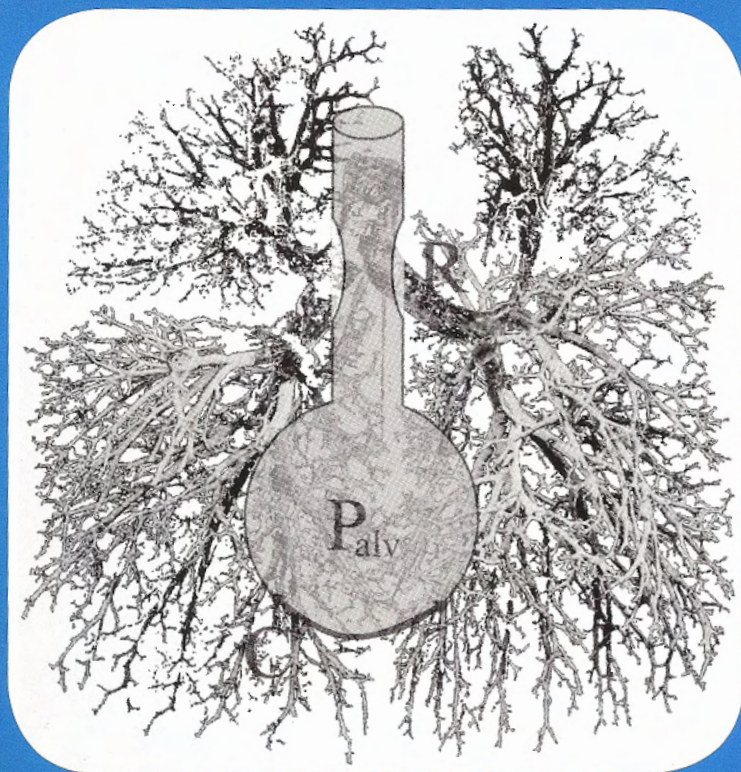


THE DYNOSTATIC ALGORITHM IN ADULT AND PAEDIATRIC RESPIRATORY MONITORING

Søren Søndergaard, MD
Institute of Surgical Sciences,
Department of Anaesthesiology and Intensive Care,
Sahlgrenska University Hospital



GÖTEBORGS UNIVERSITET

THE DYNOSTATIC ALGORITHM IN ADULT AND PAEDIATRIC RESPIRATORY MONITORING

A description of the DSA and comparison with other
models of respiratory mechanics

Thesis defended on November 8th, 2002.

Søren Søndergaard, MD

**Institute of Surgical Sciences,
Department of Anaesthesiology and Intensive Care,
Sahlgrenska University Hospital**



GÖTEBORGS UNIVERSITET

Faculty opponent:

Professor Anders Larsson MD, PhD, DEAA

Department of Anaesthesiology, Gentofte University Hospital
University of Copenhagen

THE DYNOSTATIC ALGORITHM IN ADULT AND PAEDIATRIC RESPIRATORY MONITORING.

Thesis defended on November 8th, 2002.

Søren Søndergaard, MD. Institute of Surgical Sciences, Department of Anaesthesiology and Intensive Care. Sahlgrenska University Hospital, Gothenburg University, Sweden.

Introduction: Positive pressure ventilation carries a risk of aggravating systemic and lung disease. Monitoring of ventilatory pressure and volume is important to minimize this risk. Conventionally, the *pressure* of the respiratory system is measured *outside* the patient. Tracheal pressure measurement is one step closer the alveoli and alveolar pressure can be calculated by an appropriate algorithm. Volume and pressure may possibly be reduced by using low-density gas mixtures of Helium and Oxygen.

Methods: A small fibre optic pressure transducer was evaluated for tracheal pressure measurement in paediatric patients and a polyethylene catheter for pressure measurement in adult patients. The dynostatic algorithm (DSA) is based on the equation of motion and the assumption of equal inspiratory and expiratory resistance and compliance at isovolume. The DSA utilises flow and tracheal pressure signals to calculate an alveolar P/V- and an alveolar P/t-curve continuously during ongoing ventilation. The DSA was evaluated clinically and in lung models by comparison of calculated and measured alveolar pressure. A Pitot type venturimeter was calibrated for use with low-density gas mixtures; the calibration may be incorporated in the DSA for a preliminary clinical study using He/O₂.

Results: The fibre optic pressure transducer and polyethylene catheter functioned satisfactorily in clinical pressure measurement in intubated positive pressure ventilated children and adults, respectively. The tracheal pressure recording provided an improved possibility of detecting peak inspiratory pressure and intrinsic PEEP compared to proximal measurement. The DSA reliably calculated alveolar pressure in lung models and provided a number of interesting clinical observations concerning inflection points and overdistension.

Conclusions: The Dynostatic Algorithm offers the clinician the option of improved respiratory monitoring in adult and paediatric intensive care patients.

Keywords: monitoring, respiratory mechanics, lung model, fibre optic pressure measurement, alveolar pressure, dynostatic algorithm.

ISBN 91-628-5385-6

LIST OF PAPERS

This thesis is based on the following papers, which will be referred to in the text by their Roman numerals:

I Karason S, Sondergaard S, Lundin S, Wiklund J, Stenqvist O.

A new method for non-invasive, manoeuvre-free determination of “static” pressure-volume curves during dynamic/therapeutic mechanical ventilation. *Acta Anaesthesiol Scand* 2000; 44(5): 578-85.

II Sondergaard S, Karason S, Wiklund J, Lundin S, Stenqvist O.

Alveolar pressure monitoring - an evaluation in a lung model and in patients with acute lung injury. Submitted 2002.

III Sondergaard S, Karason S, Lundin S, Stenqvist O.

Evaluation of a Pitot type spirometer in helium/oxygen mixtures. *J Clin Monit Comput* 1998 14(6): 425-31.

IV Sondergaard S, Karason S, Hanson A, Nilsson K, Hojer S, Lundin S, Stenqvist O.

Direct measurement of intratracheal pressure in pediatric respiratory monitoring. *Pediatr Res* 2002; 51(3): 339-45.

V Sondergaard S, Karason S, Hanson A, Nilsson K, Wiklund J, Lundin S, Stenqvist O.

The Dynostatic Algorithm accurately calculates alveolar pressure on-line during ventilator treatment in children. Submitted 2002.

Paper I is reproduced with permission of *Acta Anaesthesiologica Scandinavica*.

Paper III is reproduced with permission from Kluwer Academic Publishers.

Paper IV is reproduced with permission of *Pediatric Anesthesia*.

CONTENTS

ABBREVIATIONS	8
INTRODUCTION	10
THE DYNOSTATIC ALGORITHM, DSA.....	13
The dynostatic P/V curve	13
The dynostatic volume dependent compliance, VDC.....	16
Lung and chest wall mechanics.....	17
AIMS OF THE THESIS.....	19
THE RELATIONSHIP BETWEEN PRESSURE AND FLOW	20
The interventional approach, the basics	20
Pressure and flow relationship in human lungs.....	21
Rohrer laminar/turbulent, upper/lower airway model, 1915	21
Jaeger and Matthys nonlinear Venturi model, 1968	24
Papamoschou, unit airway model 1995	26
THE RELATIONSHIP BETWEEN PRESSURE AND VOLUME.....	29
The Wilson (P, S, γ , V) model, the basics of hydrodynamics.....	30
Rahn and Fenn rediscover Rohrer	32
Methods for uncovering the P/V-relation	37
Dynamic methods.....	38
The pulse method	38
Ranieri, stress index	38
Static and semistatic methods	39
The super syringe method	39
Flow interruption during a single breath.....	40
Multiple occlusions at different tidal volumes.....	40
The PEEP-wave technique.....	41
Constant flow inflation.....	42
Low flow inflation.....	42
Slow pressure ramp technique, SPRT	44
Computational approaches to respiratory mechanics.....	45

Rohrer one-compartment lung model, 1915	46
Bates, linear viscoelastic lung model 1955	46
Otis, linear serial two-component lung model 1956	49
Multiple linear regression, MLR	52
The Bertschman LOOP model 1990	56
The Guttmann SLICE method 1994.....	57
Exponential decay	58
Nikischin, Mead and Whittenberger	59
Bates and Bijaoui, MLR and time dependency	59
Inhomogeneous, nonlinear models.....	60
Fractal models of resistance, P/\dot{V} - and P/V -relationships.....	61
THE PROBLEM OF RESISTANCE	65
The interventional approach	65
Airway resistance	65
Inspiratory resistance.....	66
Expiratory resistance	68
The computational approach	70
“HAT ES EINen ZWECK?”	72
OWN INVESTIGATIONS AND RESULTS	76
ADULT SECTION.....	76
Tracheal pressure measurement in adults.....	76
The expansion of the alveolar P/V curve in time	77
Validation of the DSA in the adult lung model (Papers I & II)	79
Results of validation in the adult lung model.....	82
Application of the DSA in adult patients	83
Results of applying the DSA in adult patients	85
PAEDIATRIC SECTION	90
Tracheal pressure measurement in paediatric tubes (Paper IV).....	90
Response time.....	91
Influence of the FOPT during constant flow.....	91
Influence of the FOPT during ventilation of the lung model.....	92

Results of pressure measurement in paediatric tubes.....	92
Validation of the DSA in the paediatric lung model (Paper V).....	96
Results of validation of the DSA in the paediatric lung model	97
Application of the DSA in paediatric patients	99
Results of applying the DSA in paediatric patients	99
VOLUMETRIC MEASUREMENT IN He/O ₂ MIXTURES (Paper III)	101
Results of calibration of side stream spirometry (Paper III).....	104
SAMPLING, PROCESSING, AND CALCULATIONS (Papers I-V)	107
DISCUSSION.....	110
Is the DSA related to a lung model?	110
Can you really equate R_I with R_E ?	114
What are the advantages of <i>tracheal pressure</i> measurement?	116
Clinical impressions	118
Low-density gas mixtures in severe lung disease	120
CONCLUSIONS AND PERSPECTIVES.....	123
ACKNOWLEDGEMENTS	124
APPENDIX	127
Jaeger and Matthys.....	127
Papamoschou.....	127
Bates	127
Otis	127
Bijaoui	128
Derivation of volume correction	128
ERRATA	129
REFERENCES	130

ABBREVIATIONS

A	cross-sectional area, cm^2	MAP	mean alveolar pressure, cm H_2O
ALFI	automated low flow inflation	MBW	measured body weight, kg
ALI	Acute Lung Injury	MEF	maximum expiratory flow, L/min
ARDS	Adult Respiratory Distress Syndrome	MLR	multiple linear regression
BP	body plethysmograph	MMF	expiratory flow measured over the two middle quartiles
BVT	Biotek Ventilator Tester	MV	minute ventilation, L/min
C	compliance, $\text{mL}/\text{cm H}_2\text{O}$	ν	kinematic viscosity, η/ρ
C_d	discharge coefficient	N	nasal intubation
C_e	effective compliance (Otis)	NEP	negative expiratory pressure
C_{dyn}	dynamic compliance	O	oral intubation
CM	confidence of the mean	OD	outer diameter, mm
CMV	controlled mechanical ventilation	OI	oxygenation index
COPD	chronic obstructive pulmonary disease	OR	operating room
CV	controlled ventilation	ΔP	pressure change
DBW	measured weight	P	pressure, cm H_2O
DSA	dynostatic algorithm	P_0	stagnation pressure
E	elastance, $1/C$, $\text{cm H}_2\text{O}/\text{L}$	P_1	pressure related to airway resistance
EFL	expiratory flow limitation	P_A	alveolar pressure
η	dynamic viscosity, Ns/m^2	PBW	predicted body weight, kg
ETT	endotracheal tube	PCV	pressure controlled ventilation
f	friction factor	PEEP	positive end expiratory pressure
FOPT	fibre-optic pressure transducer	PICU	paediatric intensive care unit
g	gravitation, $9,8 \text{ N}/\text{kg}$	PIP	peak inspiratory pressure
γ	surface tension, dynes/cm	P_{lam}	pressure driving laminar flow
Hz	Hertz, s^{-1}	P_{ltt}	combined pressure in laminar, transitional, and turbulent flows
IBW	ideal body weight, kg	PLV	pressure limited ventilation
ID	inner diameter, mm	P_M	mouth pressure
IFL	inspiratory flow limitation	P_{max}	maximum inspiratory pressure
i.o.	intraoperative	p.o.	postoperative
λ	frequency modulating the fractal dimension	P_o	oral pressure
l	length, m		
LFI	low flow inflation		
LIS	lung injury score		
LSF	least square fit method		
μ	fractal dimension		

P_{oe}	oesophagus pressure	SPRT	slow pressure ramp technique
P_{plat}	pressure at end of end-inspiratory pause	τ	time constant, s
P_{tr}	tracheal pressure	t	time, s
PVLV	pressure & volume limited ventilation	T_I	inspiratory time
ρ	density, kg/m^3	TLC	total lung capacity, L
r	radius, mm	U	work performed on lung parenchyma during respiratory cycle, J
R	resistance, $\text{cm H}_2\text{O/L/sec}$	V	volume, mL
R_{aw}	airway resistance	V_A	end insp. alveolar volume, L
ΔR_{rs}	resistance relating to viscoelasticity	\dot{V}	volume velocity, L/s
Re	Reynolds' number	\bar{V}	linear velocity, m/s,
R_e	effective resistance (Otis)	VCV	volume controlled ventilation
RIP	respiratory inductive plethysmography	VDC	volume dependent compliance
R_L	resistance of lung	VILI	ventilator induced lung injury
$R_{min,rs}$	resistance relating to airway	V_T	tidal volume, mL
RLS	recursive least squares	z	difference in height, m <i>or</i> generation in bronchial tree
RMS	root mean square	ZEEP	zero end expiratory pressure
RR	respiratory rate, 1/min	ω	angular frequency, rad/s
R_{rs}	resistance related to airway and tissue		
R_{ti}	tissue resistance		
RV	reserve volume		
S	alveolar surface area, m^2		

INTRODUCTION

"In developing a mathematical model of respiratory system mechanics, our first task is to define physiologically relevant variables that can be used to describe the mechanical behavior of the system. Ultimately, these variables must be traceable to forces, displacements, and their rates, which are the fundamental variables used to describe the mechanics of any system. The variables most commonly employed to describe respiratory mechanics are pressure (a generalized force), volume (a generalized displacement), and flow (assumed to be equal to the rate of change of volume)". (41).

Respiratory failure in the guise of Acute Lung Insufficiency, ALI, or Acute Respiratory Distress Syndrome, ARDS, still exacts a great death toll from the patient population in the Intensive Care Unit (28, 114, 115). At international conferences, there is a never-ending discussion on subgroups of ALI/ARDS according to aetiology, lung mechanics, and prognosis. A number of sophisticated methods are applied to describe the evolution and resolution of the diseased lung. Few of these, if any, are applicable bedside.

The contemporary state of monitoring lung mechanics bedside is comparable to attempting from a distance of 30 feet to describe the statue of Venus from Milo (on display at the Louvre) wrapped in layers of blankets. In order to improve monitoring of patients with respiratory failure, one must get closer to the object: the alveoli. As a step in that direction, we have introduced methods of continuous measurement of tracheal pressure in adult and paediatric patients treated with positive pressure ventilation in controlled modes. As a further step in the direction of the alveoli, we have introduced the Dynostatic Algorithm, **DSA**, for continuous, on-line monitoring of respiratory mechanics.

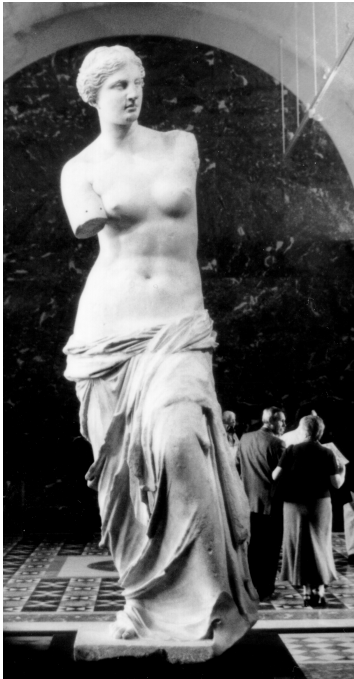


Figure 1. Venus from Milo.

A group of respiratory physiologists are discussing their findings behind her back and what the future may reveal.

The algorithm is based on tracheal pressure measurement combined with flow signal from ventilator or spirometry module. The name, dynostatic algorithm, was coined in accordance with the fact that the algorithm calculates the *static* pressure under *dynamic* conditions.

In the prototype version the algorithm provides the user with

- a total respiratory system-, a chest wall- and a lung P/V -loop as well as total respiratory system- and an alveolar P/V -curve based on tracheal and oesophageal pressure;
- calculations of initial, mid and final compliances (volume dependent compliance, VDC) as well as two-point dynostatic compliance;
- graphs displaying compliance and isovolume resistance vs volume; trends of compliance and isovolume resistance vs time;
- a strip chart displaying volume, flow, tracheal and alveolar pressure.

The algorithm has been described and documented in (95, 99, 100, 101, 179, 180, 181) and has been the subject of a thesis (97). During the development of the algorithm in our group (Ola Stenqvist, Stefan Lundin, Sigurbergur Kárasón, and Jan Wiklund) I have come into contact with a number of aspects of lung physiology and unconventional treatment of respiratory disease in the Intensive Care Unit: the use of low-density mixtures of helium and oxygen (He/O₂).

In the following paragraphs, my aim is a detailed description of the DSA in adult and paediatric applications and its relation to previous and contemporary models of lung mechanics. These models have been divided into two groups: one based on manipulation of ventilator settings in order to obtain data for analysis of respiratory mechanics (**interventional**) and another based on calculations derived from mechanical models (**computational**).

The DSA entails tracheal pressure measurement, which is easily accomplished in adult patients. In children, it presented a major challenge, which called for validation of the fibre-optic pressure transducer, a recently introduced interferometric technique. As a prerogative for using the DSA in connection with He/O₂ mixtures, the subject of measuring respiratory volumes in these conditions had to be investigated.

This presentation is an attempt to assemble those bits and pieces that have been of interest and importance to me. My situation may not be too different from the fable of the three men and the elephant, with the not insignificant increase to six men, of Indostan (167). The answer is, of course, in the lung.

The description of lung mechanics and models is relying on mathematical equations. In order not to impede reading, these have been placed in the APPENDIX with the relevant subheading.

THE DYNOSTATIC ALGORITHM, DSA

... and I thought instinctively of the troll in the fairy-tale who pops out of his hole and roars: "Who is chopping trees in my forest?"

AS Byatt, The Biographer's Tale.

The dynostatic P/V curve

We have proposed a method for the on-line calculation and display of the static P/V-curve and alveolar pressure vs time based on commercially available monitoring apparatus, a personal computer, an A/D-converter, and suitable software. We have termed the method "the dynostatic algorithm" because it **calculates** the equivalent of the static pressures under dynamic conditions. The algorithm may be seen as a reflection of the **equation of motion** stating that the total pressure exerted during controlled positive pressure ventilation is accounted for by the pressure necessary for expanding the lung parenchyma and thoracic cage, P_{elastic} , and pressure needed to overcome the flow-resistive and viscoelastic forces of airway and lung tissue, $P_{\text{resistive}}$, and total PEEP, thus:

$$(i) P_{\text{total}} = P_{\text{elastic}} + P_{\text{resistive}} + \text{PEEP}$$

or

$$(ii) P_{\text{total}} = V/C + \dot{V} \times R + \text{PEEP}$$

The first part (V/C) accounts for the elastic component of the lung and chest wall, whereas ($\dot{V} \times R$) calculates the flow-resistive component. Thus, the P_{total}/V -loop expresses the sum of these pressures. In the equation, P_{total} and flow are measured by respiratory monitoring equipment and volume is time-integrated flow, whereas C and R are unknown. The end-expiratory pressure (PEEP) represents the relation between the compliance of the lung and the volume retained above FRC in the lung: RV/C .

This version of the equation of motion has the following assumptions:

1. the relationships between pressure/flow and pressure/volume are linear equations;
2. a singular value of resistance and compliance can be specified, either for the whole cycle or for inspiration and expiration separately;
3. there is no hysteresis in the respiratory system (corollary to 2.);
4. inertia, gas compression, and gravity can be neglected.

In the DSA these assumptions are modified to the effect:

5. that inspiratory and expiratory resistances (R_{aw} , R_{ti} , but not R_{rs} which includes the ETT and ventilator circuit) are equal or almost equal at *isovolume* levels; and
6. modifies the first two to the effect that compliance and resistance may vary during the respiratory cycle AND each will be equal or almost equal during in- and expiration at isovolumes.

At isovolumetric points, one inspiratory, another expiratory, the following expressions may then be formulated:

$$(iii) P_{insp} = P_{elastic} + \dot{V}_{insp} \times R_{insp} \Rightarrow R_{insp} = (P_{insp} - P_{elastic}) / \dot{V}_{insp}$$

$$(iv) P_{exp} = P_{elastic} + \dot{V}_{exp} \times R_{exp} \Rightarrow R_{exp} = (P_{exp} - P_{elastic}) / \dot{V}_{exp}$$

$$\text{As } R_{insp} \cong R_{exp}$$

$$(v) P_{dynostatic} = P_{elastic} = (P_{exp} \times \dot{V}_{insp} - P_{insp} \times \dot{V}_{exp}) / (\dot{V}_{insp} - \dot{V}_{exp})$$

P_{insp} and P_{exp} are measured as distal (tracheal) pressures with a polyethylene catheter inserted in the tube in the adult setting (181) and a fibre-optic pressure transducer in the paediatric setting (179). Pressure, volume and flow vectors¹ for inspiration and ex-

¹ Strictly speaking, *flow* is a vector (\equiv a quantity or phenomenon that has two independent properties: magnitude and direction), whereas *volume* and *pressure* are scalars (\equiv a phenomenon that exhibits magnitude with no specific direction). In this context 'vector' will be used for both.

piration (end-inspiratory pause with zero flow is not included in the analysis) are entered into the $P_{\text{dynostatic}}$ equation in the software programme, values of pressure, volume, and flow during end-inspiratory pause are not utilised.

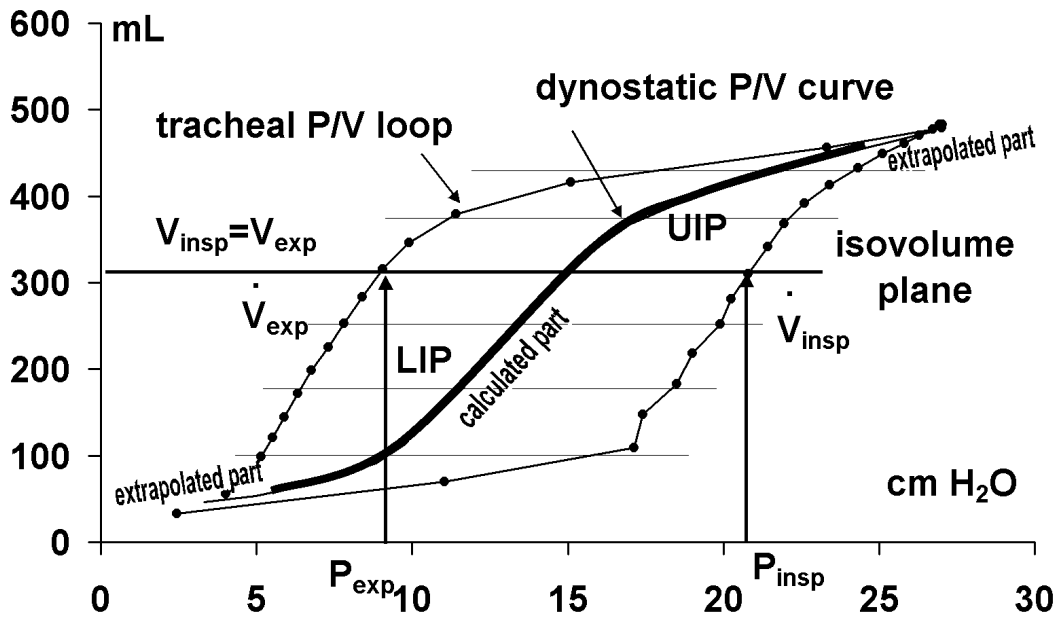


Figure 2. Method of calculation of dynostatic pressure. Vectors of pressure and flow are sampled continuously and volume is integrated from flow. Isovolum levels are set, and isovolemic values of pressure and flow are interpolated and entered into the dynostatic equation.

Calculation of P_{DSA} encompasses central inspiratory and central expiratory part pressure, volume, and flow signals (90%) stopping shortly before start-inspiration and end-inspiration and correspondingly start-expiration and end-expiration. The parts of pressure, volume and flow vectors close to start-inspiration/end-expiration and end-inspiration/start-expiration contain such rapid and large changes that the algorithm be-

comes extremely sensitive to the nonlinearity of the signals and the nominator ($\dot{V}_{\text{insp}} - \dot{V}_{\text{exp}}$) attains low values during transition between inspiratory and expiratory phases. Therefore, the central part of the dynostatic P/V-curve is automatically extrapolated to $(P_{\text{min}}, V_{\text{min}})$ and in the case of end-inspiratory pause to $(P_{\text{plat}}, V_{\text{max}})$. If no pause is present, the P/V-curve is fitted to a second-degree polynomial; the pressure value corresponding to V_{max} is calculated and the curve is extrapolated to $(P_{\text{poly-max}}, V_{\text{max}})$.

The dynostatic volume dependent compliance, VDC.

The alveolar P/V curve clearly shows zones of varying compliance. Compliance displays a nonlinear relationship between pressure and volume. This has been recognized since 1978 (189) and has emerged in a vast literature on *inflection points*, not in the strictly mathematical sense, but as an indication of a point where slope is changing in an upward or downward direction. For practical purposes the P/V curve may be divided into three segments at low, mid and high volume and compliances for these *zones* may be calculated according to specification. As default, the DSA calculates zones from 5-15%, 45-55%, and 85-95% of volume, but zone limits may be changed. The feature of VDC has been explored in (98, 99).

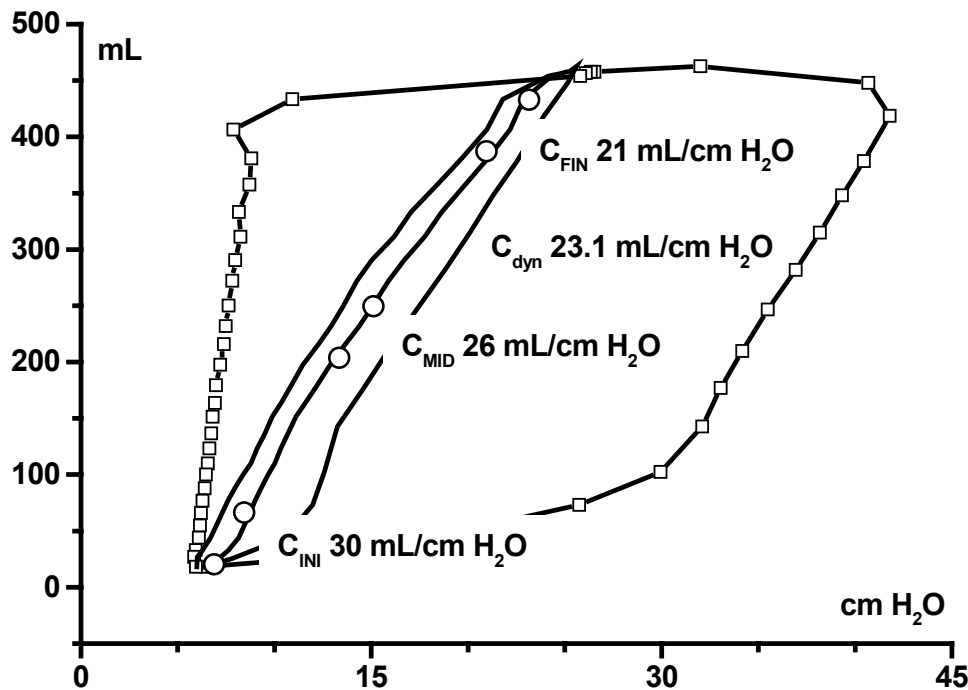


Figure 3. Volume dependent compliance. Proximal (square), and tracheal (full line) P/V loops from VCV at PEEP 5 cm H₂O and 10% end-inspiratory pause. Dynostatic P/V curve with VDC marked in circles: C_{INI}: 30, C_{MID}: 26, C_{FIN}: 21 cm H₂O. The single value of C_{dyn}: 23.1 cm H₂O demonstrates that this measurement misses the fact that compliance is gradually diminishing through the tidal volume. In cases with pronounced overdilation the tracheal P/V loop takes on a “banana” shape and the C_{dyn}-line lies *outside* the loop, which of course is not possible, cf. insert in lower part of Figure 30, p.81.

Lung and chest wall mechanics.

By measuring oesophageal pressure with a double lumen SalemTM stomach tube or a conventional stomach tube as a substitute for pleural pressure, the compliance of the chest wall and lung can be separated. The tube is passed through the nose or mouth into the stomach; the narrow lumen is filled with saline and connected to a standard pressure transducer. The larger lumen is also filled with saline whereupon the proximal end is occluded. The tube is then withdrawn slowly into the oesophagus until the

pressure curve shows maximal pressure fluctuations related to respiration and minimal artefacts from heartbeat. Correct positioning is verified by the rib cage compression occlusion test (25, 97). In the DSA algorithm the oesophageal pressure curve is smoothed over sections of eight measurement points with an averaging algorithm to decrease pressure variations caused by heart oscillations. Since the oesophageal P/V-loop does not display hysteresis, a mean value of the inspiratory and expiratory limbs at isovolume levels during inspiration and expiration is calculated, producing a *mean chest wall P/V-curve*. To obtain a *single dynostatic compliance value* for the chest wall, a best linear fit of this curve (LSM) is calculated. A lung pressure curve is calculated as the pressure difference between the tracheal (total respiratory system) and the smoothed oesophageal (chest wall) pressure curves and displayed as a lung P/V-loop. This lung P/V-loop is analysed as described for the tracheal P/V-loop (representing total respiratory system), with identification of the *lung dynostatic P/V-curve* and calculation of a *single value dynostatic compliance* and *volume-dependent compliances*.

AIMS OF THE THESIS

- To validate the Dynostatic Algorithm for calculating alveolar pressure and for displaying alveolar pressure/volume curves in a lung model and for applying it in patients during on-going ventilator treatment, based on direct measurements of tracheal pressure (Papers I and II).
- To examine the long-term feasibility of tracheal measurement in adult respiratory care (Paper II).
- To extend the DSA to calculation and display of alveolar pressure vs time (Paper II).
- To examine the possibility of monitoring tracheal pressure in paediatric intensive care with a fibre-optic catheter (Paper IV).
- To validate the DSA in a paediatric lung model and apply it in paediatric intensive care (Paper V).
- To calibrate a Pitot type spirometer for use with He/O₂ mixtures (Paper III).

The merits of Dynostatic Algorithm lie in the combination of old insights, tracheal pressure measurement and a step towards monitoring ventilatory treatment by means of calculated alveolar pressure.

Without acknowledging our predecessors, we will not be able to incorporate their findings and will run the risk of reduplicating their results - as well as mistakes.

Therefore, I intend to sketch the development of respiratory physiology in two approaches, the interventional and the computational, in order to demonstrate various approaches to the description and modelling of lung mechanics.

THE RELATIONSHIP BETWEEN PRESSURE AND FLOW

The interventional approach to respiratory system impedances focuses on the relationships between *pressure and flow* mediated by viscous pressure reduction in air and tissue, airway dimensions, and geometry; as well as between *pressure and volume* mediated by air and lung tissue elasticity; and between *volume acceleration, gas density and viscosity and airway geometry* mediated by inertance of the gas and tissue.

The interventional approach, the basics

The science of hydrodynamics describes the relation of pressure to flow of substances of known density and viscosity in single tubes and system of tubes. The human airway may be looked upon as a complex system of tubes. Traditionally, flow is characterised as laminar, transitional or turbulent. Whether flow *in a single tube* is laminar or turbulent is estimated from the value of Reynolds' number (named after the English physicist Osborne Reynolds, 1842-1912) calculated according to:

$$(vi) \quad Re = \frac{2 \times \dot{V} \times \rho}{\pi \times r \times \eta}, \text{ (the ratio between inertial and viscous forces).}$$

Values of Reynolds' number less than 2000 designate *laminar* flow (viscous forces are dominant), whereas values above 4000 designate *turbulent* flow (inertial forces dominate over the viscous forces). For intermediary values, flow is characterised as *transitional*. Driving pressure in laminar flow is calculated according to the Hagen-Poiseuille equation:

$$(vii) \quad \Delta P_{\text{lam flow}} = \frac{\dot{V} \times 8 \times \eta \times l}{\pi \times r^4},$$

stating that pressure is proportional to flow, viscosity, and length of tube, and inversely proportional to the fourth power of the radius of the tube.



Figure 4. Parabolic flow profile in laminar flow.

Driving pressure in *turbulent flow* rises exponentially with volume velocity and inversely with the fifth power of radius. It is calculated from the Fanning equation:

$$(viii) \Delta P_{\text{turb flow}} = \frac{\dot{V}^2 \times f \times l}{4 \times \pi^2 \times r^5} \quad (f \text{ (smooth pipes)} = \frac{0,316}{Re^{0,25}}, f \text{ (rough pipes)} = 0,02-0,06).$$

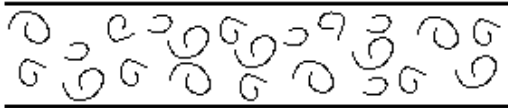


Figure 5. Flow profile in turbulent flow.

Generally, flow incorporates features of laminar as well as turbulent flow and may be estimated according to:

$$(ix) \Delta P_{\text{transitional flow}} = k_1 \times \dot{V} + k_2 \times \dot{V}^2.$$

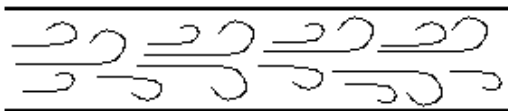


Figure 6. Flow profile in transitional flow.

Traditionally, though questionable, k_1 is ascribed to the laminar part of flow and k_2 to the turbulent part. The calculation of Reynolds' number, driving pressures in laminar, transitional, and turbulent flow are limited to smooth, unbranched tubes, a characteristic NOT found in the human bronchial tree. Alternative descriptions are called for.

Pressure and flow relationship in human lungs

Rohrer laminar/turbulent, upper/lower airway model, 1915

The Swiss physiologist Fritz Rohrer (1888-1926) laid the foundations of respiratory physiology in his dissertation "*Der Strömungswiderstand in den menschlichen Atemwegen unter der Einfluß unregelmässigen Verzweigung des Bronchialsystems auf den Atmungsverlauf in verschiedenen Lungenbezirken*" (160), for an English translation see (161). Mead (209), p. 173, announces him the "Mozart of respiratory mechanics", but the only common denominator seems to be their interest in pipes (listen to, e.g.,

KV 313, 314, 581, and 622) and the sad fact that they died at about the same age.

Rohrer's profound contribution to the understanding of pressure flow and pressure volume relationships has three headings.

First, Rohrer performed simple experiments involving flow in smooth, branched tubes. Using vapours of ammonium chloride, he was able to demonstrate laminar flow ("Parallelströmung"). From this he proceeded to develop the mathematical apparatus describing pressure under conditions of laminar and turbulent flow and states in between. Exceeding "Grenzgeschwindigkeit", defined by Reynolds' number, driving pressure equals a sum of pressures to (1) maintain turbulent flow and (2) to overcome "störende Momente", thus

$$(x) \quad \Delta P = k \times V^n, \quad n=1.7-2 \quad (\text{cp. Fanning equation, see above}).$$

Below one sixth of "Grenzgeschwindigkeit" pressure fall is calculated according to Hagen-Poiseuille. In between Rohrer presumed that pressure will have to counter a mixture of laminar flow and "störende Momente", which he defined as:

1. sprungweise Änderung des Strömungsquerschnittes;
2. Änderung der Strömungsrichtung; and
3. unregelmässige Wandung.

He generated the equations describing pressure fall in a single tube and a branched system of tubes arriving at the expression cited below; the second (squared) term encompasses these "störende Momente" as well as turbulent flow. His findings for the relationship between pressure in laminar, transitional and turbulent flow are expressed in the equation

$$(xi) \quad \Delta P_{\text{itt}} = k_1 \times \dot{V} + k_2 \times \dot{V}^2.$$

This expression has prevailed throughout the literature on respiratory mechanics since 1915, whether in connection with single or branched tubes.

His *second* great achievement was the description of the morphology of the human lung based on measurements of diameter and length of bronchi and bronchioles down to a diameter of 1 mm using calibrated bougies. He assumed a dichotomous branching

of bronchi and bronchioli. The diameters of successive generations were described as following an exponential decay. This is the first demonstration in respiratory physiology of the fact that an exponential law governs the dimensions of the lung. Proceeding from these morphometric enumerations Rohrer calculated distribution and size of pressure fall, arriving at the equation:

$$(xii) \Delta P = 0.79 \times \dot{V} + 0.801 \times \dot{V}^2.$$

This he broke down into

$$(xiii) \text{ upper airway } \Delta P = 0.426 \times \dot{V} + 0.7135 \times \dot{V}^2$$

$$(xiv) \text{ lower airway } \Delta P = 0.364 \times \dot{V} + 0.0875 \times \dot{V}^2.$$

The second term in (xvi) emphasizes the small importance of turbulent flow and “störende Momente” during **normal respiration** in the lower airway. It is worth noting that Rohrer based his description on a simple experiment and the morphology of the lung down to the tenth generation. Rohrer condensed his findings in **one** equation relating pressure and flow: ”Zwischen der Volumengeschwindigkeit in der Trachea V in Sekunden/Litern [sic] und der Druckdifferenz zwischen Alveolen und Aussenluft berechnet sich, unter möglichst genauer Berücksichtigung aller morphologischen Verhältnisse, für die Lungen nahe dem Collapszustand, die Beziehung:

$$(xv) P = 0.8 \times k \times (V + V^2) \text{ (cm H}_2\text{O)}.$$

....Diese Formel kann für alle Dehnungszustände als gültig angenommen werden.” (p. 296).

His *third* achievement was the description of the elastic properties of the lung and their incorporation in the equation of total ventilating pressure:

$$(xvi) P = P_{el_0} \pm 4.5 \times \Delta V \pm 0.8 \times (\dot{V} + \dot{V}^2) \text{ (cm H}_2\text{O)}.$$

Note that Rohrer assumed a linear relationship between pressure and volume with the elastance 4.5 L/cm H₂O. This equation is valid “..innerhalb der für die Atmung in Betracht fallenden Ausdehnung...” (p. 282). All three areas of his research interest are

summarized in his chapter on *Physiologie der Atembewegung* in *Handbuch der normalen und pathologischen Physiologie* (162).

The durable legacy of Rohrer is the realization of the complex bronchial geometry and its relation to the calculation of pressure, flow, and resistance during ventilation. Later developments have added more details to airway models and other constants into the equations together with the inclusion of the parameters of viscosity and density from the Hagen-Poiseuille and Fanning equations. The conception of the linear and constant compliance continued until far into the second half of the century.

Jaeger and Matthys nonlinear Venturi model, 1968

In 1968 Jaeger and Matthys (87, 88) sparked off renewed interest in pressure/flow in the human airway by proposing their “astute” (40) airway model. Usually, they noted, the pressure-flow relationship is described in terms of laminar and turbulent flow in uniform, non-branching tubes, but, actually, the airway is more like non-uniform, multiple branching tubes, and the transformation from laminar to turbulent flow is gradual. They likened the situation to the Venturi tube, a short tube with a concentric constriction halfway. According to the Venturi model there is a gradual transition described by a nonlinear relation between a “coefficient of discharge”, C_d , and Reynolds’ number (see APPENDIX). Jaeger and Matthys investigated the relationship between pressure, volume, and flow in human subjects, measuring P_A , V , and thoracic gas volume with a body plethysmograph, P_{tr} with a catheter six centimetres above the carina, P_M , mouth pressure, and \dot{V} at the mouth. Furthermore, they tested the relation between C_d and Re in an experimental set-up of the upper extrathoracic and lower intrathoracic airway, and demonstrated a curvilinear correspondence in a double logarithmic plot for O_2 , Ne , He and SF_6 , see Figure 7. After calculating Reynolds’ number for \dot{V} , D , ρ and η , the coefficient of discharge, C_d , should be read from the curve – as no mathematically identifiable relation exists between Re and C_d , according to Jaeger and Matthys. However, digitising the measurements in Figure 7 and performing a lo-

gistic curve fit, demonstrates that the relationship between C_d and Re is indeed predictable. This makes it possible to automate the calculation of C_d and as a corollary ΔP may be calculated after reorganising the equation (see APPENDIX).

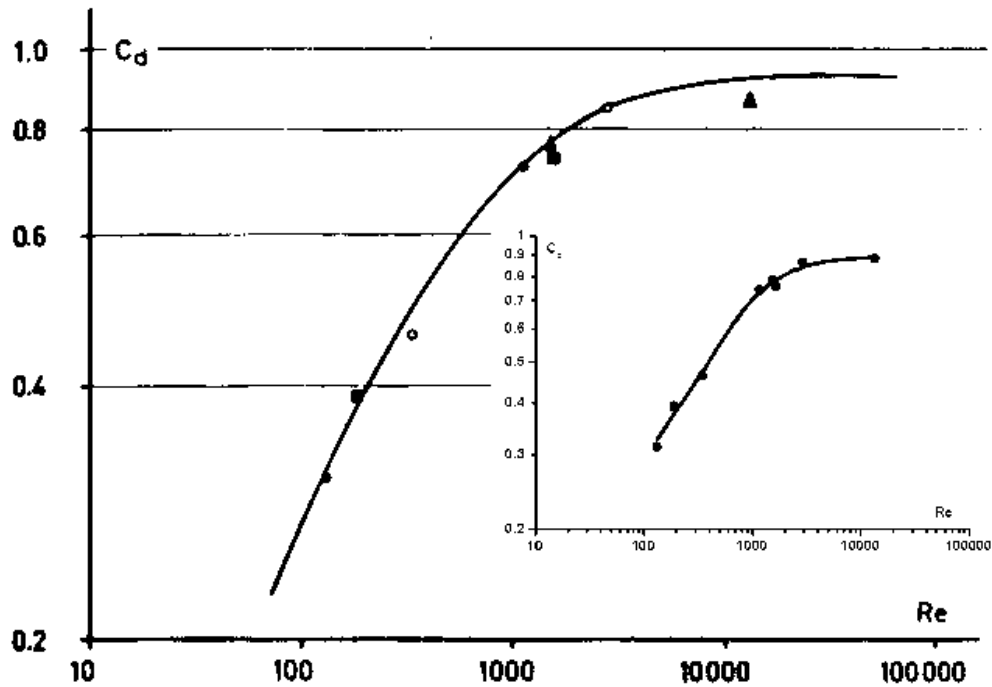


Figure 7. The Jaeger and Matthys curvilinear relationship between C_d and Re . **Insert:** the Jaeger & Matthys measurements (closed circles) digitised and fitted to a logistic function (line) χ^2 0.00059. Adapted from Jaeger and Matthys (87). Courtesy of Charles C Thomas, Publisher, Ltd., Springfield, Illinois.

The routes towards pulmonary mechanics taken by Rohrer and Jaeger and Matthys are very characteristic of the complex pressure/flow relationship. It is beyond the scope of this exposé to demonstrate the calculation of pressure as dependent on area and flow in the bronchial tree, as this would further entail a thorough description of airway geometry (the reader is referred to (83, 84, 85, 154, 206, 207, 208)), but with information on actual flow and area in ascending order of bronchial generations, it is possible with the equations adduced (see APPENDIX) to calculate the viscous pressure drop

related to each generation and thus the probable pressure at alveolar level. Were it possible to characterise a “unit” area and flow (see below), encompassing all 20-25 generations, the ΔP could be entered into the motion of equation. By contrasting the term $(\dot{V} \times R)$ in the simple version of the equation of motion with the expressions of Rohrer and Jaeger and Matthys, one realises the tremendous simplification entailed.

Papamoschou, unit airway model 1995

Papamoschou (142) contributed to this discussion by looking at the upper airway (5 generations, which seems to be the farthest anyone has dared to go in terms of “unit” dimensions) as approximated by a single pipe with effective diameter, D_{eff} , and effective length, L_{eff} , defined as a factor multiplied by the tracheal diameter. Extending from the work by Slutsky (177), Papamoschou derived a relationship between flow, pressure, effective length, and effective diameter (see APPENDIX). From this he was able to calculate the relation of pressure to flow in complete accordance with the measurements of Slutsky. In continuation, it is possible to demonstrate the pressure/flow relationship in various combinations of flow, gas mixture, and tracheal dimensions. This is demonstrated in Figure 8.

Numerous other descriptions and analyses have been given on this subject. Out of personal preference I have used Rohrer, Jaeger and Matthys, and Papamoschou as examples, but reference to the very authoritative contributions by Pedley (143, 144, 145, 146) should not be left out, nor to Drazen and Wood (53, 212). Other investigators have looked at the pressure/flow relation during *expiration*, Hardin (78) and Collins (44), and during *oscillatory* flow. This has been extensively studied by using sinusoidal flow for which flow and pressure may be expressed as a function of time. This is hardly possible for the pressures and flows generated during controlled ventilation. In sinusoidal flow at low frequency (in the range of normal breathing), resistance due to oscillation is negligible. The subject is not further pursued in this context. The reader is referred to (40).

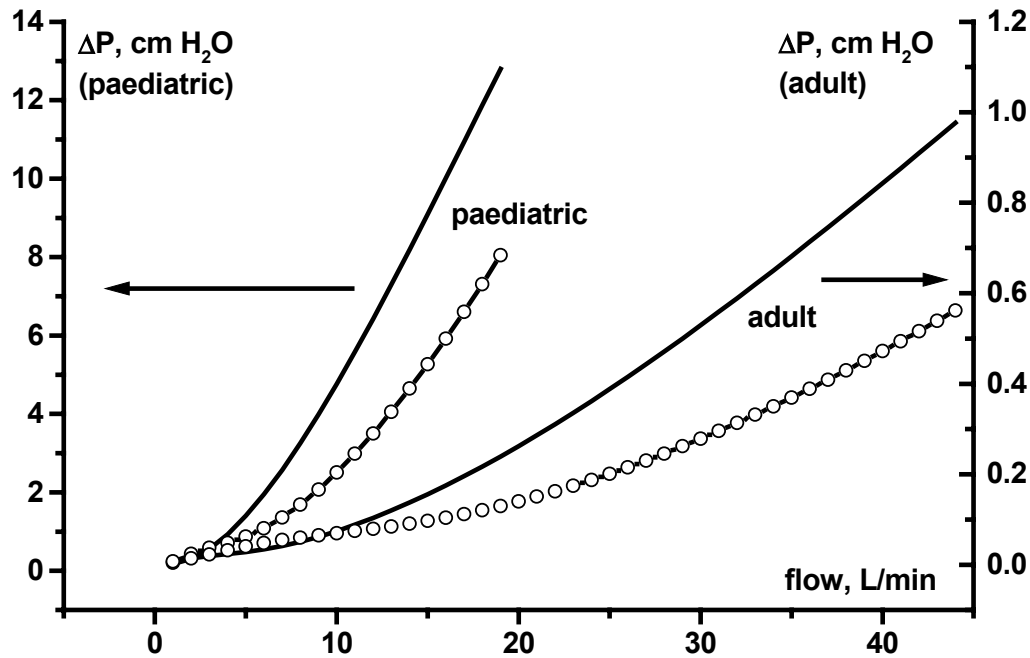


Figure 8. Pressure/flow relationship for normal and low-density mixtures. Full line: N_2/O_2 70%/30%; circled line: He/O_2 70%/30%. Left pair of lines: paediatric values to be read on Y1; right pair of lines: adult values to be read on Y2. Note that owing to the high viscosity of He/O_2 mixture, the driving pressure exceeds N_2/O_2 at low flow (laminar). The figure is based on Papamoschou (142).

In health, the viscous pressure drop is of minor importance during quiet breathing. The flow regimen is predominantly laminar. During exercise, flows may produce turbulence in the upper part of the intrathoracic airways. **In pulmonary disease** in the ICU varying degrees of inflammation, oedema, exudation, and transudation make up a highly variable clinical picture of changes in compliance and resistance.

With an understanding of the pressure/flow relationship in the airway and the factors entering this relationship, the clinician is able to choose therapeutic means to alleviate or minimize the risks inherent in positive pressure ventilation by changing flow (I:E ratio), frequency, airway diameter (bronchodilators, PEEP), density, and viscosity (us-

ing low-density gas mixtures), &c. In conclusion, the Jaeger and Matthys airway model as well as the Papamoschou model *may* offer an explanation to the possible effect of He/O₂ mixture in patients with obstructive complaints. Furthermore, introducing the gradual transition in the Re/C_d plot replaces reference to the laminar/transitional/turbulent trichotomy.

THE RELATIONSHIP BETWEEN PRESSURE AND VOLUME

The lung is the soft tissue organ par excellence. It consists of time-varying proportions of collagen, elastin, reticulin, and proteoglycans. It has been characterised as *quasi-incompressible, non-homogeneous, non-isotropic, nonlinear, viscoelastic* undergoing *large deformations* and has stimulated a wealth of modelling in biomechanics. Building blocks in this are the Kelvin, Maxwell, Voigt, and Prandtl bodies (see below, - comparable to the “mechanical alphabet” of Christopher Polhem) – and any combination of these. The choice of model is an intricate consideration of descriptive and explanatory power vs complexity and computational capacity.

The lung as a soft or bio-viscoelastic tissue is characterised by the following features:

- Stress-relaxation: Upon applying a *constant strain* (\equiv local deformation) to a material, *the stress* (\equiv internal tension) in the material will reduce over time. In lung physiology, this is demonstrated in the exponential decay of pressure during end-inspiratory pause.
- Creep: Involves applying a *constant force* to a material. The material will subsequently undergo some extension and the *strain rate* of lengthening *decreases* with time. This may be observed as decelerating volume increment during constant pressure insufflation.
- Hysteresis: The cyclic loading of a material is often path dependent. Typically, the loading curve shows higher pressures than the unloading curve for identical volumes, the difference in area representing the energy lost in the process. The P/V loop is typical of hysteresis for reasons to be elucidated below.
- Nonlinear elasticity: In a stress-strain diagram – the equivalent of the P/V diagram – the lung shows three regions of stress/strain relationship. An initial low *modulus* (\equiv stress/strain, cp. volume/pressure) region, a mid linear and final region of decreasing modulus before the tissue yields. This feature has been termed pseudo-elasticity as no constant modulus can be assigned to the tissue (3).

In the following, I shall use the Wilson exposition to present the basics of reasoning and perspective of biomechanical modelling.

The Wilson (P, S, γ , V) model, the basics of hydrodynamics

A description of models concerning the elastic properties of the pulmonary parenchyma may conveniently take as a starting point the difference in the P/V loops of saline-filled vs an air-filled lung. Hildebrandt and colleagues elucidated the mechanical behaviour of a fluid-filled lung (6, 7, 82): a saline-filled lung hardly shows any hysteresis during inflation-deflation; in contrast the normal, air-filled lung, as is well known, demonstrates a marked hysteresis. The greater part of the difference relates to the presence of surfactant. In contrast to the elastic lung parenchyma, the work performed on surfactant during inspiration is not recovered during expiration, which gives rise to the hysteretic P/V loop. This is expressed in the equation

$$(xvii) \quad \delta U = P\delta V - \gamma\delta S,$$

where U denotes elastic energy stored in tissue, the term ‘ $P\delta V$ ’ denotes the work done on the lung and ‘ $\gamma\delta S$ ’ the work “lost” in increasing lung surface, S, with surface tension γ .

Based on considerations of energy balance, Wilson (210) derived the following equations between independent variables V, γ and dependent variables P, S:

$$(xviii) \quad \frac{\delta S}{\delta V} = \frac{\delta P}{\delta \gamma} \Rightarrow \delta S = \frac{\delta P}{\delta \gamma} \times \delta V,$$

stating that rate of increase of alveolar surface area, S, is a linear function of volume with the ratio ‘ $\delta P/\delta \gamma$ ’ as a constant. This is brought out in the following figures:

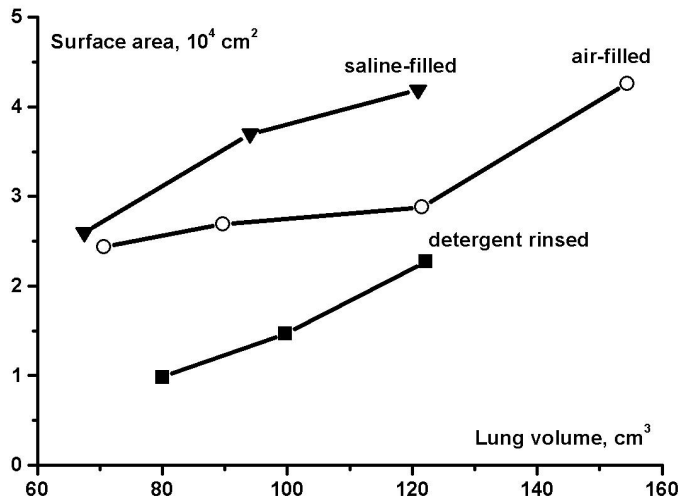


Figure 9. Surface area as function of lung volume in saline-filled, air-filled and detergent-rinsed rabbit lungs. An identical linear relationship is evident in the three circumstances, only the constant varies. The saline-filled surfactant-free lung exerts the lowest pressure (surface tension zero), whereas surface tension is increased in the detergent-rinsed lung, exerting the greatest pressure. The curves do not allow extrapolation to $V = \text{zero}$ as this entails negative surface or “lung implosion”. The figure is based on data from Wilson (210).

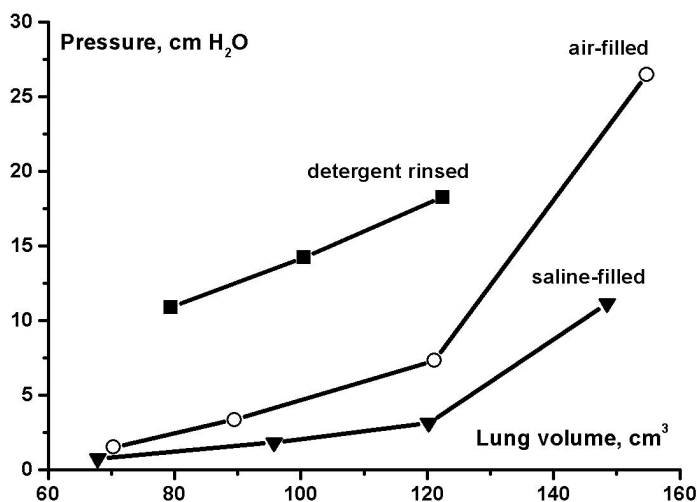


Figure 10. Pressure as function of volume in saline-filled, air-filled, and detergent-rinsed rabbit lungs. Saline-filled lungs have the highest compliance. The figure is based on data from Wilson (210).

The variables V, S may also be chosen as independent variables, thus:

$$(xix) \quad \frac{\delta\gamma}{\delta V} = -\frac{\delta P}{\delta S} \Rightarrow \delta P = \frac{1}{\delta V} \times \delta\gamma \times \delta S,$$

stating that pressure increase is inversely related to increase in lung volume with $\delta\gamma \times \delta S$ as a constant. The function is demonstrated in Figure 10.

Wilson utilised these relationships to demonstrate the intricate relationships between pressure, volume, surface tension, and surface in a three-dimensional diagram describing possible combinations of surface area, pressure, and volume obtained in a rabbit lung preparation.

These rather complicated interrelations draw attention to the fact that the description of the elastic properties of the lung involves - as a first approximation - the elastic properties of the lung parenchyma (which may be divided into a number of compartments) and the characteristics of surfactant, which in disease is either deficient or malfunctioning (27, 49).

These are the elements under consideration in the various attempts to describe the pressure/volume relationship, whether from an interventional or a computational approach.

Rahn and Fenn rediscover Rohrer

Rahn (155) and Fenn (57) rediscovered the work of Rohrer and laid the foundations of modern respiratory mechanics by analysing the relationship in a pressure/volume diagram. They described a sigmoidal static P/V-curve of the total respiratory system in individuals with normal lung function (Figure 11). The initial compliance, below functional residual capacity, was considered lowest. At FRC, the compliance became highest and then decreased successively with increasing volumes. The total respiratory system P/V-curve is the sum of chest wall compliance and lung compliance. With in-

creasing tidal volumes the static chest wall P/V-curve will show increasing compliance while the static lung P/V-curve will show decreased compliance. The fall in lung compliance is larger, however, as the total respiratory system compliance also decreases with higher tidal volumes (34).

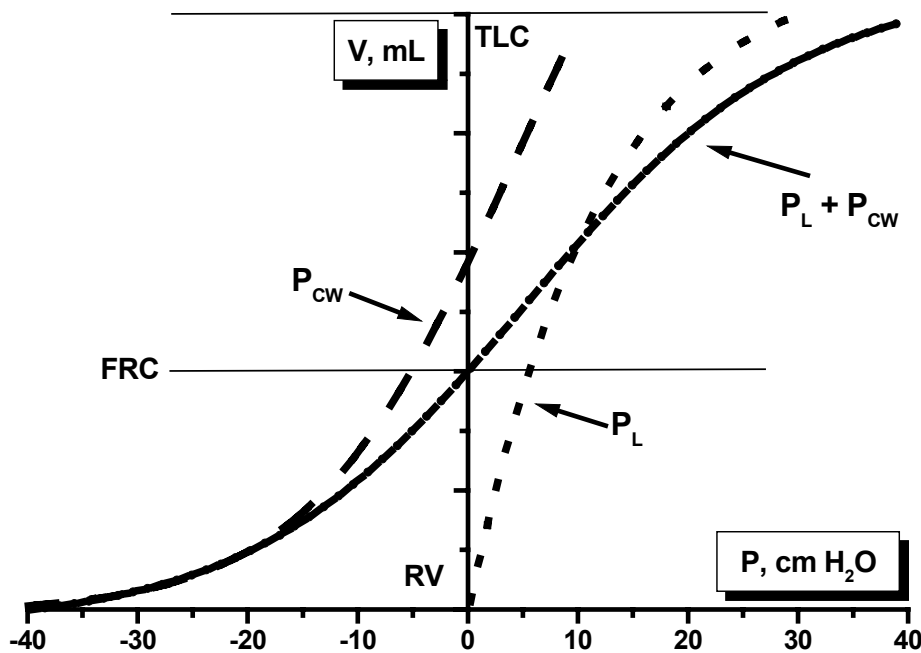


Figure 11. Rahn diagram of total respiratory system, chest wall, and lung with schematic illustration of static P/V-curves of the total respiratory system, chest wall, and lung traced from residual volume (RV) to total lung capacity (TLC). Notice that chest wall compliance increases with increasing volume, whereas lung compliance decreases. The curve for the total respiratory system, a sum of the other two curves, crosses the zero pressure line at functional residual capacity (FRC).

In 1972, Falke (56) traced dynamic P/V-loops in patients with ARDS at different PEEP levels and showed increased compliance with recruitment. In 1975, Suter (188) identified an optimal PEEP level in the treatment of ARDS patients, where maximum

oxygen transport coincided with highest FRC and static compliance of the total respiratory system. This was explained by movement of the tidal volume on a hypothetical curvilinear P/V-curve with an inflection at low tidal volume similar to that identified in normal subjects but lying at other volume and pressure levels in ARDS patients. In 1981, Lemaire evaluated static respiratory system mechanics in patients with ARDS and noted a sigmoidal static P/V-curve with a prominent lower inflection point (109). In 1984, Matamis (122) proposed the use of the *lower inflection point* (LIP) to titrate PEEP and suggested that the initial portion of the static P/V-curve was a sign of progressive alveolar recruitment that would be completed once the curve became linear. This has later been questioned, see below An *upper inflection point* (UIP) indicating overdistension of alveoli had also been described but it seems not to have been used to identify an upper pressure limit during ventilator treatment and empirical pressure limits were used instead (1, 36, 37, 183, 194). In the ACCP 1993 consensus report about mechanical ventilation, it was stated that there were no data indicating that any ventilatory support mode was superior for patients with ARDS (176). However, results from animal models and trials using a limited upper pressure approach in ARDS patients (63, 81) led to the recommendation of keeping the end-inspiratory plateau pressure below 35 cm H₂O. An appropriate PEEP level was recognised as useful to support oxygenation and possibly helpful in preventing lung damage. It was recommended that the PEEP level should be identified by an empirical trial but should be minimised as it could also have deleterious effects in terms of cardiovascular effects and overdistension.

Numerous mechanisms have been proposed to explain the behaviour of lung mechanics in patients with lung injury. These include increased surface tension because of surfactant inactivation, airway block caused by air-liquid interfaces and bubble formation in small airways, reflex bronchoconstriction and peribronchial oedema (121).

The P_L/V curve (Figure 11) represents a summation of airway and tissue volume response to applied pressure, thus demonstrating the intrinsic interplay between alveolar recruitment, alveolar surface-air interface (surfactant), the integration of alveoli into the interalveolar mesh of collagen, elastin and vessels, bronchiolar opening pressures, the compliance of conducting airways and volume increase. Carney (39) showed by dynamic microphotography that increase in alveolar volume was minimal during inflation (Figure 12), whereas the number of alveoli increased. Hickling (80) demonstrated in a mathematical model that continuing recruitment could account for the course of the P/V curve and this was also shown in Jonson (92) and Vieira (203). Lichtwarck-Aschoff has made an elegant demonstration of the stepwise increase in volume in terms of Hounsfield units during a fast CT scan in three horizontal slices, see Figure 13.

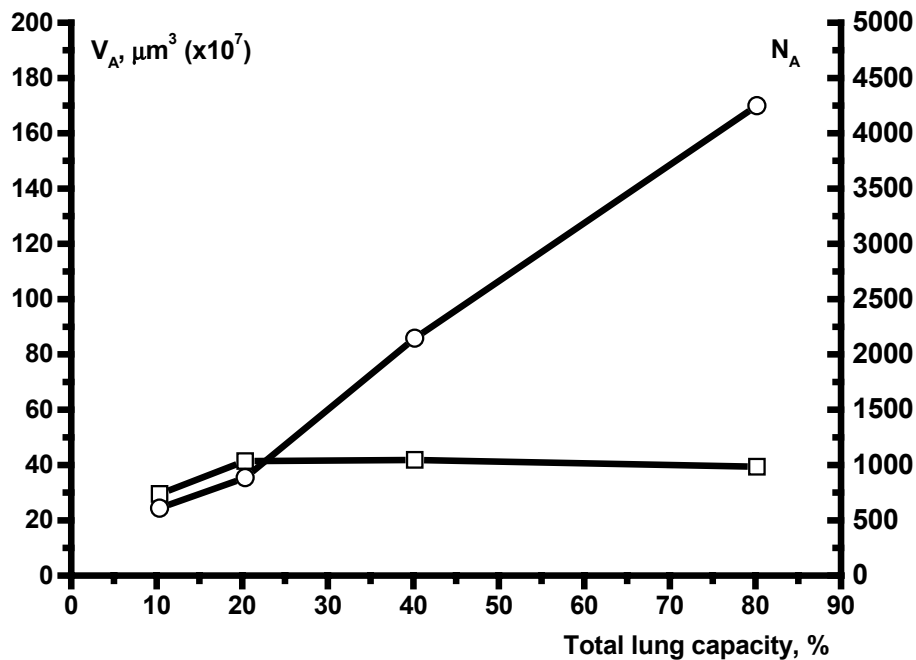


Figure 12. Volume increment during inflation. Increase in number/cm³ (N_A , open circles) and volume (V_A , open squares) of alveoli during inflation from residual volume to 80% of total lung capacity. V_A is minimal, whereas N_A is steadily increasing. Modified from Carney (39) with permission.

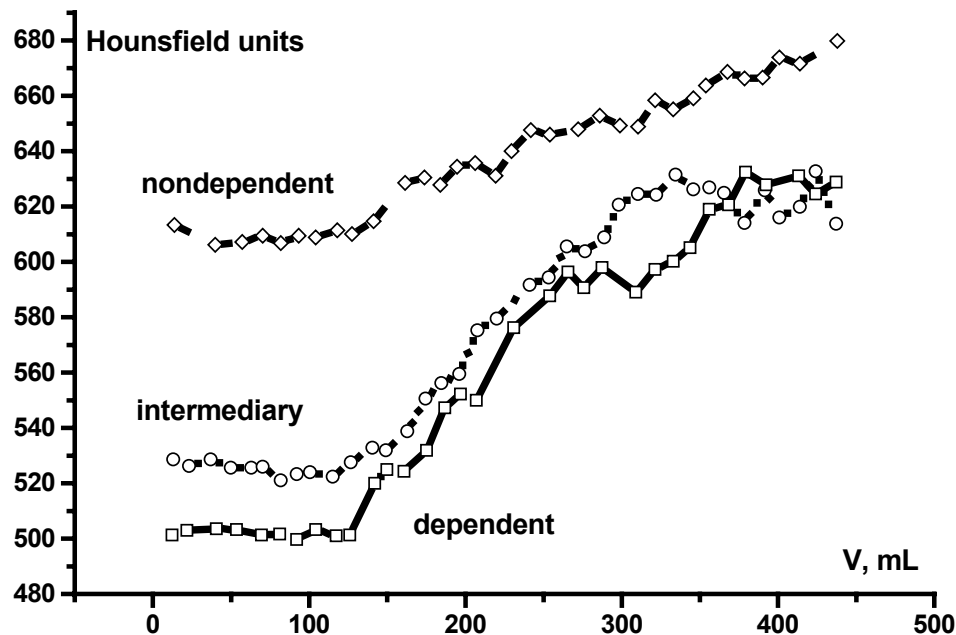


Figure 13. Three zone CT scan during volume increment. CT scan of near-diaphragmatic part of lung in a healthy pig. Densitometry was performed in three zones during insufflation of the lung: a dependent, an intermediary, and a non-dependent. The upper zone shows a linear increase in volume, whereas the lower two do not contribute to volume increment until a volume (and associated pressure) of app. 150 mL is reached, when they both contribute in an avalanche pattern of volume increment. The figure was kindly put at my disposal by Dr. Michael Lichtwarck-Aschoff.

The interpretation of the lower inflection point as a point of recruitment seems in need of a modification. Rather, recruitment is a pan-inspiratory process. Still, the segment between the LIP and the UIP is seen as representing a zone of optimal compliance within which ventilation should preferably occur (2, 124). The above discussion represents a modification of the *dictum* “open up the lung and keep it open” (106), as it seems as the lung is continuously “opened” through the whole inspiratory phase and not in an all-or-none fashion around the lower inflection point.

Methods for uncovering the P/V-relation

Since Asbaugh (5) described the syndrome of ARDS in 1967, the pressure/volume relationship in the respiratory system in ARDS patients has been analysed to assess respiratory mechanics and used as a tool for diagnosis (32), prognosis (62) and treatment (1, 56, 188). During the last 30 years, there has been a steady flow of articles in the scientific literature concerning various methods of tracing P/V-curves.

The following paragraphs are – with permission – modified from (95).

It has been assumed that the true values of the P/V relationship in the alveoli could only be obtained during static/semistatic conditions, i.e. no flow/low flow conditions, because of confounding factors complicating measurements under dynamic conditions caused by (46):

- friction along the endotracheal tube, airways and lung and chest wall tissues affecting flow (viscous forces);
- elastic forces within the lung and chest wall (elastic forces);
- stress adaptation units within lung and chest wall tissues (viscoelastic forces);
- inertial forces at the start of inspiration and expiration;
- compressibility of thoracic gas;
- inhomogeneity within the respiratory system; and
- distortion of the respiratory system from the configuration during muscle relaxation (e.g. high intra-abdominal pressure).

The first three factors are supposed to be those that provide the most important opposing forces against flow. These factors are also considered to be flow, volume and fre-

quency dependent (20, 21, 47, 55, 152, 174). They all have a systemic basis and may be fitted into a physiological model, see below.

The interventional approach may conveniently be divided into

- Dynamic methods
- Static or semistatic methods
- Constant flow methods
- Constant pressure methods

The methods rely on the ventilator-treated patient being sedated and muscle relaxed.

Dynamic methods

The pulse method

The pulse method was proposed by Surratt (187). This method is based on the assumption that when inspiratory flow is constant during passive inflation of the relaxed respiratory system, the rate of change of airway pressure is related to the compliance of the respiratory system. An upward displacement of the curve would therefore be a sign of increase in compliance and indicate recruitment while a downward deflection would be a sign of decreased compliance and indicate overdistension. A group led by Barnas has developed a system depending on an external computer to drive a ventilator to produce a *quasi-sinusoidal flow pattern* and collect data at eight combinations of frequency and tidal volume using a simplified Fourier transformation for analysis (70).

Ranieri, stress index

Ranieri (158), extending his findings in static respiratory P/V curves at conventional (high V_T) at ZEEP vs low V_T at PEEP 10 cm H₂O and comparison of static vs dynamic compliance (156, 157), documented the use of the “stress index” looking at the contour of the inspiratory *pulmonary* pressure trace, P_L , during constant flow ventilation in an *ex vivo* animal model. The rat lungs were ventilated in one of three modes:

- (i) low volume, stress: low volume (V_T 7.3 mL/kg), low PEEP (3.9 cm H₂O),
- (ii) minimal stress: low volume (V_T 7.5 mL/kg), high PEEP (14.9 cm H₂O), and
- (iii) high volume, stress: high volume (V_T 16 mL/kg), high PEEP (20.6 cm H₂O).

The P_L/t curve during inspiration was fitted to a power function: $P_L = \alpha \times t^b + c$, 'α' being slope of curve, 'c' offset at $t = 0$. The coefficient 'b' mirrored the shape (upward convexity: $b < 1$, straight: $b = 1$, downward convexity: $b > 1$) of the P_L/t curve. Values of $b < 0.9$ and > 1.1 were significantly correlated with a U-formed distribution of the concentrations of cytokines, TNF-α, IL-6, and MIP-2 as well as clinical lung injury scores. This method implies the assumption of constant resistance and influence of viscoelastic elements during constant flow inflation. The stress index concept seems a readily applied practical tool in setting the ventilator, but has so far been validated only in an animal model of VILI.

These dynamic measurements will be influenced to some extent by both viscous and elastic properties of the respiratory system and are time-consuming, as they require several study breaths at each level to obtain data. The method is furthermore restricted to VCV and includes the assumption of constant resistance during inspiration.

Static and semistatic methods

The super syringe method

The super syringe method has generally been considered as gold standard for measuring static P/V-curves (113). It makes use of a 1.5-2 L syringe which is used to inflate and deflate the lungs stepwise with 100 mL aliquots with a 2-3 sec pause at each step (34). The method has several drawbacks. The volume history of the lungs must be standardised before using the super syringe with several large breaths from the ventilator and the patient must be disconnected from the ventilator. The super syringe manoeuvre takes between 30 and 90 seconds and gas exchange during the manoeuvre,

gas decompression and temperature and humidity changes of the inspired gas will cause artefacts (34, 45, 61). The method is time-consuming and potentially dangerous to the patient.

Flow interruption during a single breath

The flow interrupter technique during constant flow inflation, from zero end expiratory pressure, is a combination of the interrupter and elastic subtraction methods proposed by von Neergaard and Wirz to measure airway resistance (133, 135). It was further developed by Gottfried (69) to measure respiratory mechanics using a pneumatically operated valve to produce a series of rapid occlusions (0.2 s) either during passive deflation following end-inspiratory occlusion or during both inspiration and expiration (67, 68). Most patients studied with this method have shown a linear P/V relationship and it has never been used clinically, probably because of its additional equipment requirements (34). Furthermore, it is doubtful whether frequency-dependent viscoelastic forces are brought to rest in 0.2 seconds.

Multiple occlusions at different tidal volumes

These methods are based on a large number of interrupted breaths at different tidal volumes during constant inspiratory flow from zero end expiratory pressure, and usually during both inspiration and expiration, each interruption yielding a point on the static P/V-curve. The first method was described by Levy in 1989 (110) but it has been refined over the years (30, 91, 190). In its later version, it uses an external device to override the frequency set by the ventilator to keep constant inspiratory flow at different volumes, and predefines the volume history and distribution of points on the pressure/volume curve. About 20 study breaths are sampled with at least three normal breaths between each (to stabilise the lung volume history) and occlusions are performed during both inspiration and expiration. Servillo (171) recently published a study using this method and concluded that it was safe, easy and rapidly performed.

A similar method has been described by Sydow (192) where a pneumatic valve, automatically controlled by a computer, was used to achieve repeated inspiratory and expiratory occlusions lasting six seconds. Two normal breaths were interspersed between each study breath. The authors used the super syringe technique as a reference and found substantial differences in the static P/V-curves produced by the two methods. The occlusion method showed no hysteresis and very few inflection points were identified even in patients with severe ALI. The super syringe method showed hysteresis even if corrected for gas exchange, temperature, and humidity. The authors suggested that the correction factors were insufficient and the volume cumulative super syringe method altered the lung volume history at each step while the occlusion method gave measurement points independent of each other.

The PEEP-wave technique

The PEEP-wave technique was proposed by Putensen (153) and is based on calculation of static compliance after tracing the difference in expiratory volumes before and after a PEEP change. A similar method was used by Valta (198), who calculated static compliance at different PEEP levels and followed changes in lung volume by respiratory inductive plethysmography, RIP.

These methods or similar ones have been used by many authors in studies (2, 58, 156, 157) and as reference methods (113, 159, 173). They are seldom used clinically though they avoid the problem of disconnection and gas exchange inherent in the super syringe method. This is probably because they are time-consuming with respect to both data recording and analysis, they are technically complex, and they require substantial additional equipment to perform the procedure. They also require standardisation of the volume history of the lung between study breaths. The number of normal

breaths between study breaths has varied from one study to the next (58, 69, 91, 110, 113, 156, 159, 173) and sometimes the number is not reported.

Constant flow inflation

In order to avoid the need of intermittent airway occlusions, minimise the influence of airway resistance, and increase the speed of analysis, constant *low flow* inflation methods have been proposed.

Low flow inflation

To minimise the effect of viscous resistance, Mankikian (120) used the *very low constant inspiratory flow* of 1.7 L/min and allowed deflation to occur passively at a controlled constant flow. He compared this method with the super syringe method and concluded that they produced identical P/V-curves. As the super syringe method was not corrected for gas exchange, the flow used has probably been so low that continuous gas exchange caused similar artefacts in both methods (93).

The past few years have seen the publication of several articles concerning low flow inflation using different flow velocities. They all try to identify a clinically applicable “single breath” method that can be used to analyse respiratory mechanics instead of the time-consuming static occlusion methods. For this purpose, commercially available ventilators with varying amounts of sophisticated extra equipment have been used. In 1997, Servillo (173) introduced the *automatic low flow inflation* (ALFI) method using an external computer to control the ventilator to give a flow velocity of 15 L/min. The in vitro determined endotracheal tube resistance was subtracted, as was the airway resistance determined previously from a normal breath (calculated as the ratio between the area of the pressure volume loop and the area of the flow volume loop according to Varène (199)). The authors used the static occlusion method as reference and found good agreement except at high volumes, where the ALFI curve

showed less compliance. Recently Servillo and colleagues have demonstrated that the low flow and occlusion technique result in identical values for UIP (172). In 1999 Lu (113) presented P/V-curves obtained with flows of 3 and 9 L/min and used the inflation limb of the super syringe and the static occlusion method as reference. Because of technical limitations of the ventilator, the tidal volumes were 500 mL with 3 L/min and 1500 mL with 9 L/min. The authors concluded that the reference methods and 3 L/min flow P/V-curves were identical while the 9 L/min flow curves were affected by resistance and shifted to the right but to a degree that was not clinically relevant. No correction factors were used. Rodriguez (159) also published a study in 1999 using a flow velocity of 7 L/min and a tidal volume of 1100 mL and used the static occlusion method as a reference. They concluded that the curves obtained with the two methods were similar.

The correct flow rate for low flow inflation is difficult to determine. If the flow rate is too low, the P/V-curve will be affected by continuous gas exchange and if the flow rate is too high it will be affected by the resistive components of the endotracheal tube and conducting airways, necessitating a number of correction factors, which will introduce uncertainties of their own. If the ventilator is not able to provide constant flow from the very beginning of inspiration, it will affect the initial part of the P/V-curve, showing a lower compliance.

The normal flow range methods are not considered reliable, because of the effect of resistance. None of the static or semistatic methods have come into routine clinical use, even though the basic techniques have been known for over two decades. This has primarily been blamed on the slowness and inconvenience of the methods, but also on their requiring additional technical equipment both for data sampling and for analysis. In recent papers, an effort has been made to simplify the technological part and/or make the analysis faster. The quickest analysis with the low flow inflation

technique is reported to be about 2 minutes (113), and with the static occlusion method about 10 minutes (171).

None of the static/semistatic methods can be used to perform continuous monitoring of respiratory mechanics. They are all intermittent and require interruption of the on-going ventilator treatment and replacing it with a special state of flow, i.e. no flow, low flow, or sinusoidal flow that is never encountered during normal breathing or during normal ventilator treatment. These static or semistatic measurements are then used to try to predict the behaviour of the respiratory system during dynamic conditions.

When collecting data with the static occlusion method, a standardised lung volume history is necessary so that the results will not be affected, as has been shown with changes in low flow P/V-curves after recruitment manoeuvres (191). These methods therefore do not reflect the “only true” P/V-relationship in the respiratory system, as it will vary with different ventilator settings and recruitment. Neither is it clear what information *static/semistatic* methods provide for the description of a *dynamic* system, where compliance and resistance are considered to depend on volume, flow velocity and respiratory rate (20, 21, 47, 55, 152, 174). It seems, in a way, inappropriate to evaluate a dynamic system only with static/semistatic methods. It would also be of major value to be able to follow on-line, at the bedside, what happens with respiratory mechanics when ventilator settings are changed.

Slow pressure ramp technique, SPRT

Instead of using low flow inflation, the use of a slowly increasing pressure ramp has been suggested, e.g. 3 cm H₂O/s for 10 seconds. If this results in a volume of 1.2 L, flow *on an average* amounts to 7.2 L/min, which qualifies as a low flow inflation (LFI). The method was introduced by Newman (138). In the commercially available version of the SPRT (P/V tool in Galileo Gold Ventilator, HAMILTON MEDICAL AG, Rhaezuens, Switzerland), an initial PEEP release is performed before the pressure

ramp is applied. The P/V curve is updated continuously during this manoeuvre and the curve is analysed by placing two cursors delimiting the mid portion of the P/V curve from which compliance is calculated. The cursors typically may be placed at the lower and upper inflection points – if present. The method has not been validated, but is at present being applied in clinical investigations (May 2002). According to personal communication (Josef Brunner), the method yields results equivalent to the LFI method.

As with LFI, similar objections may be raised: the result is dependent on choice of pressure ramp – a slowly increasing pressure ramp implies a lower flow and thus fewer contributions to flow resistive pressure as the pressure ramp must counter compliance as well as resistance. Furthermore, as flow is not inherently constant, it may vary owing to the ramp contributing to varying values of compliance, and may thus induce varying contributions to overcome resistance. The idea of applying a pressure ramp is reminiscent of the Suki “volume avalanche” (186) concept and the P/V tool may open up to the perspective of “fractal volume increment” during ventilation.

Computational approaches to respiratory mechanics

The interventional approach focuses on

- the characterization of the viscous pressure reduction due to airway dimensions, geometry, and gas composition in terms of density and viscosity;
- the static and dynamic aspects of elasticity of lung and chest wall; and
- the inertial forces coming into play at frequencies in the range 60/min and upward.

In contrast, the computational approach aims at fitting values of the variable impedances of elasticity, resistance, inertance, and viscoelasticity in a formulation of the equation of motion minimising the squared differences between measured and calculated values. This is performed by multiple linear regression, MLR. Ideally, there should exist a one-to-one correlation between the components of the mechanical model, the formulation of the equation of motion, and the anatomical structures of the

lung. The choice of version of the equation of motion depends on the sophistication and preferences of the investigator, the purpose of modelling, and the access to and magnitude of computer processing facilities. The descriptive power of the model must be weighed against its predictive power and simplicity. This trade-off will become obvious in the following.

Rohrer one-compartment lung model, 1915

A one-compartment model of the respiratory system consists of two components: a conductive, resistive system of one tube and a distensible, non-hysteretic elastic container shown in Figure 14 together with its rheological representation.

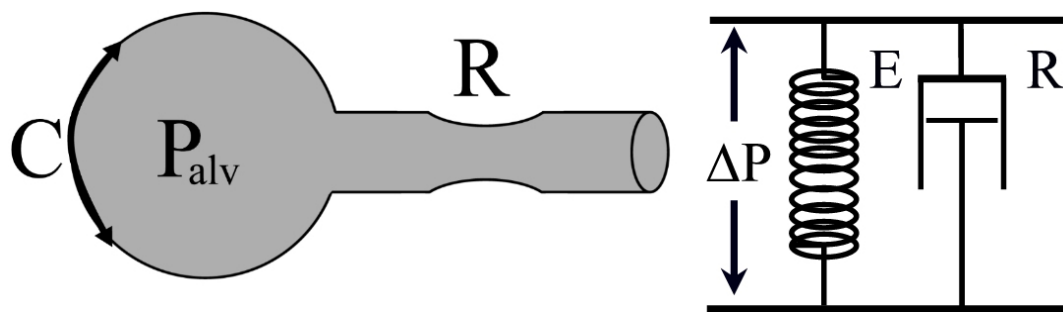


Figure 14. Voigt body consisting of spring and dashpot representing flow resistance and elasticity of the lungs.

The relationship between flow and the pressure difference during filling and emptying the container is formulated in the *equation of motion*:

$$(xx) \Delta P = EV(t) + \delta V / \delta t \times R, \text{ cf. p. 13.}$$

This equation is the basis of multiple linear regression, cf. p. 52.

Bates, linear viscoelastic lung model 1955

Although attractive, the linear, single-compartment model cannot explain certain mechanical phenomena presented by the respiratory system, such as:

- the slow decay in pressure observed after an end-inspiratory occlusion;

- the double-exponential profile of expiratory pressure and volume;
- the frequency dependence of resistance and elastance in RR 1-120; and
- the quasi-static pressure/volume hysteresis in isolated lungs.

These phenomena have been ascribed to ventilation heterogeneity, *Pendelluft*, and/or viscoelasticity. Thus D'Angelo (47) demonstrated that the additional resistance during end-inspiratory pause decreased as flow increased or - correspondingly - T_I decreased, and that ΔR_{rs} increased as volume increased at constant T_I .

Based on the work of Mount (130), Bates and associates (for a review see (23)) proposed a model capable of describing these four characteristics of pulmonary mechanics. The model is extended by the inclusion of a series-coupled spring and dashpot, a Maxwell body, in parallel with the spring of the two-component model: this assembly of a spring and a Maxwell body is termed a **Kelvin body** (Figure 15).

During inspiration, increasing pressure and volume expand the spring of the Maxwell body simultaneous with the dissipation of energy into the dashpot.

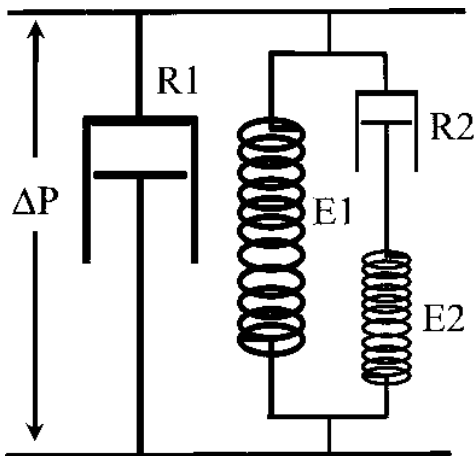


Figure 15. Kelvin body is the base of the Bates' model. In the original version, one Kelvin body accounted for the lung and another in parallel for the chest wall.

Intuitively, one may appreciate that with increasing frequency, $E2$ will not have the time necessary for dissipating its energy into $R2$, and total resistance will diminish. During expiration, the springs $E1$ and $E2$ dissipate their energy into the $R1$ and $R2$ in an exponential decay. By lowering frequency, the $E2$ will have plenty of time for dissipation, and total resistance will go up. This is demonstrated in the following Figure 16 and Figure 17, based on (126). The model was “ventilated” with a sinusoidal pres-

sure signal and the viscoelastic resistance and elastance were calculated (see APPENDIX). Using values for R_{aw} , R_2 , E_1 , and E_2 according to D'Angelo (48), Figure 16 and Figure 17 can be constructed.

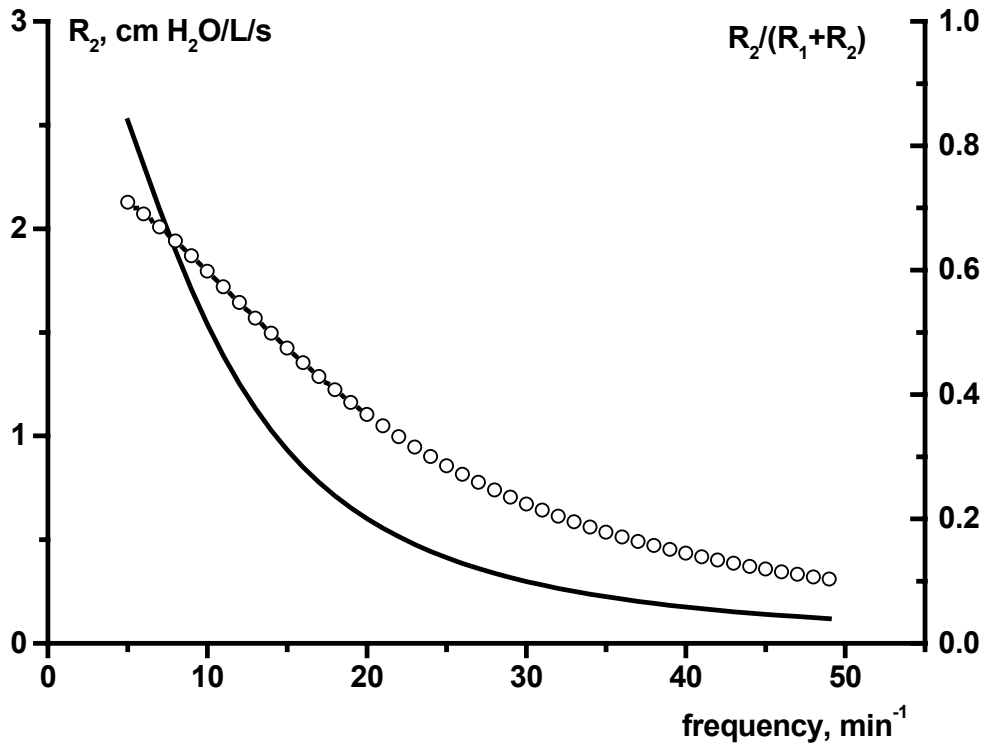


Figure 16. Resistance as function of frequency in Bates' viscoelastic model. Tissue resistance, R_2 (Y1 axis, full line), as a function of respiratory frequency in Bates' viscoelastic model, using values and equations indicated above. Note that tissue resistance diminishes with increasing frequency, but that the tissue resistance makes up approximately one third to one half of total resistance at normal frequency (Y2 axis, circled line). The figure is based on Milic-Emili (126).

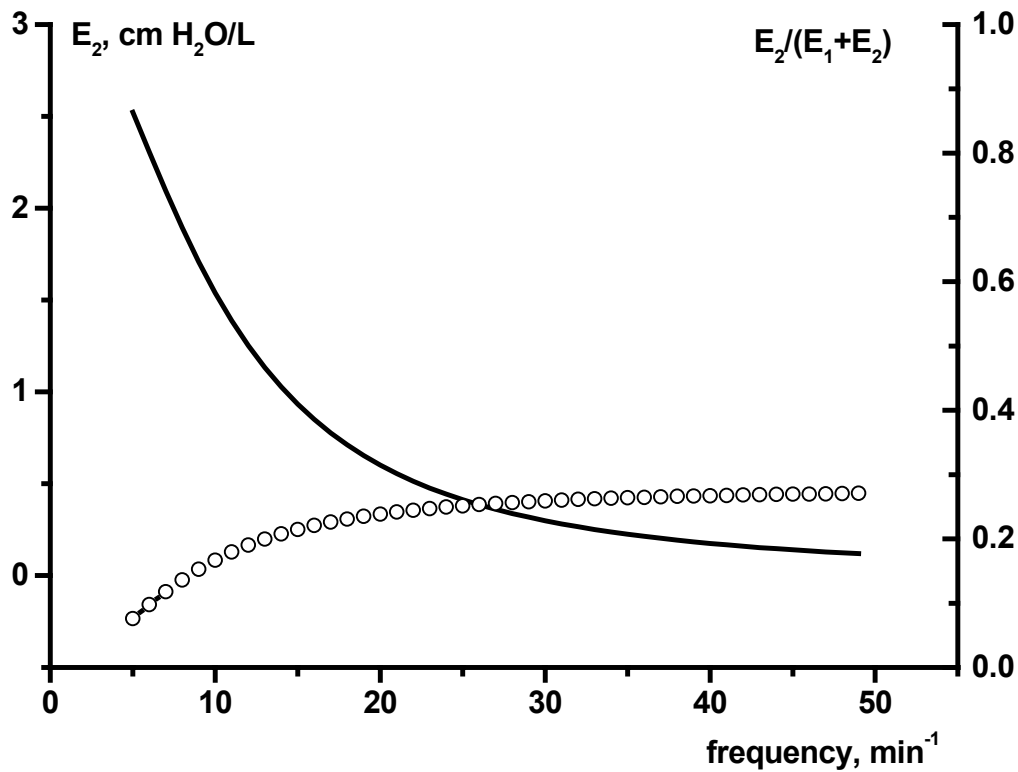


Figure 17. Elastance as function of frequency in Bates' viscoelastic model. Tissue elastance, E_2 (Y1 axis, full line), as a function of respiratory frequency in Bates' viscoelastic model, using values and equations indicated above. Note that tissue elastance diminishes with increasing frequency, but that the tissue elastance makes up approximately one fourth of total elastance at normal frequency (Y2 axis, circled line). The figure is based on Milic-Emili (126).

Otis, linear serial two-component lung model 1956

In order to account for these observations (heterogeneity, *Pendelluft* and viscoelasticity), Otis (141) thoroughly investigated experimentally and clinically the behaviour of a parallel system of two *linear* Voigt bodies (Figure 18) under the assumption of negligible inertance using sinusoidal flow and pressure signal. In the motion of equation, resistance is replaced by *effective* resistance, R_e , and compliance by *effective* compliance, C_e (see APPENDIX).

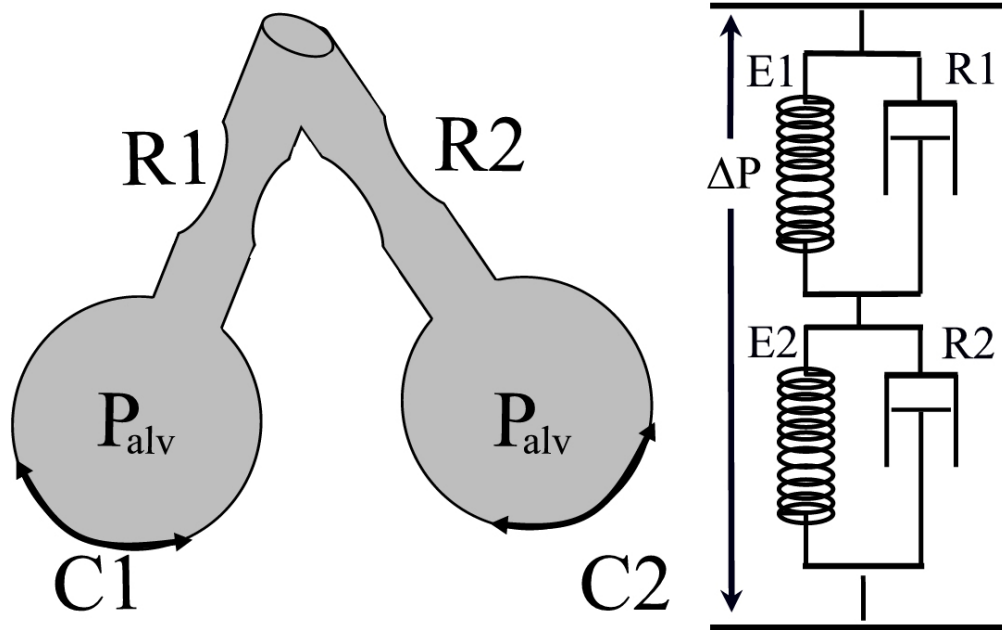


Figure 18. The Otis linear serial two-compartment model and its rheological representation (terminology is confusing: this model may be encountered as *parallel*, the term referring to its electrical representation).

Otis also demonstrated that resistance as well as compliance were frequency dependent. In a person with normal lungs, compliance was remarkably constant irrespective of breathing frequency, supposedly due to equal time constants of lung compartments. Challenging normal lungs with histamine, thus increasing resistance threefold, the frequency dependency was disclosed due to inequality of time constants as illustrated in the figure below.

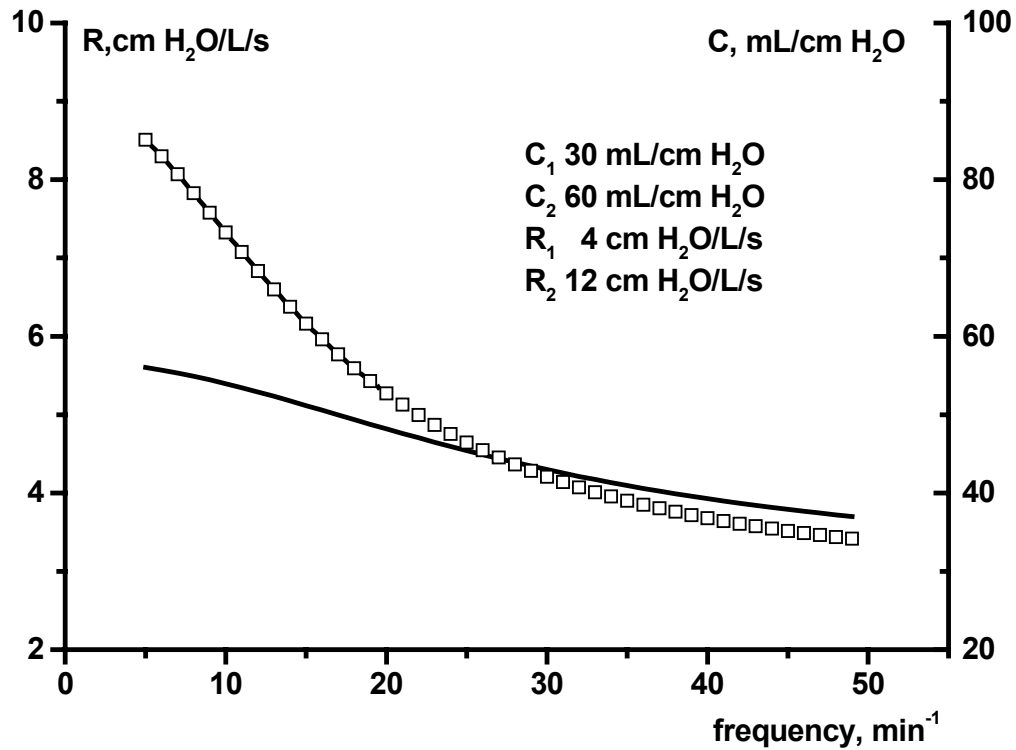


Figure 19. The Otis equation applied on two-compartment model. Otis parallel linear model with compliances and resistances of the two compartments as indicated. Effective resistance: full line, Y1-axis; effective compliance: squared line, Y2-axis. Notice frequency dependence of resistance and compliance. The figure is based on Otis (141).

Otis performed model and patient experiments with his parallel linear model and found very good correlations.

These components – Kelvin, Maxwell, Voight body, serial, parallel arrangements – can be multiplied in the models, and be assigned different threshold values, time constants, resistances, elastances, &c. in order to approximate the observations of respiratory mechanics made in experimental animals, in healthy subjects and patients. The anatomic correlates can be represented by collagen and elastin fibres interwoven with

cellular matrix and vascular structures in what has been termed the “integral fiber strand” (Weibel).

If reasonably easily accessible equations can be formulated for the various models, it will be equally easy to ascertain their descriptive performance in model and human investigations. The attraction of these models resides in the fact that they provide estimates of lung mechanical entities (R_1 , R_2 , E_1 , E_2) which may prove of importance in following the clinical course of a patient.

Multiple linear regression, MLR

The equation of motion

$$(xxi) \quad \Delta P = EV(t) + \delta V/\delta t \times R + \delta \dot{V}/\delta t \times I + PEEP$$

predicts that four elements enter into the calculation: a pressure to distend the container ($EV(t)$), a pressure to overcome friction in the single tube of the system when air is flowing ($\delta V/\delta t \times R$), a pressure related to the acceleration of air ($\delta \dot{V}/\delta t \times I$), and any pre-existing pressure in the lungs (PEEP). Further, it predicts that there exists a linear relationship between a constant E and $V(t)$, between $\delta V/\delta t (= \dot{V})$ and a constant R , as well as between $\delta \dot{V}/\delta t$ (acceleration) and a constant I . There is interdependency neither between E and $V(t)$, nor between $\delta V/\delta t$ and R , nor any relation to time, in the sense of “flow - ” or “volume history” of the system, apart from the temporal aspect of volume and flow, $\delta V/\delta t$. The model contains no predictions about frequency-related changes in E and R . A mechanical analogue consists of spring and a dashpot in parallel, a so-called Voigt body (Figure 14). The lung may be modelled as one-compartment with a single Voigt body or as two compartments, if the dynamics of the chest wall is included. The container may be seen as the total number of alveoli. This adds the assumption that pressure is equal and that elastance, E , is uniform in all alveoli. The tube may be seen as an ensemble of all bronchi and bronchioli. This adds an assumption of equal or singular resistance in the system. The term $(\delta \dot{V}/\delta t \times I)$ is usually omitted as inertance amounts to only a minor part of the total impedance of

the respiratory system at normal frequencies ($<60 \text{ min}^{-1}$). Recently, though, inertance has been reintroduced as a parameter of possible importance in the monitoring of the course of acute respiratory distress syndrome, see (103). This assembly of equations is solved by the statistical method of Multiple Linear Regression. In MLR, the constants E and R (and I, if included) are substituted so that the squared difference between calculated value and actual value of pressure is minimised. The method is also termed Least Square Fit-method (LSF or LSM).

The function of MLR is readily available in most statistical spreadsheet programmes. The MLR method was first used by Wald (204) and later by Uhl (197). It has gained an enormous spread and may be encountered in some variant in almost any work on respiratory mechanics. The equation may be duplicated, one accounting for inspiratory pressure, volume, and flow, the other accounting for expiratory pressure, volume, and flow in each sampling point. At each (sampling) point in the respiratory cycle the above equation accounts for the relationship between P, \dot{V} , and V. In parallel with measurements for “interventional” methods, MLR is preferably performed on a relaxed respiratory system without muscular effort, see Iotti (86).

In Table 1 the results of four investigations calculating resistance with the MLR are shown.

The Voigt body is viscoelastic, because it may store and dissipate energy, but it will not exhibit relaxation, gradual stress decrease against time, or the opposite, creep, the gradual decrease of lengthening against time at constant tension. Contemplating the intricate relationships between flow and pressure as well as volume and pressure described previously, it becomes hard to accept a linear relationship between variables and parameters; nor can the idea of a constant value of E and R for the whole cycle, or for inspiration and expiration separately, be readily accepted. In order to handle the nonlinearity of the \dot{V}/R - as well as the E/V-relationship, additional elements have been added to the equation either covering the whole cycle or the inspiratory and expiratory phases separately. This has been attempted in respiratory monitoring in adults

as well as in children in controlled and spontaneous ventilation, cf. (50, 94, 140, 148, 165, 200), thus

$$(xxii) \quad \Delta P = E \times V(t) + \delta V / \delta t \times R_1 + \delta V / \delta t \times \underline{\underline{R_2 \times V}} + P_0$$

- resistance varies linearly with volume.

$$(xxiii) \quad \Delta P = E_1 \times V(t) + \underline{\underline{E_2 \times (V(t))^2}} + \delta V / \delta t \times R + P_0$$

- elastance varies quadratically with volume.

$$(xxiv) \quad \Delta P = E \times V(t) + \delta V / \delta t \times R_1 + \underline{\underline{(\delta V / \delta t)^2 \times R_2}} + P_0$$

- resistance varies quadratically with flow

accounting for laminar and turbulent components of flow resistance, ad modum Rohrer (160). It becomes increasingly difficult to attach physiological correlates to each constant as their number increases in models incorporating nonlinear elements. Generally, these equations result in good correlation with measured pressures, slightly better the greater number of constants included in the equation, and notably so when resistance in contrast to elastance is varied with volume. The importance of this, however, seems to diminish with increasing PEEP in COPD patients, possibly indicating that flow restriction plays a diminishing role as airway calibre is increased by PEEP (200). This seems to be in concert with the demonstration of expiratory flow restriction being successful only when negative expiratory pressure is applied (105), either alone or in combination with bronchoconstrictive medication (201).

Table 1. Results of resistance calculations using MLR.

Reference	Equation	Subjects	R_I	R_E	$R_I:R_E$
Uhl (197)	Separate in- and exp. R and C, MLR	Six healthy spontaneously breathing	2.47	2.47	1:1
Officer (140)	E_{tot} , R_I , R_E in composite MLR (increasing R^2 with inclusion of nonlinear element in calculation of R_E).	Seven normal	1.36	1.87	1:1.4
		Seven asthmatic	3.08	3.67	1:1.2
		19 COPD	7.41	7.9	1:1.1
Mols (128)	MLR performed on six volume slices	16 ARDS patients	$R_I=R_E$ within volume slices.		
Peslin (148)	MLR on in- and exp. vectors separately (tube resistance excluded).	12 ALI patients, three combinations of end-inspiratory pause and PEEP	15.7	13.4	1:0.9
			14.0	17.8	1:1.3
			9.1	13.6	1:1.5

The Bertschman LOOP model 1990

Bertschmann and colleagues have presented another variation on MLR. In their first presentation(29), the authors utilised the vectors of *proximal* pressure, volume, and flow during the respiratory cycle in the MLR. In their second paper (75) the method was refined by excluding parts of the flow signal (and corresponding parts of volume and pressure vectors) from the calculation, viz. the parts showing very rapid changes or very low values: during inspiration 0-20%, 80-100% of flow samples, end-inspiratory pause and end-expiratory samples of less than 20 mL/s. The LOOP method calculates single values of compliance and resistance.

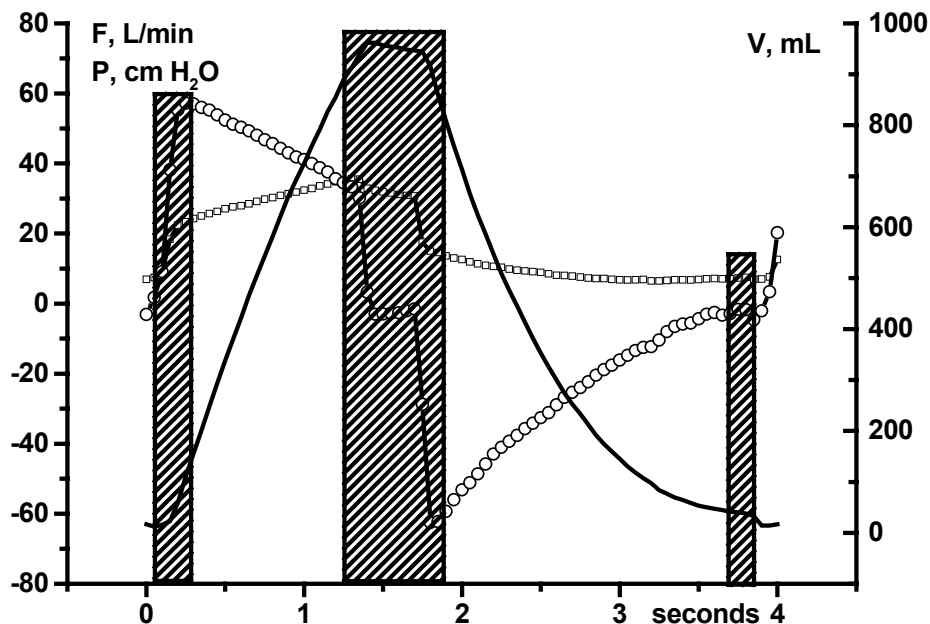


Figure 20. Vectors of pressure, volume, and flow vs time entering MLR in Bertschmann's LOOP concept demonstrated in recording from patient 3. Circled line: flow; squared line: pressure; full line: volume. Hatched areas denote parts of vectors excluded from multiple linear regression calculation of resistance and compliance. By definition - leaving out the nonlinear segments - it can account neither for these nor for the frequency-dependent element of viscoelasticity.

Using simulated respiratory data, Bertschmann and colleagues were able to show better congruence between data and recalculated values when excluding these three sections of the pressure, volume, and flow vector. I have compared calculation of alveolar pressure using this method (based on *distal pressures*) with MLR performed on inspiratory and expiratory vectors separately (I/E LSF) and with the DSA, cf. p. 82. The LOOP approach has later been superseded by the SLICE method.

The Guttman SLICE method 1994

The SLICE method was introduced in 1994 (73). It is based on a linear one-compartment model using *calculated tracheal* pressure (71), volume and flow and the equation of motion. The tidal volume is divided into six slices. In each slice pressure, volume and flow, representing inspiratory as well as expiratory values, are entered into a Least Square Fit algorithm producing *one* slice-resistance and *one* slice-compliance. The implicit assumption is that inspiratory and expiratory resistances as well as inspiratory and expiratory compliances are equal within each slice. In a lung model the SLICE method gave good correlation with measured values, and in patients, the SLICE method calculated dynamic end-inspiratory pressures from compliance values closely matching measured values. Later it was demonstrated that ARDS patients show different patterns of compliance through the range of tidal volume and not surprisingly the same could be found concerning resistance (127, 129). In the SLICE method the assumption of equal resistances is tacitly accepted and no discussion is found concerning its validity. The method is using calculated tracheal pressure. In adult as well as paediatric setting the calculation of tracheal pressure is very sensitive to the presence of secretion (102, 179), which will influence calculations unpredictably. It is an observandum that the SLICE method restricts the tidal volume excursion to six slices (in order to obtain acceptable number of measurements and signal/noise ratio for the MLR to function properly) – this implies that the slices may hide the position of inflection points, or force them to a position between slices.

Exponential decay

It is obvious that during mechanical ventilation *inflation* is active whereas *deflation* of the lungs is passive. During expiration the Voigt body demonstrates an exponential decay of pressure as the energy of the spring (distended lungs and chest wall) is dissipated into the resistance (bronchial tree and lung tissue), which is expressed in $P_{el} = -P_{res}$. This can be rewritten as

$$(xxv) \quad \frac{\delta V(t)}{\delta t} = \frac{E}{R} \times \delta t, \text{ which is integrated to}$$

$$(xxvi) \quad V(t) = A \times e^{-t/\tau_{rs}}$$

expressing that the volume vector is fitted to an exponentially decaying function of time with a specific time constant. The time constant, τ , of an exponential decay equals resistance multiplied by compliance. Note that it is the resistance and compliance of the *total* respiratory system including the tube, thus $1/C_{rs} = 1/C_{aw} + 1/C_{ETT}$ and $R_{rs} = R_{aw} + R_{ETT}$ and that the C_{aw} and R_{aw} may be composed of one or more alveolar components. Taking this into account, one may proceed to acknowledge that decay of viscoelastic pressure as well as pressure and volume during expiration in the Kelvin body (representing the pulmonary component to the exclusion of the ETT) may be better explained in terms of a biexponentially decaying function. During inflation, E_L is strained and its energy is dissipated into the dashpot continuously into the end-inspiratory pause, returning the E_L to its equilibrium length. During expiration, the E_L is compressed and, once again, it dissipates its energy into the dashpot accounting for the slow time constant of the biexponentially decaying function. This has been described by Chelucci (42, 43): he found a fast expiratory compartment with time constant of 0.35 - 0.50 sec corresponding to $\sim 80\%$ of V_T exhaled within one τ vs a slow compartment with a time constant of 3.3 - 4.7 seconds accounting for $\sim 20\%$ of V_T within one τ . The biexponential approach may solve some of the problems in mechanically ventilated patients with and without COPD as pointed out by Rossi and Polese (163), e.g. modifications in the viscoelastic properties of the respiratory tissues

due to the underlying disease and to the insertion of an end-inspiratory pause in the ventilator settings, and the nonlinearity of the resistance and gradual obstruction of the endotracheal tubes.

Nikischin, Mead and Whittenberger

Nikischin (139) has presented another approach in order to handle the nonlinearity of resistance and compliance. First, resistance is calculated at isovolume planes by a modification of the Mead and Whittenberger (123) method:

$$(xxvii) \quad R = (P_I - P_E) / (\dot{V}_I - |\dot{V}_E|)$$

This modified Mead and Whittenberger method of resistance calculation assumes equal in- and expiratory resistance at isovolume planes, whereas resistance according to the original method - as stated in the 1953 article – is calculated as $R_I = P_{insp} -$

$P_{elastic} / \dot{V}_I$ and $R_E = P_{exp} - P_{elastic} / \dot{V}_E$ at each isovolume plane. In their study, Mead and Whittenberger had a linear P/V relationship and did not find differences between in- and expiratory resistances at normal breathing frequency and tidal volume. In the Nikischin modification compliance is calculated in a second step according to:

$$(xxviii) \quad C = V / (P - (R \times \dot{V}))$$

As a corollary, inspiratory and expiratory compliances are equal as well, as pointed out by Muramatsu (131) in a commentary to Nikischin. By using this approach, Nikischin showed better congruence between measured and calculated proximal pressures in intubated paediatric patients than that obtained by using the MLR method. As will be evident below, the Nikischin approach is very similar to the dynostatic algorithm, and as such, it does not seem surprising that it works better than MLR.

Bates and Bijaoui, MLR and time dependency

Extending from Bates' viscoelastic model, Bijaoui (31) presented a method based on an equation including frequency dependency of viscoelastic elements (see APPENDIX).

The equation was applied as a *Recursive Least Squares* (RLS) procedure in a MatLab application on animal and model data showing inspiratory flow limitation (IFL). The RLS implies that the procedure continuously includes “new” and excludes “old” data, thus a memory function is introduced according to the proposal of Lauzon (108). The method was compared with a modification of the Mead and Whittenberger calculation of resistance. Mead and Whittenberger assumed a single value of elastance for the whole breath calculated from “no-flow” endpoints at start and end of inspiration before calculating R_I and R_E by subtracting elastic pressure ($E \times V$) from total pressure obtaining flow-resistive pressure, which was divided by flow. The identification of endpoints is precarious if flow is not reaching zero value. Bijaoui, therefore, introduced a calculation of a more “robust” value of elastance based on data from the whole respiratory cycle (see APPENDIX). Calculating the “robust” ($E \times V$), this elastic pressure is subtracted from total pressure, leaving flow-resistive pressure. Resistance over the cycle can then be calculated by dividing P_{res} with flow. Bijaoui compared resistance values at different IFL thresholds calculated by the RLS and the modified Mead and Whittenberger method and found them in good agreement. Her method of calculating elastance is reminiscent of the Varène method applied to resistance (199). The identification of IFL from variations of resistance through the breath turned out unconvincingly, which the authors ascribed to the fact that “R and E still varied somewhat without any IFL”. In this animal model with presumably constant elastance, RLS works as well as a modified Mead and Whittenberger method for calculating resistance. The Bijaoui approach is attractive because it incorporates a frequency- and time-dependent formulation of the equation of motion based on the Bates model with viscoelastic elements.

Inhomogeneous, nonlinear models

In a series of articles, Fredberg, Lutchen, and Suki have described their development and evaluation of nonlinear models of lung mechanics (59, 60, 116, 117, 118). In its latest version, the model comprises two “generations”: a single central airway and an

inhomogeneous, parallel assembly of pathways characterised by a distribution of resistances, inertances, tissue damping, and tissue elastances. This assembly is arranged in cascade with a polynomial nonlinear block. Exciting this model with an especially composed flow, the pressure response is registered as airway pressure. The computational challenge of this model lies in the “excavation” of best-fit values of the distribution of airway and tissue resistances and elastances as well as coefficients of the nonlinear polynomial block. In animal models with induced bronchoconstriction, calculations on the inhomogeneous nonlinear model gave the best fit compared with calculations on homogeneous (consisting of only a single set of airway resistance and elastance) linear and homogeneous nonlinear models.

Model simulations abound, but clinical studies are few, the clinical tools are complex and the computations even more so.

Fractal models of resistance, P/\dot{V} - and P/V -relationships

Recently a new approach to the analysis of biological phenomena in general and respiratory physiology in particular has emerged: fractal analysis. The concept of fractal geometry was developed by Mandelbrot (119) to quantitatively describe the random variations in size and shape seen in natural objects. It is still not decided what role and insights it provides for clinical respiratory monitoring, but as it seems very promising, it will be shortly mentioned. The bronchial geometry has been extensively described from a fractal point of view by (208) and (136) based on the studies of Weibel (207) and Raabe (154). West and Nelson have shown that the dimensions of the bronchial tree are better described by an inverse power law modulated by a harmonic frequency²

$$(xxix) \quad \overline{d(z)} = \frac{A_0 + A_1 \times \cos(2\pi \times \ln z / \ln \lambda)}{z^\mu}.$$

² The reader is referred to West: ”Beyond the principle of similitude...” I am indebted to Mats Larsson and Håkan Andreasson at the Centre for Applied Mathematics and Statistics, Chalmers University of Technology, Gothenburg, for trying to enlighten me on the rather complicated mathematics involved in the West exposition.

Displaying the generation, z vs diameter in a double logarithmic plot a.m. West shows excellent agreement between theoretical and actual measurements. This interpretation is in contrast to the ‘exponential decay’-description adopted by Rohrer (and Weibel) as their predicted diameter deviates increasingly from observed values from the 10th generation.

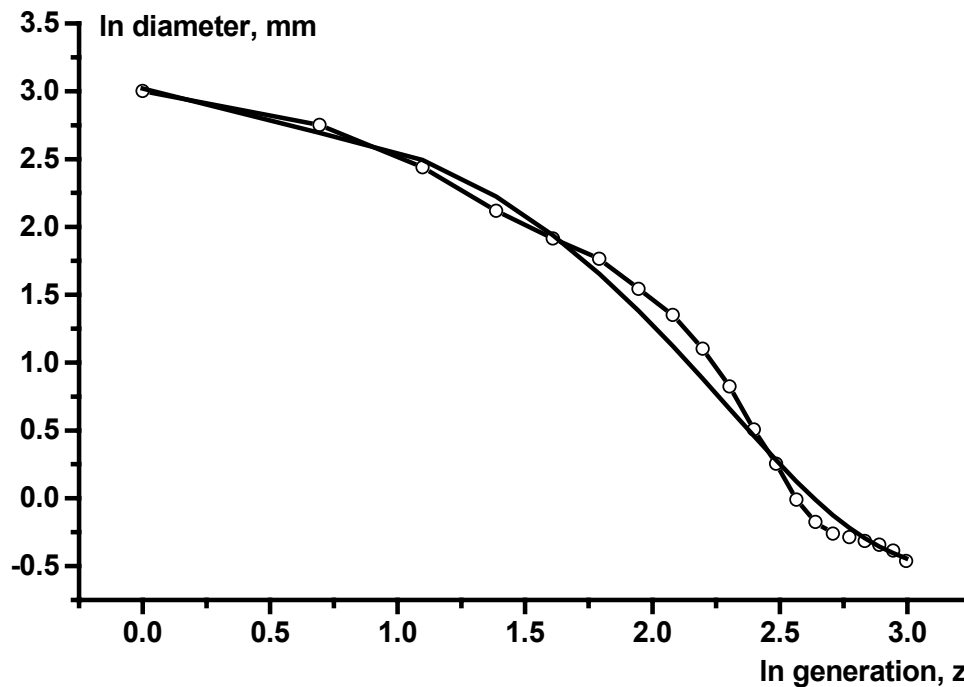


Figure 21. Generation in bronchial tree graphed vs diameter of bronchioles in a double logarithmic plot. Circled line: data from Raabe (154), full line: curve fit performed in TestPoint application according to the above equation (208). Regression coefficient 0.991 between original data and fitted curve; regression equation shows $\alpha = 1$, and constant = zero.

Suki (185, 186) measured resistance by oscillatory technique and catheters wedged in peripheral bronchioli during very, very low flow inflation. This was combined with a model of volume increment and a random distribution of threshold opening pressures in the bronchiolar system subserving alveolar compartments. He demonstrated the occurrence of “volume avalanches” as bronchiolar segments open up and described the

drop in resistance according to fractal properties. One objection is the extremely long and unphysiological inflation³. One may suspect that the spectacular result is confined to this specific experimental situation.

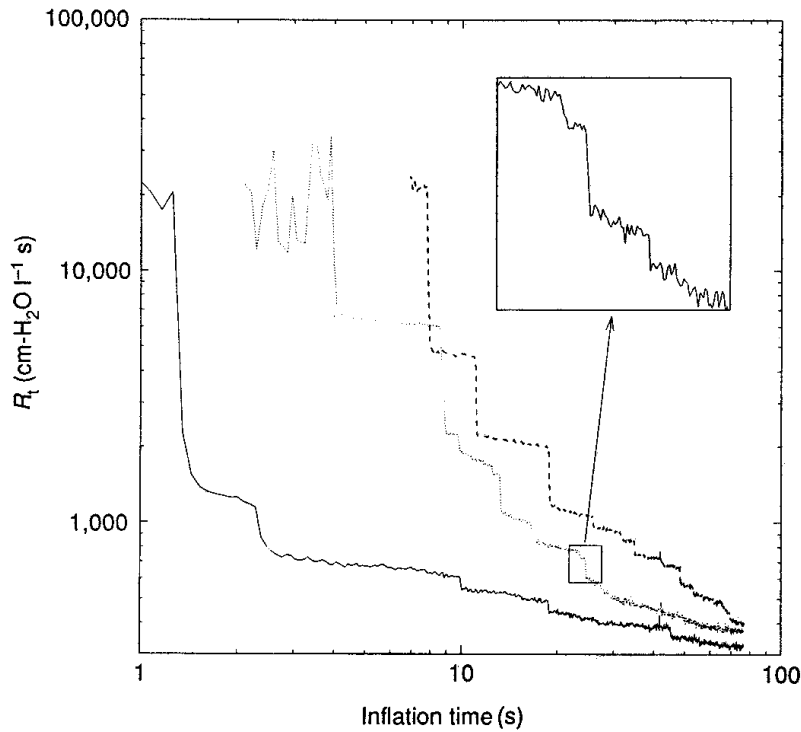


Figure 22. Suki demonstration of resistance avalanches. An animal lung was slowly inflated by applying negative pressure in a closed chamber. A long polyethylene catheter is wedged in a bronchiole. Resistance is measured by forced oscillation technique resulting in resistance decreasing in avalanches. These drops correspond to avalanche opening of groups of alveoli. Reproduced with permission from (186).

³ I know of no species in animal kingdom with a respiratory rate of 40/h. The physiological spectrum may be illustrated by the *mus musculus* (100-250 min⁻¹), the *macaque* (32-50/min) and the 60 tonnes sperm whale, *physeter macrocephalus*, with an RR of 6-7/min.

During the early phases of this study, I had occasion to measure tidal volumes in patients spontaneously breathing a mixture of either air or He/O₂. The distribution of tidal volumes – according to fractal analysis – showed a fractal “orderliness” in air-breathing *vs* a chaotic pattern when He/O₂ was used. One may hypothesize that control of tidal volume in some way is related to density mediated by flow or speed of distension of airways (unpublished observations). Similar observations are reported in (52, 184).

A very rich source of knowledge and examples is found in Bassingthwaite (22). Studies and findings derived from fractal analysis have provided important insights into pulmonary perfusion/ventilation (64, 65, 66) but have yet to be incorporated in clinical respiratory monitoring.

The equality of inspiratory and expiratory resistance is *the* central assumption of the DSA. It may therefore be worth devoting a few words to the

THE PROBLEM OF RESISTANCE

Δος μοι που στω την γην κινησω.

Give me a place to stand and I will move the Earth, Archimedes (287-212 BC).

The interventional approach

Airway resistance

The resistive components of the breathing circuit, the endotracheal tube, and respiratory system cause a variable distortion of dynamic airway pressure measurements, depending on the measurement site. When the pressure is measured at the Y-piece or ventilator, the endotracheal tube is the element causing the largest distortion in airway pressure measurements (72). Investigations have shown that this impedance is predictable and may be estimated with great accuracy as long as the tube is placed in a test bench; thus algorithms have been proposed for the calculation of tube resistance in adult sized (71) and paediatric dimensions of ETT (76, 196) based on the second order polynomial of Rohrer. Jarreau has presented a most elaborate algorithm (89) including length of tube, ID, curvature, flow, density and viscosity of gas mixture for calculation of impedance in paediatric tubes. Algorithms for the detection of secretions - slowly, but surely - obstructing the tube lumen have also been advanced (74). The problems of measuring airway pressure at the Y-piece or ventilator for the calculation of tracheal pressures can be avoided, though, by *direct measurement*. This can be accomplished by inserting a pressure line through the lumen of the endotracheal tube (71, 102, 134). However, it is not possible to measure pressure directly in the alveoli and there is no consensus about how to measure the pressure drop between the tip of the endotracheal tube and alveoli during inspiration and expiration in the intubated patient (in animal experimental set-ups the alveolar capsule technique has been employed (24, 59)). Many approaches, both interventional (upsetting ongoing ventila-

tion) and computational (with more or less palatable assumptions of resistance), have been used to estimate airway resistance but neither provides a clinically applicable 'gold standard' method for gauging inspiratory and expiratory resistances.

Classically, airway impedances have mainly been considered to be caused by a frictional component, in phase with flow, and an elastic component, in phase with volume. The frictional component is considered to occur between the tip of the endotracheal tube and alveoli owing to opposition to motion of air and tissue, and the elastic component between the alveoli and the pleural surface owing to tissue elastance. However, the bronchial tree does not behave as a rigid tube system and the pressure losses along the airway are therefore dependent on lung volume (33) and flow. They are also strongly influenced by the respiratory rate, cp. p. 46. This makes comparisons of resistance values difficult unless the volume and flow are standardised (20, 21, 47, 55, 152, 174). Airway resistance is a highly complicated component to describe (as detailed in the preceding paragraphs on pressure-flow relationship in the human airway) and using only a single value to describe the resistance behaviour of a whole breath or the inspiration and expiration separately is an unjustified simplification. Different approaches to obtain resistance calculations have been used in the literature.

Inspiratory resistance

The flow interrupter technique is the most common method used during constant flow inflation. After a very rapid occlusion, the airway pressure drops instantly from a maximum followed by a slower decay to a plateau. The rapid pressure drop to an intermediary P_1 is considered mainly to represent airway resistance and the slower decay is ascribed to tissue viscoelasticity, Pendelluft, serial or parallel inhomogeneities. By dividing the pressure differences ($P_{\max} - P_{\text{plat}}$) by the preceding constant, the airway, $R_{rs, \max}$ (airway + viscoelastic resistance), is calculated. The difference

$(P_{\max} - P_1)$ divided by flow results in $R_{rs,\min}$ (airway resistance). The drop from P_1 to P_{plat} enters the calculation of the additional resistance ΔR_{rs} , the measurements are illustrated in Figure 23.

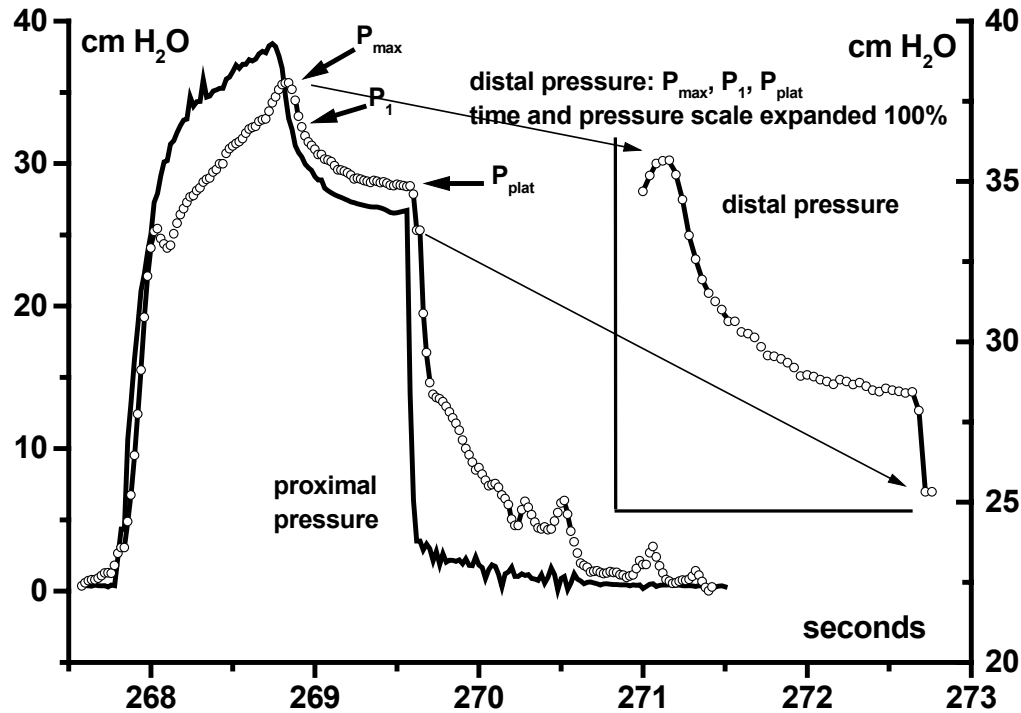


Figure 23. Recording of proximal and distal (tracheal) pressure in patient 5. Proximal pressure: full line; tracheal pressure: circled line, VCV (constant flow) demonstrating P_{\max} , P_1 and P_{plat} entering calculations of $R_{\max,rs} = (P_{\max} - P_{\text{plat}}) / \dot{V}_{\text{insp}}$, $R_{\min,rs} = (P_{\max} - P_1) / \dot{V}_{\text{insp}}$, and $\Delta R_{rs} = R_{\max,rs} - R_{\min,rs}$. Note that P_1 is not clearly defined in proximal and distal pressure recordings and may only - in this tracing - be identified artificially. Not even enlarging the pressure vector of interest (insert) purports any better possibility of identification of P_1 .

If oesophageal pressure is measured simultaneously, as a substitute for pleural pressure, the lung and chest wall resistances may be partitioned. The closing time of the ventilator valve has to be sufficiently rapid so that flow will cease almost immediately (133). Pesenti has presented data on $R_{rs,\max}$, $R_{rs,\min}$ and ΔR_{rs} in normal subjects, COPD

and ARDS patients at different PEEP levels (147) during inspiration and expiration. His results are shown graphically in Figure 24.

Expiratory resistance

Flow interruption is also used during expiration. The flow is passive, however, and therefore decelerating and the resistance calculated only represents the resistance at the point of occlusion (164). Airway pressure rises rapidly after occlusion followed by a slow increase representing viscoelastic components.

The passive exhalation time constant method assumes the respiratory system to behave as a single or double compartment. The exhalation time course of lung volume above resting volume is fitted by a first or second-degree exponential equation. Its time constants, τ , i.e. the product of resistance and compliance, represent the time needed to exhale 63% of lung volume above resting volume (133). The method has some drawbacks, as mentioned p. 58.

The results of measuring resistances by interrupter technique and a.m. Comroe are shown in Figure 24. For comparison, mid-inspiratory and mid-expiratory resistances in ventilator-treated patients, also measured with the interrupter technique, have been shown to be 2 and 2.2 cm H₂O/L/s respectively (ratio 1:1.1) in patients with normal lung function, 3.4 and 3 cm H₂O/L/s respectively (ratio 1:0.9) in patients with ARDS and 20 and 50 cm H₂O/L/s respectively (ratio 1:2.5) in patients with COPD (30, 91).

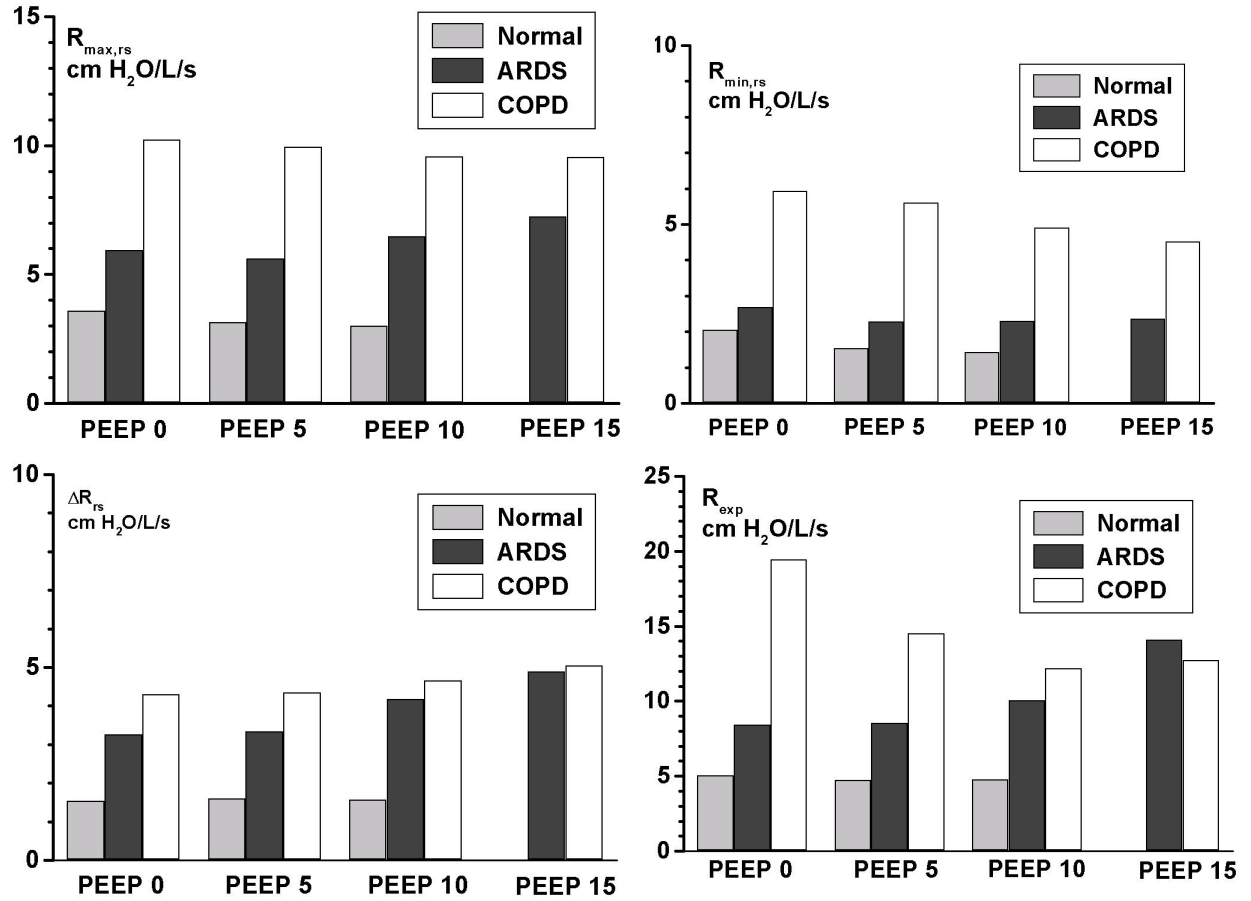


Figure 24. Pesenti presentation of resistance measures. $R_{\max,rs}$, $R_{\min,rs}$, ΔR_{rs} , and R_{exp} for three groups, normal subjects, ARDS, and COPD patients at PEEP levels 0, 5, 10, and 15 cm H₂O. Inspiratory resistance components were measured by the end-inspiratory occlusion method to the exclusion of tube and ventilator circuit. Expiratory resistance was calculated according to Comroe: estimating alveolar pressure from $V_{0.5exp}/C$, subtracting this value from tracheal pressure, thus obtaining flow resistive pressure and dividing this by flow at $V_{0.5}$. In ARDS inspiratory resistance increases due to increase in ΔR_{rs} with increasing PEEP, whereas in COPD airway resistance diminishes with increasing PEEP owing to dilatation of airways. Using these methods R_I and R_E are within the same range and comparable, apart from R_E at PEEP 0 in COPD, but PEEP 0 cannot be considered “state of the art”. The figure is based on resistance values reported in Pesenti (147).

The computational approach

The interventional methods depend on an inspiratory square-wave flow curve and an end-inspiratory pause. The MLR approach is independent of ventilation mode. Basically, it entails one value of resistance within the subvector being entered into calculation. If P-, V-, \dot{V} -vectors of a *whole* breath is utilised, the resistance value will cover the *whole* cycle. If the cycle is broken down in inspiratory and expiratory vectors, two values, R_I and R_E , are calculated. The principle is illustrated in Figure 25. The inspiratory and expiratory vectors may be further subdivided and subjected to MLR. Inspiratory and expiratory isovolume subvectors may be entered, and it may be possible to enter isovolume singular P-, V-, \dot{V} -values from 10-20 consecutive breaths.

A number of other approaches have been proposed. Some of them calculate inspiratory resistance; some expiratory resistance, and some calculate a combination of inspiratory and expiratory resistances, but none has acquired wider acceptance, and no further mention is made. The reader is referred to Table 2 and (79).

Resistance calculation a.m.	Equation
Neergaard (135)	$R = (P_m - PEEP) - ([V_m/C]) / \dot{V}_I$
Krieger	$R = (P_I - P_E) / (\dot{V}_I + \dot{V}_E)$
Bergman (26)	$R = \tau / (V_T / [P_{plat} - PEEP])$
Comroe	$R = (V_{0.5}/C) / (\dot{V}_{0.5})$
Suter	$R = (P_{max} - P_{plat}) / \dot{V}_I$
Jonson	$R = \Delta P / \dot{V}_E$

Table 2. Six methods for calculation of resistance.

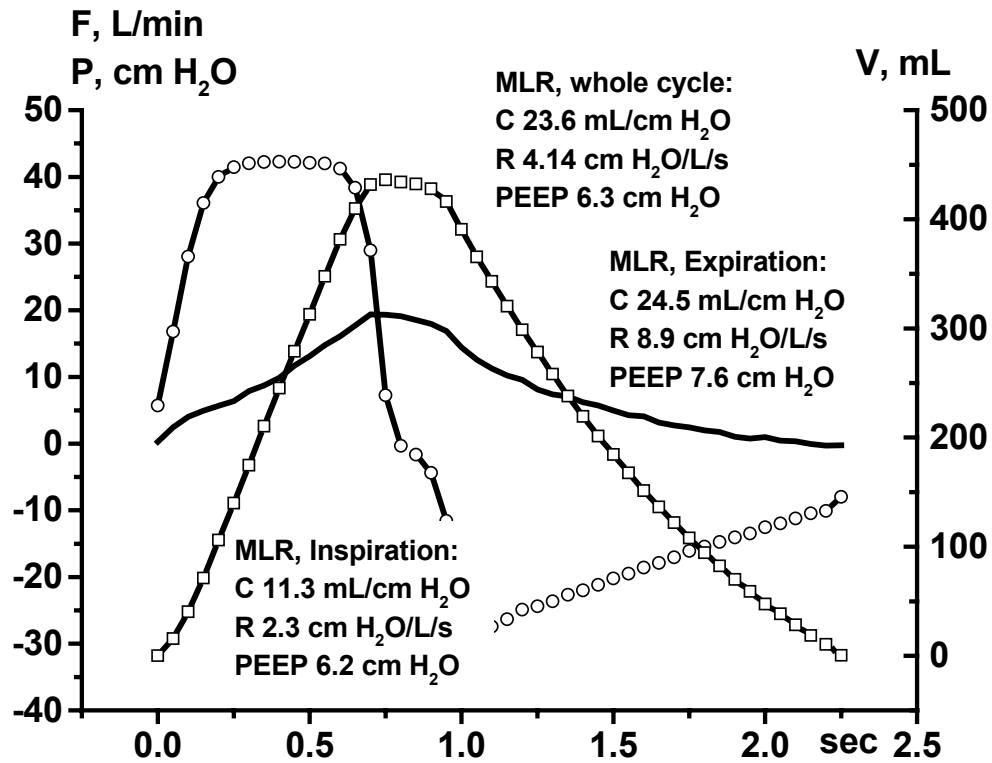


Figure 25. Recording from patient showing resistances and compliances derived from MLR to the exclusion of inertance. Circled line: flow; squared line: volume; black line: transpulmonary pressure. A mean value of ten cycles was calculated for *transpulmonary* pressure (tracheal-oesophageal pressure), volume, and flow during VCV. Note that this approach entails the assumption of one-valued compliance and resistance for the range of calculation: inspiratory, expiratory or complete breath and that in this example only the PEEP values are comparable.

“HAT ES EINEN ZWECK?”⁴

After revelling in the computational exercises, one may ask “hat es ein Zweck?” The different methods for calculation of resistances arrive at differing results, which also seems to be the conclusion in reviews on this topic: “The results are dependent on method used”. The consensus seems to be as evanescent as its subject. Concerning MLR, the analysis must be based on a reasonable model of lung mechanics. It must contain constants and relations that provide results making sense physiologically and pathophysiologically speaking, showing reasonable trends useful for clinical *jugement* and planning of therapy. The primary aim, though, of the majority of investigations using MLR has been to *reproduce* the proximal pressure signal, whatever model chosen. It does seem futile, however, to discuss an equation that will only *duplicate* what is already measured, instead of using data to calculate variables that are not accessible to measurement – e.g. alveolar pressure.

The ultimate aim of studying lung mechanics by testing *in vivo* and *in vitro* models of varying complexity must be to gain a better understanding of disease processes and the intensivist’s therapeutical possibilities to intervene accordingly. A number of investigations have looked into mortality due to acute respiratory distress syndrome (28, 114, 115), others have looked into ventilatory strategies that may reduce the incidence of barotrauma and/or mortality in children (149, 195) and adults (1, 4, 35, 37, 183). The adult studies primarily targeted on high vs low V_T . Targeted V_T was calculated on either predicted or ideal body weight. It has been commented that this V_T may differ considerably in obese populations, and that the actually delivered volume, irrespective of body weight, distends – and damages - the lungs. In two studies achieved pressure was defined as P_{peak} and in three as P_{plat} , although it is recognised that P_{peak} is depend-

⁴ “What’s the idea?” – muttered by an elderly lady in an old people’s home when encouraged to join the basket weaving.

ent on ventilatory mode, I:E ratio, tube dimensions, and frequency. Plateau pressure is not defined in ventilators without end-inspiratory pause in the PCV mode. Further, no information was provided on the presence or absence of intrinsic positive end expiratory pressure (PEEP_I). Proximal (\equiv above tube) peak pressure, used in these studies as a target parameter, does not reflect PEEP_I, and may differ considerably from *tracheal* peak pressure depending on the inspiratory:expiratory (I:E) ratio, respiratory rate, tube size and mode, i.e. pressure or volume controlled ventilation (PCV, VCV). Recalling that these investigations probably involve a number of obese patients, the transpulmonary pressure would have been more appropriate as target measure. It has also been commented that the PLV gains its merits from the comparably low V_T – or in other words that the conventional ventilation should actually be termed *destructive ventilation*. According to the study by Luhr (115), ARDS patients in Scandinavia were treated with a V_T of 8 mL/kg. Thus, the use of high V_T of 12 mL/kg seems to have been abandoned in Scandinavia. A recent study of ventilatory settings in Scandinavian ICUs found a median V_T of 7 mL/kg (96).

To my knowledge, no investigations have been performed looking into alveolar peak or mean pressure as target measures, and though it at present seems chimerical, a preliminary proposal might be that the alveolar pressure/volume curve should be obtained *continuously* during therapeutic ventilator treatment and be included in prospective studies of protective ventilation.

Table 3. Investigations in protective vs conventional ventilation. Targets in parentheses are secondary. Adapted from (166).

Study	No	Target VT		VT achieved		Target Pres- sure		Pressure achieved		PEEP		Outcome measures	Results	
		PLV	CMV	PLV	CMV	PLV	CMV	PLV	CMV	PLV	CMV		PLV	CMV
Amato (1)	53	≤6	12	387 mL	738 mL	P _{peak} (20-40)	∞	P _{peak} 24.0	45.5	13.2	9.3	28 day mortality	38%	71%
		MBW											(p<0.001)	
Stewart (183)	120	≤8	10-15	6.8	10.1	≤30	50	24.3	33.5	9.6	8.0	In- hospital mortality	50%	47%
		IBW											(p<0.007)	
Brower (37)	52	5-8	10-12	7.3	10.2	P _{plateau} (<30)	(<55)	24.9	30.6	Not indicated		Several	50%	46%
		PBW											(p<0.007)	
Brochard (36)	116	6-10	10-15	7.3	10.7	(≤25)	(≤60)	24.5	30.5	9.6	8.5	60 day mortality	46.6 %	37.9%
		DBW											(p<0.007)	
ARDS Net (4)	861	6	12	6.5	11.4	(<30)	(50)	26	37	8.1	9.1	death	31%	40%
		PBW											(p<0.007)	

OWN INVESTIGATIONS AND RESULTS

ADULT SECTION

Tracheal pressure measurement in adults

One major feature of the DSA is the measurement of pressure distal to the tip of the tube in the trachea via a polyethylene catheter or a fibre-optic pressure transducer. This pressure is clearly different from proximal pressure owing to the tube resistance (but is not identical to total PEEP in the sense of extrinsic + intrinsic PEEP, intrinsic PEEP being the value obtained when subtracting extrinsic PEEP from total PEEP during zero flow in prolonged expiratory pause (54)).

The direct measurement bypasses all problems of impending tube obstruction by secretions and even makes it possible to monitor the development of tube resistance without resorting to further mathematical exercises in detection of flow restriction (38, 74).

In adults a polyethylene catheter is passed through a special connector Figure 26.

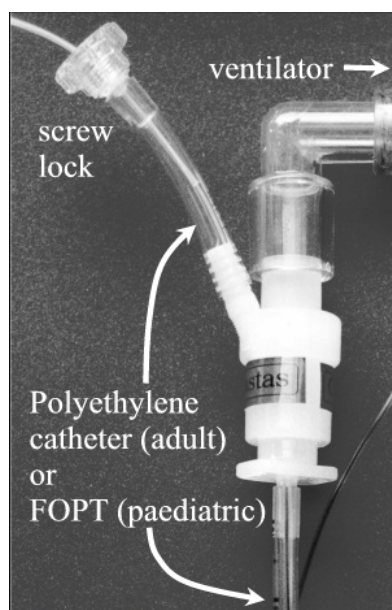


Figure 26. Connector for introducing end-hole polyethylene catheter in adult and FOPT in paediatric ETT. The tip of the catheter/FOPT is positioned at or just outside the tip of the ETT.

Pressure is measured at end-hole of catheter and corresponds exactly with reference tracheal pressure in bench test. The method has been validated in (102), see discussion (111).

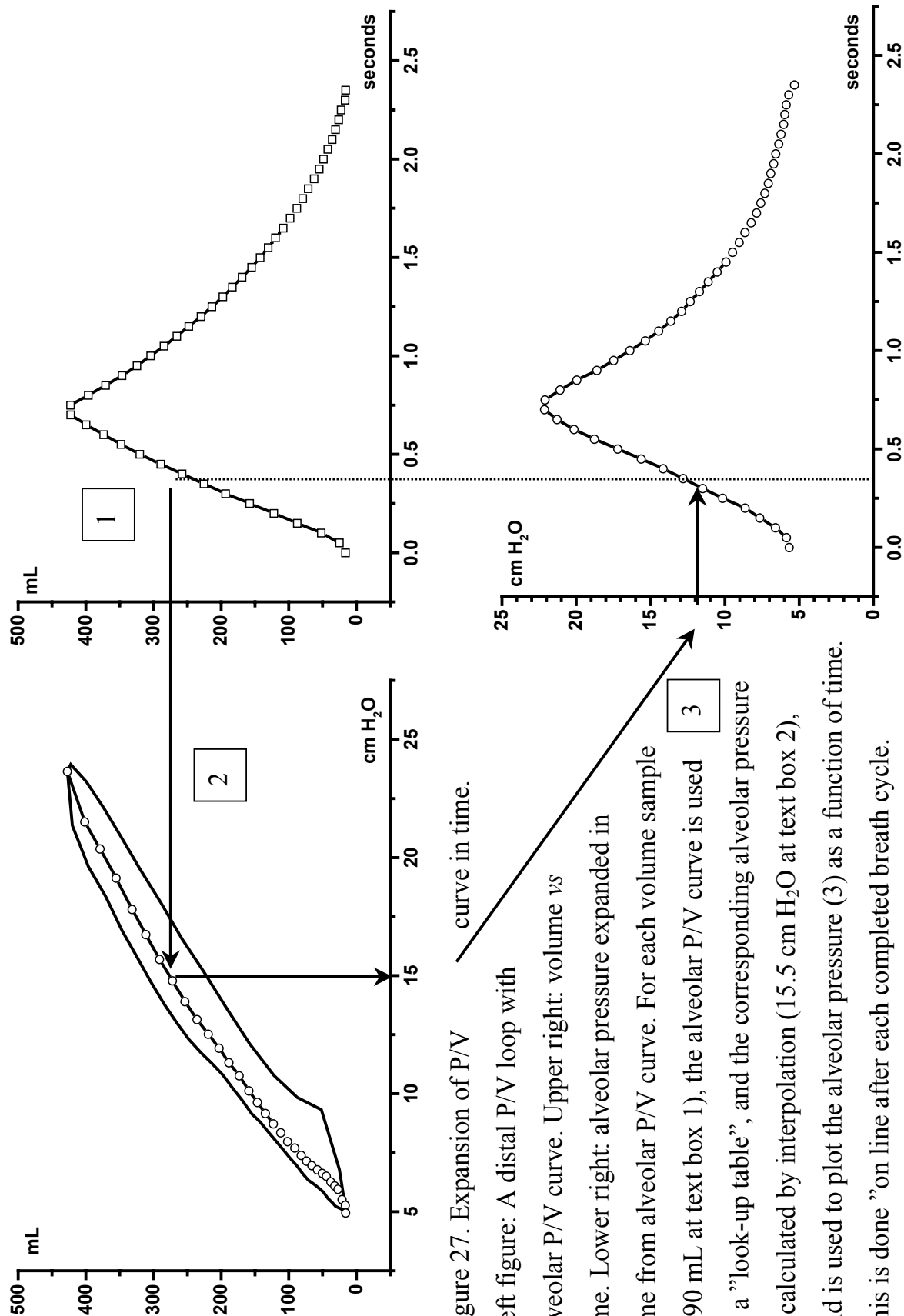
One of the aims of Paper II was the demonstration of the feasibility of long-term tracheal measurement. Ten consecutive patients from the Intensive Care Unit and Recovery Room were entered into the study. The pressure line was air filled and the pressure transducer connected to Datex AS/3. Peak/end expiratory pressures were registered hourly from the display. Duration of catheter in place, duration of active measurement and number of air flushes to clean catheter were registered.

In all cases but one, tracheal pressure was measured continuously for the whole period of ventilator treatment, mean 33 h with 30 measurements and 18 suction procedures. The pressure line became obstructed and an air-flush was necessary on an average of every second hour.

The expansion of the alveolar P/V curve in time

It is a tautology that ventilation is proceeding in time. The P/V curve does not exhibit this temporal dimension, but clearly, it may be seen as superposed inspiratory and expiratory limbs. The temporal expansion of the P/V curve was calculated on a template of volume and time, and displayed continuously. This implies that the alveolar pressure during end-inspiratory pause is constant at the level of plateau pressure (because volume is constant), and does not demonstrate the decay normally attributed to viscoelastic properties of the lung, Pendelluft, or compartmental inhomogeneities.

The principle is illustrated in Figure 27.



Validation of the DSA in the adult lung model (Papers I & II)

The lung models for testing the adult application of the DSA were built from a Biotek Ventilator Tester (BVT) in combination with a Servo 900C ventilator. The BVT was equipped with a plastic trachea, which was intubated with a 7 mm ID endotracheal tube. A resistance unit was inserted between the BVT and the trachea. The resistance unit was cut in Plexiglas™ with two symmetric lumina with a diameter of 17 mm, cf. Figure 28. By inserting two one-way valves into the conduits, the unit functioned as a one-way circle. The lumina of the expiratory and inspiratory lumina were changed by inserting pipes, OD 17 mm, with differing ID: 12, 7, 5, 4.5, and 4 mm.

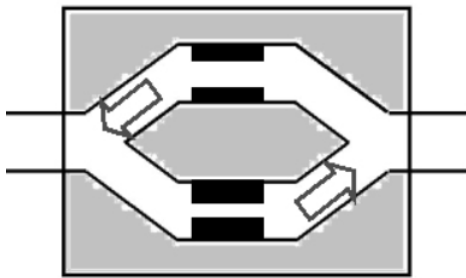


Figure 28. The resistance unit cut in Plexiglas™. Arrows indicate one-way valves. Inspiration through upper, larger diameter. Expiration through lower smaller diameter. $R_I:R_E$ 1:1.4, indicating a 40% larger resistance during expiration.

The pressure/flow relationship of the pipes in the resistance unit was characterised by differential pressure measured with a digital manometer (Digital Manometer, Revue Thommen AG, Waldenburg Swiss) at increasing flows measured with Calibration Analyser, series RT-200 model 12640 (Timeter Instrument Corporation, Oregon Pike, Lancaster, USA).

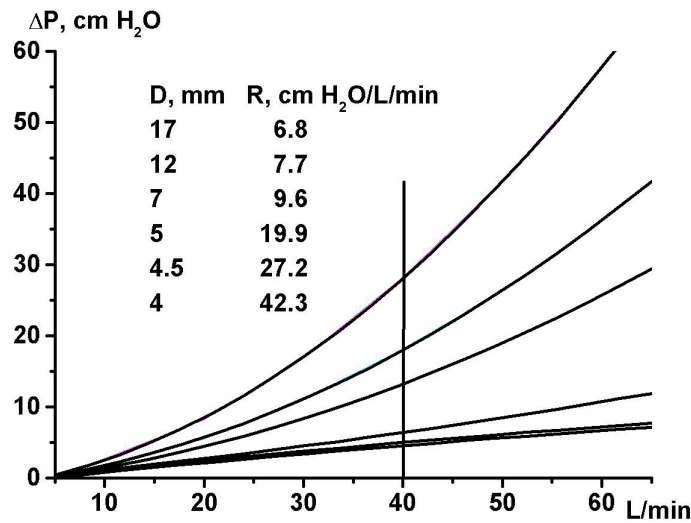


Figure 29. Pressure/flow characteristics of the resistance unit. A second order polynomial fit of pressure/flow relationship in six pipes. The resistance of a particular pipe was defined as the resistance at a flow of 40 L/min. D: diameter in mm, R: resistance in cm H₂O/L/min. The pressure/flow relation is linear for 17 and 12 mm (laminar flow) whereas it becomes nonlinear at ID 5, 4.5 and 4 mm (turbulent flow). At 7 mm, the relationship may be described as intermediary to linear and nonlinear relationship.

$R_I:R_E$ ratios were defined – arbitrarily - as resistance at flow of 40 L/min, cf. Figure 29. A low compliant catheter was inserted into the tube lumen and the tube was connected via Pitot type spirometer to the Y-piece and ventilator tubing (Paper I). In order to add a viscoelastic component to the model, a container with a low viscous fluid was placed on the lid of the BVT. This had the effect of restraining the initial rise of the lid, thus creating a lower inflection point. A spring impeded the lid excursion towards end of inspiration, thus creating the equivalent of an upper inflection point (Paper II).

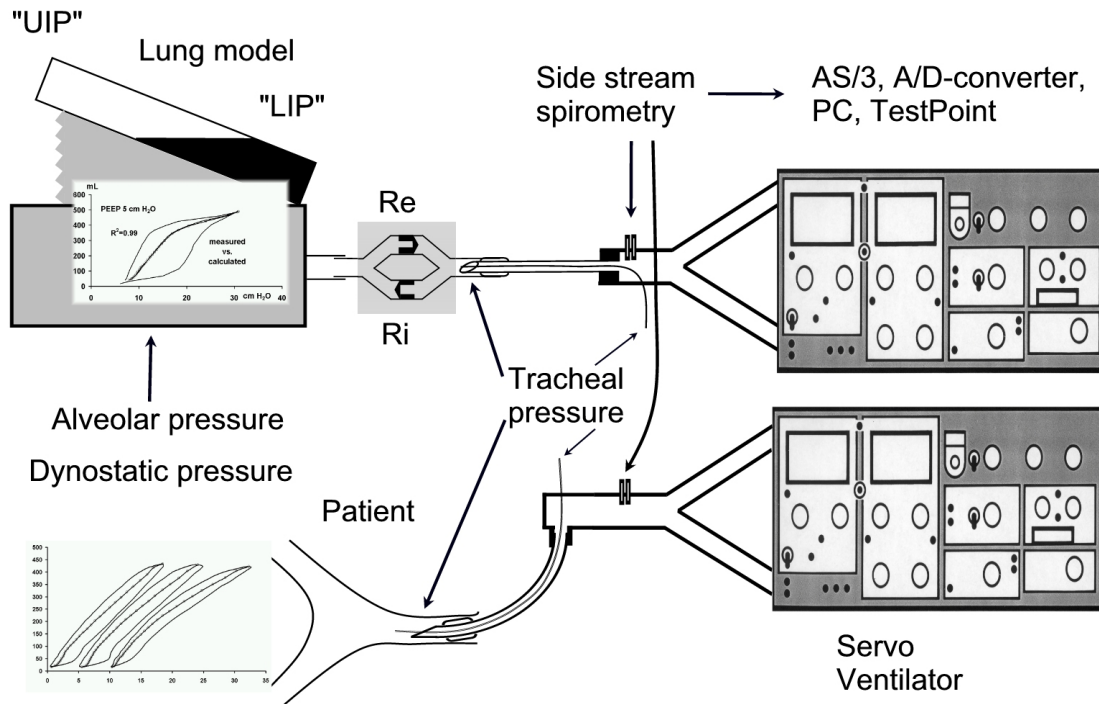


Figure 30. The lung model used for validation of the DSA in adult applications. The clinical situation is mirrored below. The diagram on the Biotek Ventilator Tester illustrates a P/V loop in VCV with $R_I:R_E$ 1:1.4 and PEEP 5 cm H₂O. The PEEP level has “pushed” the P/V loop past the lower inflection point created by the viscoelastic load. The calculated and measured model alveolar pressures coincide. In the clinical situation, three P/V loops are shown at PEEP 0, 5, and 10 cm H₂O with signs of increasing overdistension.

Measurements were performed in volume controlled (VCV) and pressure controlled (PCV) modes. The ventilatory settings were varied according to inspiratory time, T_I , 25, 33, and 50%; end-inspiratory pause 0 or 10%; PEEP 5, 10, and 15 cm H₂O; V_T 250, 500, and 750 mL, compliance 20, 35 and 50 mL/cm H₂O, and respiratory rate 20 breaths/min. Twenty settings were studied. Ratios of inspiratory:expiratory resistance ($R_I:R_E$) 1:1, 1:1.4, 1:2.1, 1:2.8, 1.4:1, and 2.8:1 were established in the resistance unit. Data were sampled for 15-20 respiratory cycles, analysis performed on 3-5 cycles and

averaged. The calculated dynostatic P/V curves were compared with the P/V curves measured in the alveolar component of the lung model (Paper I).

In Paper II, the dynostatic and alveolar P/t curves were compared by various statistical measures.

Results of validation in the adult lung model

Paper I investigated the behaviour of the DSA in a one-compartment lung model with a number of ratios between inspiratory and expiratory resistance. Dynostatically calculated P/V curve was compared with measured P/V curve. The DSA functioned satisfactorily with $R_I:R_E$ ratios ranging between 1:2.3-2.3:1 as judged from R^2 , slope and constant, as shown in Table 4.

←Increasing R_I				$R_I=R_E$	Increasing R_E →		
$R_I:R_E$	4.6:1	2.3:1	1.4:1	1:1	1:1.4	1:2.3	1:4.6
VCV							
r^2	0.88	0.97	0.99	0.99	0.99	0.95	0.86
α	1.79	1.16	0.96	0.99	0.86	0.78	0.72
K	1.83	1.13	0.17	-0.09	0.26	0.21	-0.32
PCV							
r^2	0.93	0.97	0.99	0.99	0.99	0.98	0.88
α	1.39	1.03	0.95	0.92	0.90	0.79	0.75
K	2.70	1.42	0.53	0.51	0.45	0.32	-0.37

Table 4. Comparison of calculated and measured alveolar pressure. Statistical analysis $R_I:R_E$ variations on the dynostatic algorithm. Mean results of three breaths for the coefficient of regression r^2 , α and constant K from comparisons of P_{dyn} and P_{alv} ($P_{dyn} = \alpha \times P_{alv} + K$) at seven $R_I:R_E$ ratios during VCV and PCV. The dynostatic algorithm performs well as long as the inspiratory resistance is up to 2.3 greater than the expiratory resistance or vice versa.

In Paper II a viscoelastic component was added to the lung model and respiratory excursion was restricted, thus creating the equivalent of a lower and upper inflection point. The aim was to investigate the congruence between calculated dynostatic pressure *vs* time and measured alveolar pressure *vs* time. There was an excellent agreement: R^2 0.98, slopes 0.98 ± 0.02 , intercepts 0.02 ± 0.2 , bias $0-0.22$ cm H₂O, RMS 0.47-2.2 cm H₂O, when the inspiratory and expiratory resistances of the airway were equal or differed in ratio by less than 40%. Within the range of $R_I:R_E$ known from the literature (cp. p. 70) the correlation coefficient ranged from 0.986 to 0.996 with slope of the regression equation ranging from 0.86 to 0.99 for a systematic variation of I:E, PEEP, compliance, $R_I:R_E$, V_T , ventilatory mode and end-inspiratory pause.

The performance of the DSA in calculating the alveolar pressure in the adult lung model was compared with the performance of the Bertschman LOOP method, p. 56. The LOOP method was modified to the effect that *distal* and not *proximal* pressures were entered in the MLR. Results of regression analysis for all combinations of $R_I:R_E$, ventilatory modes and gas densities showed R^2 DSA 0.97 > LOOP 0.93 with slope DSA 0.99 > LOOP 0.83 and intercept, Y_0 DSA $-0.2 < \text{LOOP } -2.4$ (unpublished results).

In the presence of low-density gas mixtures (spirometric volumes corrected according to Paper III), varying $R_I:R_E$ and viscoelasticity, the DSA resulted in correlation coefficients of 0.97-0.98 with slopes 0.99-1 and intercepts at $-0.63 - 0.07$ (unpublished data).

Application of the DSA in adult patients

Paper I aimed at demonstrating information obtainable from the dynostatic *P/V curve*. Ten patients were entered into the study, six men and four women. Age ranged from 39 to 76 years with a mean of 56.3 years. The patients had been ventilator-treated for two to 28 days with a mean of 8.8 days. Oxygenation Index (P_aO_2 (mm Hg)/ $F_I O_2$) ranged from 68 to 218, mean of 126.

Test procedure in patients: all patients were measured during VCV and PCV ventilation. The test protocol was modified as dictated by the clinical situation. Basically, three tidal volumes were used: 4, 8 and 12 mL/kg, three PEEP levels: 4, 8 and 12 cm H₂O (as zero end-expiratory pressure was not considered safe for the patients) and three I:E ratios: 1:2, 1:1 and 2:1.

Paper II aimed at evaluating the DSA in terms of alveolar pressure vs time. Ten patients with acute lung injury were entered consecutively from the Intensive Care Unit. Age varied from 46 to 81, mean 62 years, Oxygenation Index ranged from 103 to 248 with a mean of 166. Lung Injury Score was calculated according to Murray (132) and ranged from 1.5 to 3.25, mean 2.4. Patients were sedated and muscle relaxed during the investigation. Sampling of volume, flow, and tracheal pressure was performed as described in lung model. The patients were ventilated with a Servo 900C or a Servo 300 ventilator. Measurements were performed during VCV and PCV. The basic ventilator settings were V_T 8 mL/kg, PEEP 10 cm H₂O and I:E ratio 1:2. Then, by changing one parameter at a time, three V_T , 4, 8, and 12 mL/kg, three PEEP levels 5, 10, and 15 cm H₂O, and three I:E ratios; 1:2, 1:1, and 2:1, were studied. Ventilator settings were modified according to the clinical situation. The DSA is adhering to the fact that lung mechanics is frequency dependent. By changing ventilatory settings, e.g. including an end-inspiratory pause or occlusion, the mechanic conditions of the lung are changed and the “no-pause” calculation of the alveolar pressure cannot be validated by the “pause/occlusion” calculation. Therefore, the maximum alveolar pressure as calculated by DSA was compared with the end-inspiratory pause pressure, cf. Figure 31.

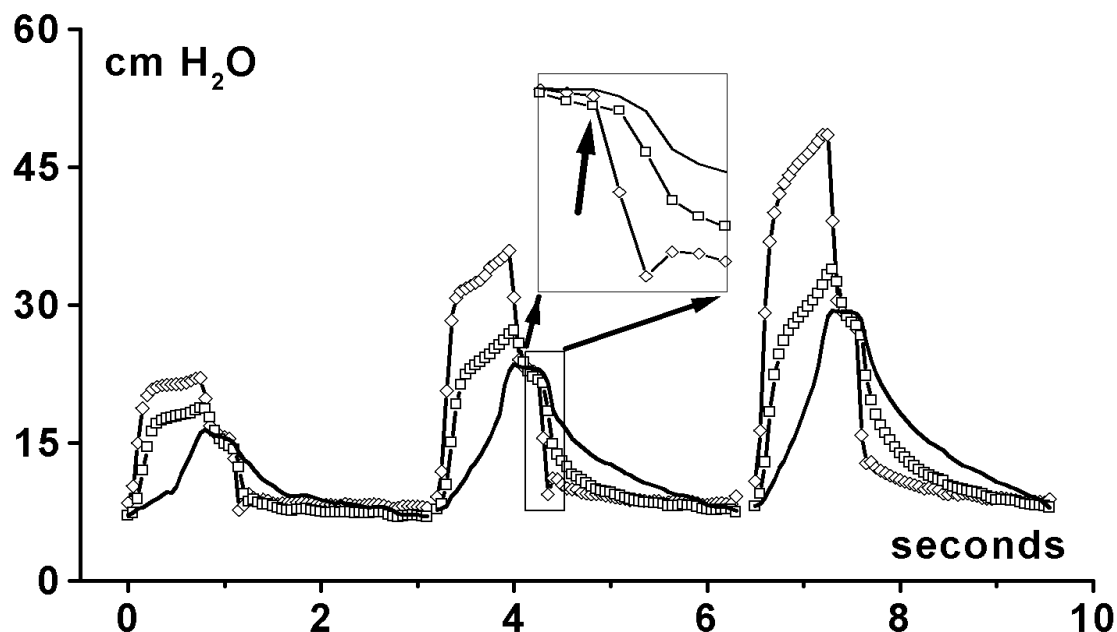


Figure 31. Comparison between peak P_{alv} and P_{plat} . Patient 1, PEEP 5 cm H_2O , VCV at tidal ventilations of 300, 500 and 700 mL on a common time scale. Diamonds: proximal pressure, squares: tracheal pressure, full line: dynostatic alveolar pressure. **Insert** demonstrates end-inspiratory pause and early expiratory period. Arrow marks values of proximal and alveolar pressure utilized in Bland and Altman analysis of agreement between the two pressures. The three pressures are highly congruent at the end of the end-inspiratory pause at all tidal volumes. Note that there is a point during inspiration where the alveolar pressure increases more rapidly, indicating that there is an upper inflection point. This can be seen neither in the proximal nor in the tracheal pressure measurement.

Results of applying the DSA in adult patients

- No obvious lower inflection point/zone was revealed by the dynostatic P/V curve in any of the patients studied. An upper inflection *zone* could be seen when the large tidal volumes or when small tidal volumes in combination with high PEEP levels were used. Compared with conventional calculation of compliance, it was

evident that the conventional curve would actually be *outside* the tracheal P/V loop in cases showing overdistension. The use of inverse I:E ratio ventilation produced intrinsic PEEP and signs of overinflation during both VCV and PCV (Paper I).

- Bland and Altman analysis showed that the maximum alveolar pressure was on average 0.32 cm H₂O lower than the end-inspiratory pause pressure and the precision was 0.97 cmH₂O. This is demonstrated in Figure 32.

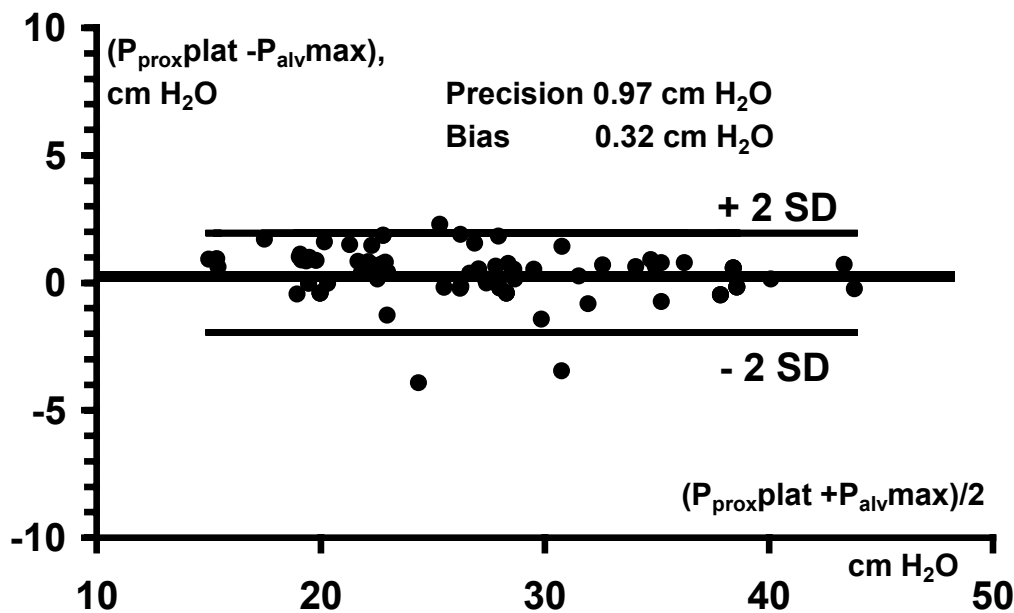


Figure 32. Bland and Altman plot of agreement between P_{proxplat} and P_{alvmax} showing good agreement of proximal plateau pressure and maximum alveolar pressure in six patients in ventilatory cycles with end-inspiratory pause, cf. Figure 31.

The relationship between the dynostatic P/V curve and the tracheal loop was different in VCV and PCV. With increasing inspiratory time, the inspiratory flow becomes slower during VCV ventilation but is unchanged during PCV. This leads to the dynostatic curve getting closer to the inspiratory limb of the tracheal loop in VCV with increasing inspiratory time, but the position of the dynostatic curve in relation to the inspiratory limb of the tracheal loop in PCV remains unchanged as inspiratory flow is the same irrespective of inspiratory time, see Figure 34.

- Setting an extrinsic PEEP of 8 cm H₂O and increasing the I:E ratio in VCV from 1:2, where proximal, tracheal and alveolar pressures coincide at beginning of inspiration, to 1:1 and 2:1, an increasing discrepancy occurs between proximal and tracheal pressures due to build-up of PEEP_I, which is reflected in the dynostatic P/V curve as well as in the alveolar pressure vs time curve. In contrast to this, the proximal loop does not disclose the build-up of PEEP_I. The rise in mean alveolar pressure is higher than the rise in PEEP_I with increasing I:E ratio irrespective of VCV or PCV. Thus, in VCV with extrinsic PEEP level of 8 cm H₂O, changing from I:E ratio 1:2 to 2:1 leads to an increase in PEEP_I from 0 to 4 cm H₂O and a rise in mean alveolar pressure from 12 to 18 cm H₂O, whereas the same procedure in PCV leads to an increase in PEEP_I from 0 to 7 cm H₂O and a rise in mean alveolar pressure from 13 to 22 cm H₂O, see Figure 7 in Paper II.
- The rate of rise of the alveolar pressure in PCV is the same irrespective of I:E ratio, whereas during VCV increasing I:E ratio leads to decreasing rate of rise in alveolar pressure, see Figure 7 in Paper II. This pattern is duplicated in the volume vs time plot, leading to increasing time of a certain volume being present in the lung, “volume persistence”, in PCV compared with VCV with increasing I:E ratio (Paper II), see Figure 33, unpublished data.

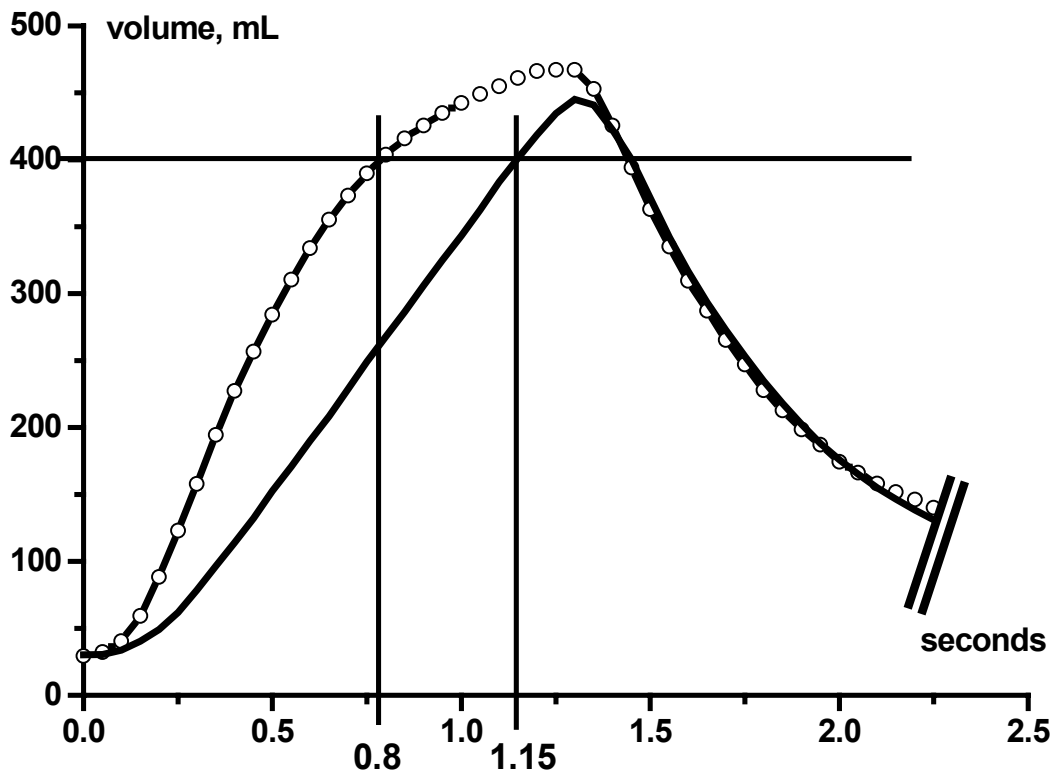


Figure 33. Recording from patient of volume vs time in VCV (full line) and PCV (circled line). During VCV 400 mL is delivered in 1.15 s, whereas in PCV an identical volume is delivered in 0.8 s, *ceteris paribus*. This indicates that the 400 mL in PCV will exchange gases 0.35 s longer than the 400 mL in VCV. This has been termed “volume persistence” and may be part of the explanation for better oxygenation in PCV. Volume persistence is effected – in this case – to the “cost” of a higher mean alveolar pressure in PCV (20 cm H₂O) vs VCV (17 cm H₂O).

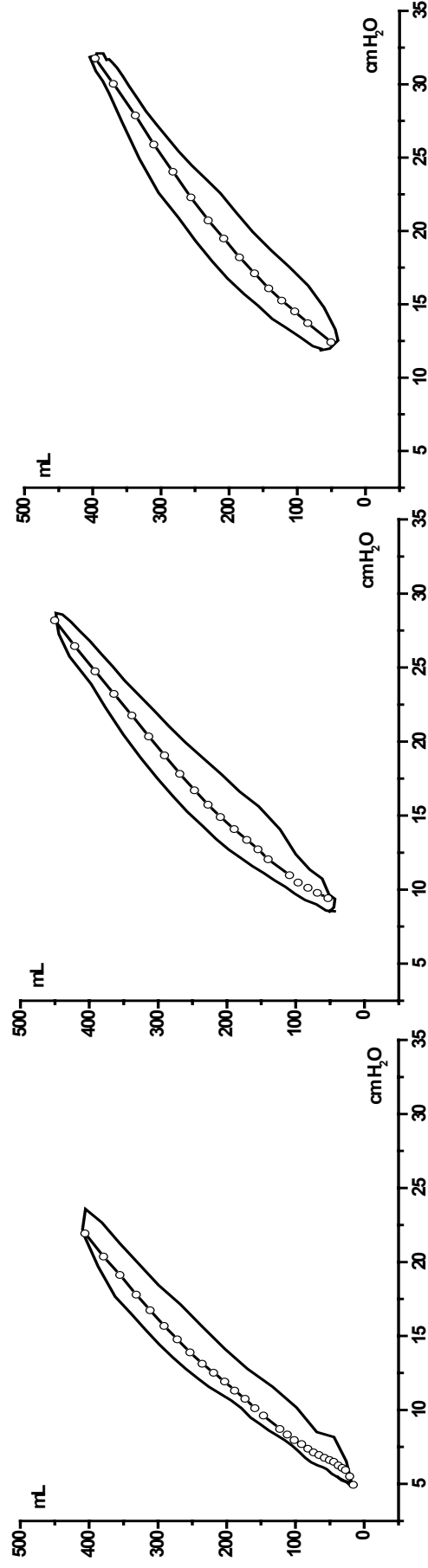


Figure 34. Increasing I:E ratio during PCV caused development of intrinsic PEEP while the extrinsic PEEP was unchanged. Note unchanged relation of alveolar P/V curve to inspiratory limb of tracheal P/V curve and signs of overinflation in spite of unchanged tidal volume owing to increasing intrinsic PEEP. *This figure replaces figure 3 in Paper I.*

PAEDIATRIC SECTION

Tracheal pressure measurement in paediatric tubes (Paper IV)

In children, the dimensions of the ETT preclude the use of polyethylene catheters. Even if one were to use the smallest dimension, e.g. 0.86x1.27 mm (ID/OD), the time constant is prohibitive. For this dimension the time constant, τ , is 6.3 ms. This means that input pressure is related to 95% of its value in 3τ , 18.9 ms, thus introducing damping as well as phase lag compared to flow measurement. Using a larger dimension, e.g. 1.1x1.57 mm reduces τ to 3.95 ms, which may be acceptable in paediatric monitoring. The outer dimension, though, creates intrinsic PEEP by impeding expiratory flow. A technique based on small sized (1 mm) fibre-optic has been tested in adult respiratory monitoring with good results (51) and (unconvincingly) in paediatric ETTs (104). I have had the opportunity of introducing the use of a very small sized optic fibre in paediatric ETTs: the SAMBA fibre-optic system (Samba Sensors AB, Gothenburg, Sweden).

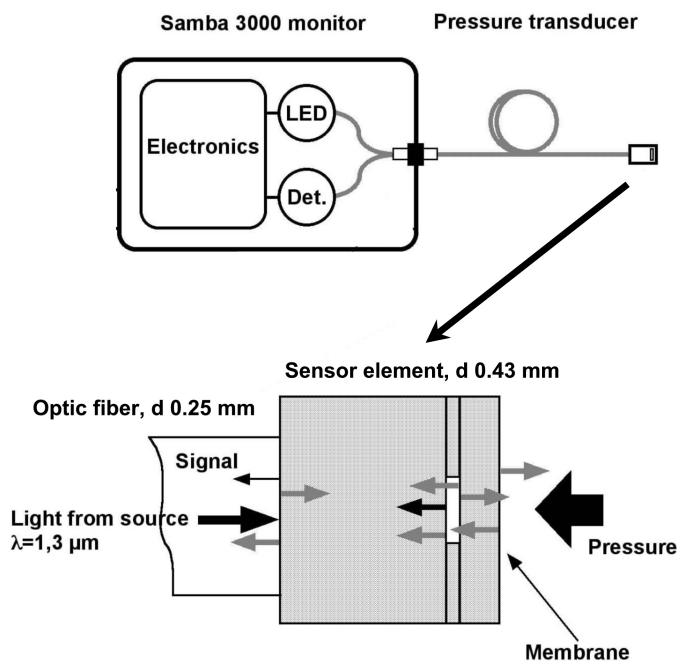


Figure 35. The fibre-optic pressure transducer system consisting of sensor element, optic fibre, and monitor. A PC programme in LabView is interfacing the pressure transducer. An analogue output is available for independent sampling by A/D-converter and custom-made programming.

The fibre-optic pressure transducer (FOPT) used for tracheal pressure measurement consists of a silicon sensor chip 0.42 mm outer diameter (OD) micromachined in silicon and attached to an optical fibre 0.25 mm OD. The pressure transducer uses a microcavity for sensing of the pressure. It is based on the interferometric principle (Fabry-Perot) that the deflection of the microcavity membrane by pressure results in a change in the reflected light intensity when the interference conditions inside the cavity are modified (214). The optic fibre is unshielded for the length passing through the tube. Outside the tube, a 1 mm plastic sheath protects it for about 40 cm. The remaining length of the fibre is covered in a 3 mm rubber sheath. The “naked” part of the fibre is passed through the connector and ETT in situ, protected, and stabilized inside a polyethylene catheter (1.1x1.57 mm). When the pressure transducer is in position at the tip of the tube, the sheath is retracted to a position outside the lumen of the ETT, but inside the introducing branch of the connector, see Figure 26, p. 76.

Much effort was dedicated to the development of user interface (software programmes) with the Samba Sensor and TestPoint in terms of absolute vs relative pressure measurement, calibration, scaling, and sampling.

The fibre-optic pressure transducer was thoroughly tested before being put to clinical use (Paper IV):

Response time.

A balloon was attached to a plastic trachea of 9 mm ID. The trachea was intubated with an ETT no. 6. The FOPT was introduced and advanced to the tip of the tube via the connector, see Figure 26. The balloon was inflated to 60–80 cm H₂O and burst with a flame. Reference pressure was measured via a side hole in the trachea. Pressure signals were sampled at 3 kHz from the analogue output of the FOPT monitor and a bridge amplifier to a TestPoint application.

Influence of the FOPT during constant flow

Pressure/flow relationships were studied in a system of respiratory tubing, a pressure transducer (proximal pressure), a connector for the introduction of the FOPT into the

ETT of neonatal or paediatric dimensions (3, 4, 5, and 6 mm ID), a model of a neonatal or paediatric trachea with a wide bore side hole for reference pressure measurement to minimise the Venturi effect, and a pressure transducer for measuring tracheal pressure. ETT 3 and 4 mm ID were flushed with air in inspiratory or expiratory direction at flows of 1, 2, 3, 4, or 5 L/min, and ETT 5 and 6 mm ID were flushed at flows of 2, 4, 6, 8, and 10 L/min. The flows were considered representative of clinical flows. Pressure reduction was calculated and displayed as a function of flow.

Influence of the FOPT during ventilation of the lung model

A Servo 900C (Siemens Elema, Solna, Sweden) was connected with paediatric tubing to ETT 3, 4, 5, or 6 mm ID, a trachea and a paediatric lung model. The system was ventilated with air at a frequency of 40 breaths/min and inspiratory-to-expiratory ratios of 1:2, 1:1, and 2:1. Volume was measured with side-stream spirometry incorporated in Datex AS/3 spirometry module. Tracheal pressure was sampled at 25 Hz at the tip of the tube via the FOPT inserted through the lumen of the ETT, and reference pressure was measured at a side hole in the model trachea via a conventional pressure transducer.

Results of pressure measurement in paediatric tubes

The application of the fibre-optic pressure transducer in paediatric respiratory monitoring demonstrated (Paper IV):

- that the fibre-optic pressure transducer occupied 0.7% of the cross-sectional area of an ETT 3.0, 0.4% of ETT 4.0, 0.25% of ETT 5.0, and 0.17% of ETT 6.0;
- that the pressure/flow relationship was curvilinear for all dimensions, flow rates in both inspiratory and expiratory directions, and was fitted to a second-degree polynomial. The presence of FOPT did not in any case increase the pressure fall significantly across the tube, and t-test did not reveal any significant differences between presence vs absence of sensor, or between inspiratory vs expiratory flow direction;

- a response time of 1.3 ms to a step change in pressure, see Figure 36.

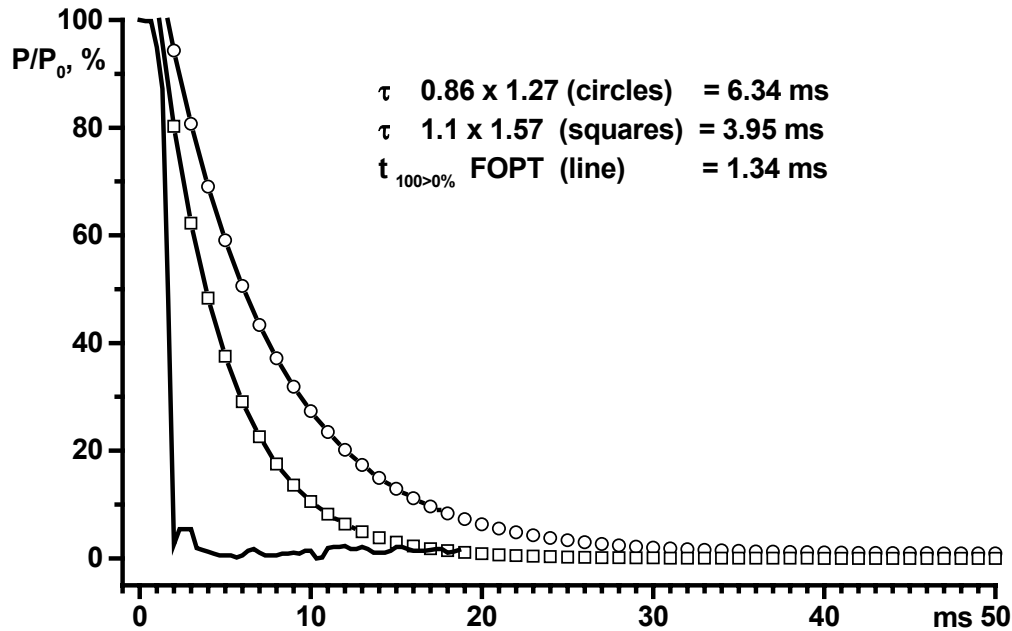


Figure 36. Pressure changes when bursting a balloon was measured with two diameters of polyethylene catheters, 0.86x1.27 and 1.1x1.57 mm, and FOPT at sampling speed of 3 kHz. Abscissa in milliseconds, ordinate shows pressure as percentage of pressure before balloon burst. The pressure decay from the polyethylene catheters has been fitted to an exponential decaying function, and time constants have been calculated. In the case of the FOPT, it does not make sense to speak of ‘time constant’, as pressure drop is complete in approximately 1.3 ms.

- that calculating pressure drop across tube according to the Guttman polynomial expression including an inertial component (71) and according to the more complex formula of Jarreau (89) did not result in any convincing congruence with measured pressure drop and became erroneous if slight amounts of secretions were added to the tube lumen, cf. Figure 37 and Figure 38;

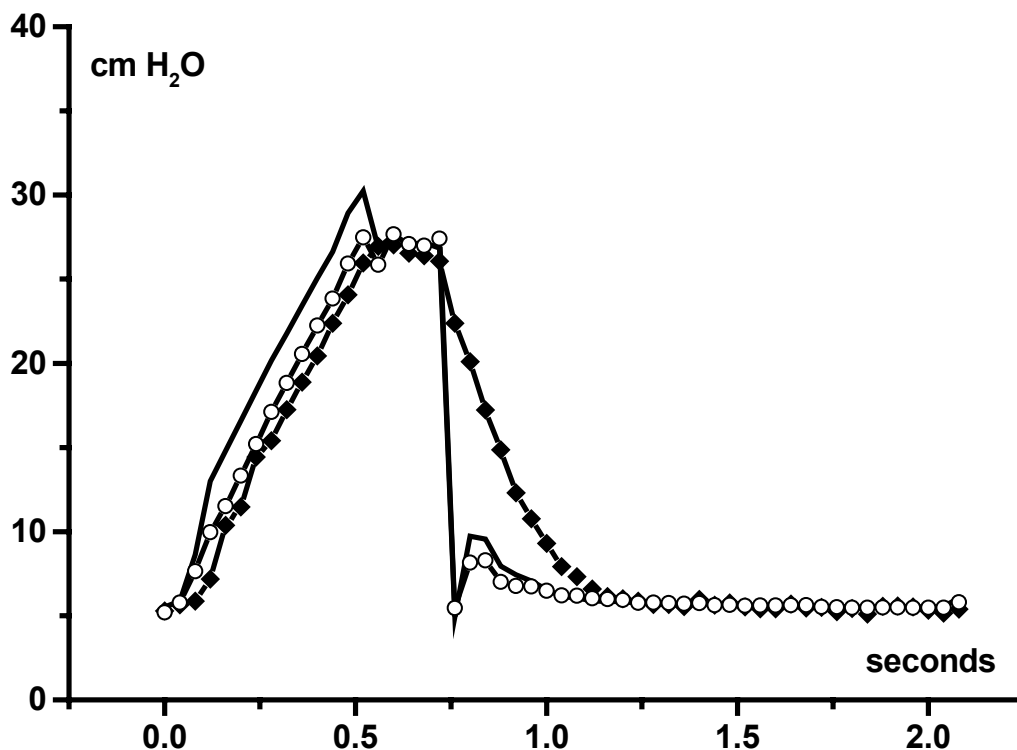


Figure 37. Guttman algorithm for P_{trach} I⁵. *Clean* ETT 4. Full line: P_{prox} measured by conventional pressure transducer; circles: P_{trach} calculated a.m. Guttman; filled diamonds: P_{trach} measured with fibre-optic pressure transducer. The Guttman algorithm works well during inspiration, but cannot reproduce the slowly decaying expiratory pressure. The oscillations at start of expiration may be ascribed to the functioning of the ventilator valves.

⁵ Drs. Lichtwarck-Aschoff and Guttman have in a personal communication pointed out that Figure 8 in Paper IV, is a serious misrepresentation of their algorithm for the calculation of tracheal pressure in paediatric tubes, as only the viscous pressure drop is displayed and not the ΔP equalling proximal pressure minus viscous pressure drop. With the kind assistance of Dr. Lichtwarck-Aschoff, I have now corrected my programming.

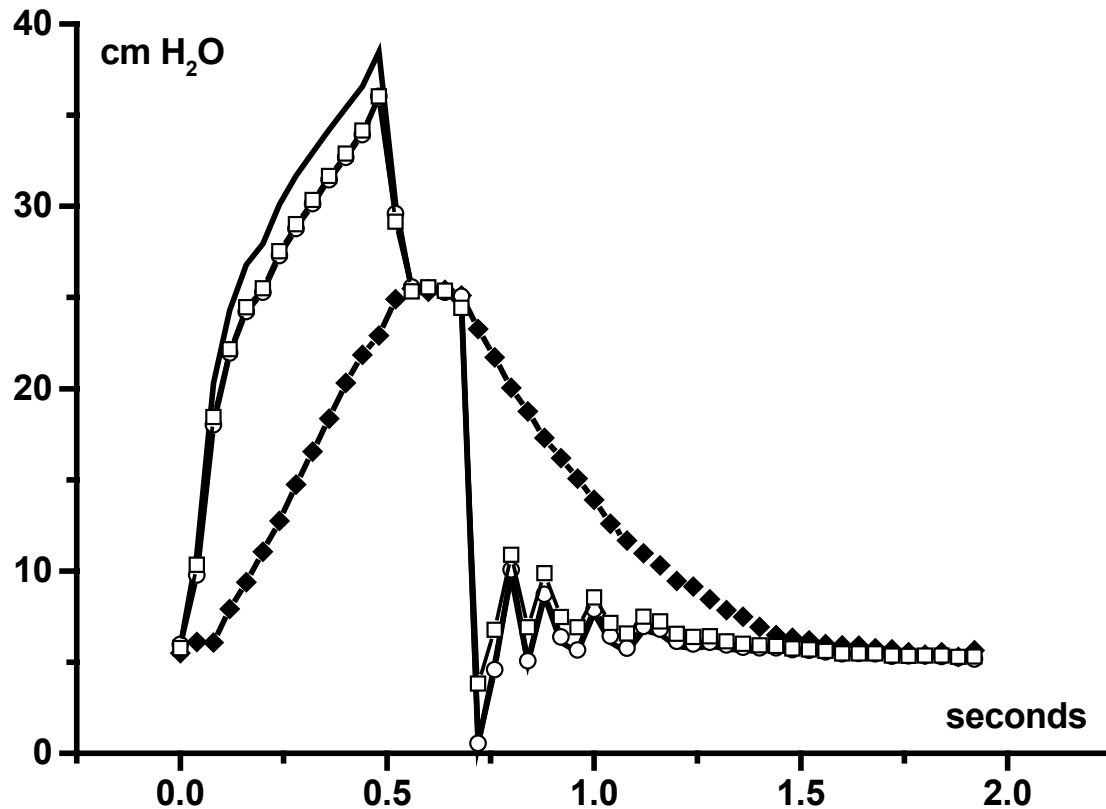


Figure 38. Guttman algorithm for P_{trach} II. ETT 4 with secretion amounting to 10% of tube volume ventilated in lung model. Legends identical to Figure 37, *squares*: P_{trach} calculated a.m. Guttman (according to Lichtwarck-Aschoff). The Guttman algorithm does not work in the presence of secretion⁶. The minor differences between Dr. Lichtwarck-Aschoff's and my calculation are explained by the fact that Dr. Lichtwarck-Aschoff left out the inertive component of his calculation. Oscillations at start expiration are more pronounced owing to higher pressure and flow during VCV setting.

⁶ In continuation of above correspondence, Dr. Lichtwarck-Aschoff concedes that the Guttman – as well as any other algorithm for calculation of viscous pressure drop in tubes, e.g. Blasius, Ito, Jarreau – will fail, naturally, if inner diameter and wall contour are changed by secretions. This may possibly be remedied by algorithms for detection of tube obstruction, however cf. discussion p. 116.

The conclusion, therefore, remains unchanged: algorithms aiming at calculation of tracheal pressure based on proximal pressure and flow are prone to fail if/when secretions occur. It remains unclear why the algorithm does not mirror the slowly decaying pressure during expiration.

- that comparing pressure measurements with distal reference pressure transducer and fibre-optic pressure transducer resulted in regression coefficients close to unity, which may also be construed as a “passed” of the conventional pressure transducer! Equations for three positions of the pressure transducer relative to the tip of ETT showed slopes close to 1.0 and intersections with the y-axis of less than 0.4 cm.

Validation of the DSA in the paediatric lung model (Paper V)

The BVT is not suited for simulation of paediatric ventilatory settings as there is no access to the paediatric “alveolar” compartment. A paediatric lung model was constructed from a 1 L ventilating bag enclosed in a wooden casing with a hinged lid, the IKEA model (Papers IV and V). At the inlet, a constriction with an opening of 4 mm was inserted. Upper and lower inflection points were produced by adding a fluid-filled cylinder to the lid and a spring connecting the base and lid of the model, Figure 39.

The compliance of the model varied from two to ten mL/cm H₂O.

The model was ventilated with a frequency of 30 or 40 breaths/minute and minute volumes (MV) of 2, 3, 4 L/min with ETT no. 3; 2.5, 3.5, 4.5 L/min with ETT no. 4; 3, 4, 5 L/min with ETT no. 5, and 4, 5, 6 L/min with ETT no. 6. The ratio between time for inspiration and time for expiration (I:E-ratio) was varied between 1:2, 1:1, and 2:1, PEEP was increased from 0 to 5 and 10 cm H₂O. These settings were repeated in VCV and PCV. Sixty settings were tested. Analogue signals were sampled from FOPT and Servo ventilator at 50 Hz to a TestPoint application. Comparison between calculated and directly measured alveolar pressure was made and results expressed as regression equation, RMS, R² and Bland and Altman plots with bias and precision.

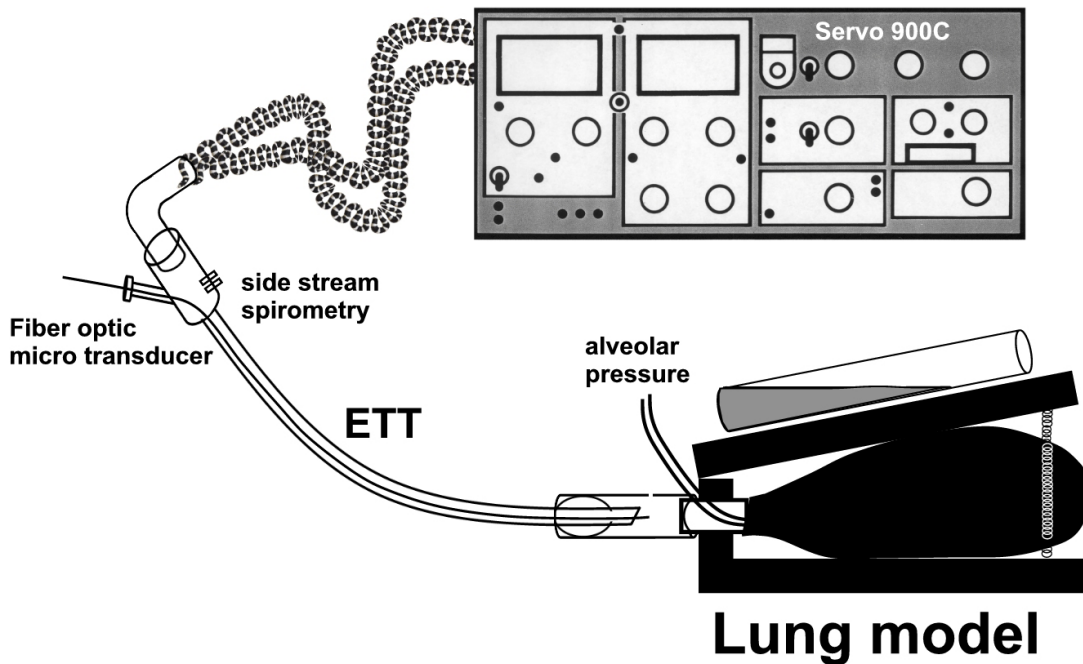


Figure 39. The paediatric lung model for the validation of the DSA consisted of a 1 L ventilating bag enclosed in a hinged wooden casing. A container with low viscous fluid was placed on lid and a spring connecting lid and bottom produced a lower and an upper inflection point during tidal ventilation. Pressures were measured in ventilating bag (\approx alveolus), and at tip of ETT with the fibre-optic pressure transducer. Side stream spirometry was sampled, but not utilised in this set-up.

Results of validation of the DSA in the paediatric lung model

The validation of the DSA in the paediatric model resulted in

- an overall R^2 (SD) of 0.98 (0.015) between calculated alveolar pressure according to DSA and measured alveolar pressure, a slope of 1.03 (0.08) and intercept -0.40 (1.02). Bias and precision were 0.001 (range -2.39 -1.98) and 0.93 (0.46); see Figure 40 and 3a-d, PaperV.

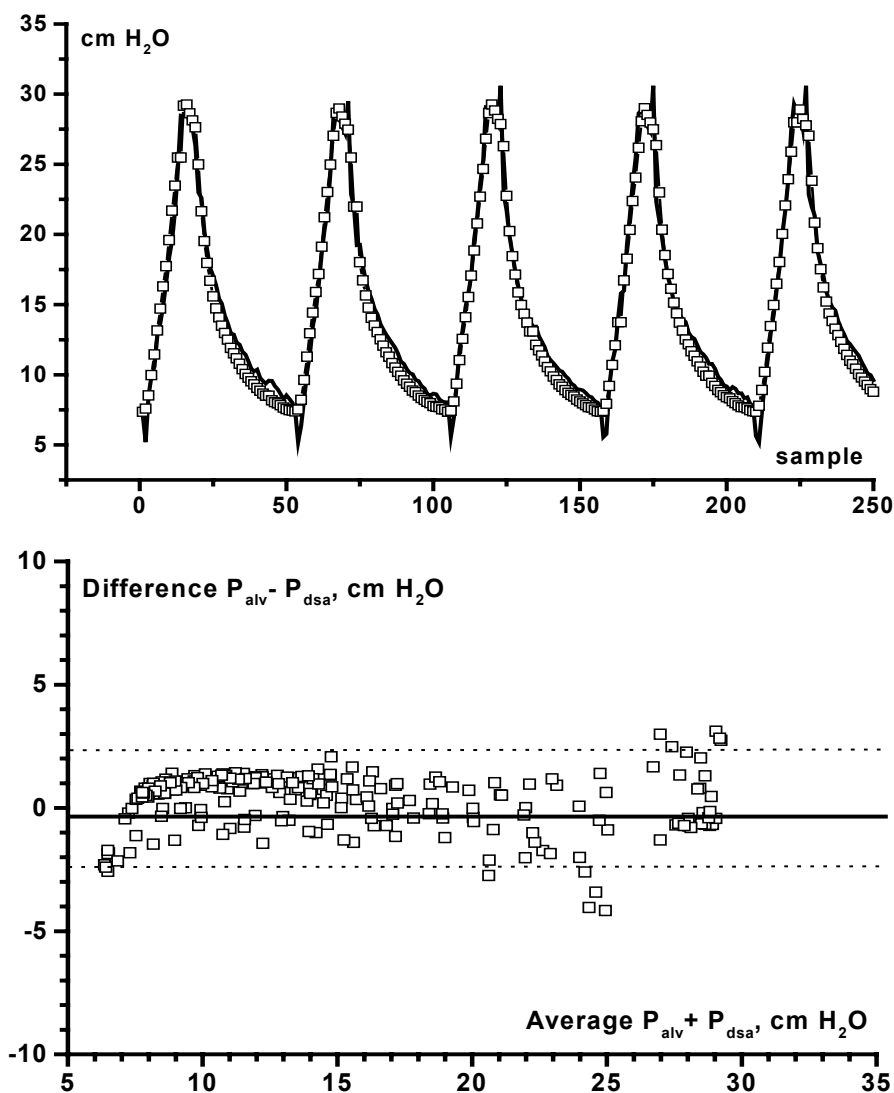


Figure 40. Agreement between calculated and measured alveolar pressure demonstrated in model recording of VCV, ETT 4, MV 3.5 L/min, I:E 1:2, PEEP 5 cm H₂O. Legends (upper figure): full line: P_{alv} measured in lung model, squared line: calculated alveolar pressure according to DSA; (lower figure): full line: bias; dotted line: $\pm 2SD$. Statistical measures: bias 0.31 cm H₂O, precision 1.15 cm H₂O, RMS 1.19 cm H₂O; regression equation: $P_{dsa} = P_{alv} \times 1.02 + 0.58$, R^2 0.97. The DSA estimates alveolar pressure in the clinically important phase towards end-inspiration in excellent agreement with measured pressure. The positive difference at high pressures as well as negative difference at low pressures is due to artifactual spikes in model pressure signal.

- When a version of the equation of motion including a nonlinear component was used for calculating alveolar pressure, regression equation was $P_{dsa} = P_{alv} \times 1.02 - 0.14$ with R^2 (SD) 0.96 (0.03), SD $\alpha \pm 0.07$ and SD intercept ± 1.00 . Bias and precision were -0.1 (range -2.72-1.76) and 1.15 (0.65). This procedure did not contain filters for handling the zones of fast transition; these are the main sources of mismatch between calculated and measured values (unpublished data).

Application of the DSA in paediatric patients

Ten patients were entered consecutively from the OR and PICU after cardiac (five), gastrointestinal (two), dental (two), and orthopaedic surgery (one). Eight patients were orally intubated, two were intubated by nasal route. No selection criteria concerning age or weight were applied. Ages varied from two weeks to nine years with a mean of 2.3 years, median 1.6 years; weights from 3.5 to 17 kg, mean 9.1 kg, median 9 kg. The patients were ventilated with Servo 300 in the PICU and Servo 900 in the OR. None of the patients had primary lung disease, and changes in ventilator settings were made only to demonstrate the potential of the dynostatic algorithm in monitoring tracheal and alveolar pressures.

Results of applying the DSA in paediatric patients

The clinical application of the DSA gave a number of findings:

- The clinical application of the pressure sensor was somewhat demanding. First, the length of connector and tube was measured and marked on the fibre-optic pressure transducer. Then the FOPT was introduced into the paediatric tube by way of a polyethylene catheter, which was retracted to a position outside the connector, see Figure 26, when the transducer was in place at the tip of the ETT. If the FOPT protruded beyond the tip of the tube, it tended to get stuck in the tracheal mucosa.
- The function of the FOPT was undisturbed by routine nursing procedures, such as wound dressing and positioning for radiography.

- The optic fibre sensor showed a tendency to zero drifting, which was easily corrected in TestPoint acquisition software, as PEEP pressure at zero flow was present in ventilator or spirometry tracings between tidal breaths.
- The pressure/volume loop measured in the ventilator differed in several respects from the loop measured below the tube. The area of tracheal P/V loop was approximately one third of the ventilator P/V loop and it was impossible from the shape of the ventilator P/V loop to read the tracheal PIP, PEEP or P_{plat} , see Figure 41.

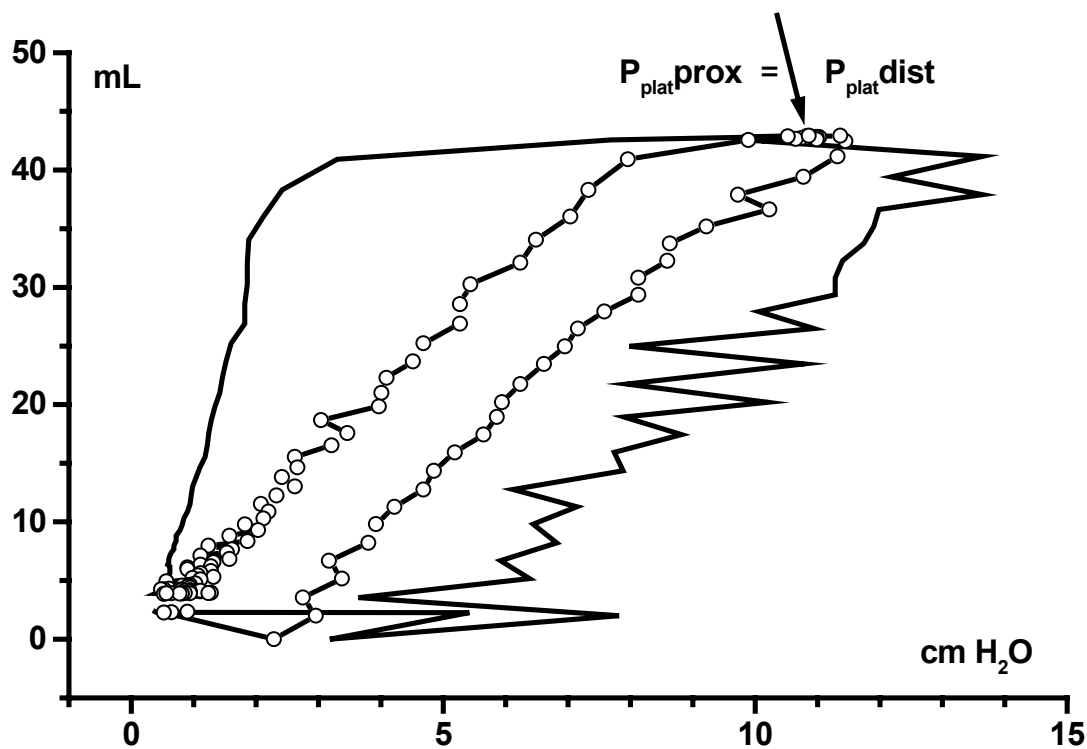


Figure 41. Proximal vs distal pressure measurement. Volume controlled ventilation with ETT 3 at PEEP of zero cm H₂O and 10% end-inspiratory pause. Proximal P/V loop: full line. Distal P/V loop (circled line) composed of signal from FOPT and integrated flow signal from ventilator. Note that the tracheal loop is completely concealed within the proximal loop and there is no possibility of knowing true peak, plateau pressure or PEEP level from proximal loop.

- The ventilator pressure profile is characterised by a linear increase in VCV and a step change in PCV. This difference is attenuated in the tracheal pressure profile and even more so in the alveolar pressure profile as calculated by the DSA, where both seem to rise almost linearly, see Figures 5a and 5b in Paper V.
- The differences between mean pressure calculated from proximal pressure (ventilator) and DSA-calculated alveolar pressure were small and lower in VCV than in PCV. The near-equality of the pressures, however, concealed an underestimation of inspiratory maximum alveolar pressure as well as an overestimation of minimum expiratory alveolar pressure, see Figures 5a and 5b in Paper V.
- Recordings of tracheal P/V loops for smaller dimensions of ETT 3.5 mm ID showed that intrinsic PEEP is generated owing to tube resistance when I:E ratio was changed from 1:2 to 1:1 and 2:1. The intrinsic PEEP during expiration did not show up in the ventilator loop. No lower inflection point was visible.
- Initial, medial and final compliances were seen to decrease as I:E ratio increased due to increased PEEP_I.
- With continuous measurement of pressures from ventilator or Y-piece and trachea as well as flow, the resistance of the endotracheal tube and ventilatory tubing could be monitored and displayed as an analogue trace or a digital value, see Figure 10 in Paper IV.

VOLUMETRIC MEASUREMENT IN He/O₂ MIXTURES (Paper III)

During the fourth decade of last century helium/oxygen mixtures (heliox) made their way into the treatment of airway obstruction. The American pulmonologist Alvin R. Barach described in a series of publications the use and benefits of *heliox* (10, 11, 12, 13, 14, 15, 16, 17, 18, 19). During the Second World War its use diminished owing to war time efforts and the emergence of other therapies for obstructive diseases (168, 169, 170). In the past three decades a number of case descriptions have been published where heliox has been used in paediatric and adult cases of upper and lower airway obstruction caused by asthma, foreign body, malignant compression or infection, and

its use has indisputably been very rewarding in these cases. Recently Hansen (77) and Ball (8) have summarised the publications on case series and clinical trials.

The theoretical benefits of using a low-density gas mixture have attracted intensivists as an option in the ventilator treatment of acute respiratory distress syndrome, ARDS, in spite of the fact that this condition primarily lowers the compliance of the respiratory system, whereas the aerodynamic effect of heliox primarily is attributed to cases with increased airway resistance. A number of problems, however, relate to the changes in density and viscosity compared to oxygen-in-air as normally used in treatment of respiratory failure. Solutions to these have been proposed in (211) using a modified Pitot tube in paediatric intensive care and in (150) during gas flow measurements during exercise.

An algorithm to correct volumetric signals of Datex-Ohmeda side stream spirometry module was developed using the Pitot tube described in Meriläinen (125), cp. APPENDIX for a full derivation.

It may be noted that calculation of flow is based on turbulent flow in the D-lite. At low linear velocity, laminar flow reigns and the software resorts to tabulated values of pressure/flow relationship (personal communication, P. Meriläinen). At laminar flow, pressure difference is calculated according to Poiseuille's law using viscosity rather than density. Mixtures of N_2/O_2 show a linear relationship, increasing approximately $0.3 \mu P/\%O_2$ in the range 20-80% (183-200 μP), whereas mixtures of He/O_2 behave according to a peculiar curvilinear relationship; the difference in viscosity varies between 205 and 222 with a maximum at $F_{I}O_2$ 0.6 of 222 μP , cf. (90, 151). As viscosity enters the equation for ΔP_{lam} in the numerator, driving pressure will actually be increased in laminar flow. This is illustrated in the Papamoschou model (see p. 26) at low flows where the He/O_2 pressure curve is relatively *higher* than the N_2/O_2 curve, albeit at very low absolute pressure. This could indicate that the viscosity and density of heliox is not conducive to flow in peripheral airways. In terms of oxygenation, it must be taken into consideration that bronchiolar laminar convective flow is changing

into diffusive mixing in the distal part of the airway, and that the He/O₂ mixture will facilitate diffusion of CO₂ and O₂, as gas mixing is inversely related to density.

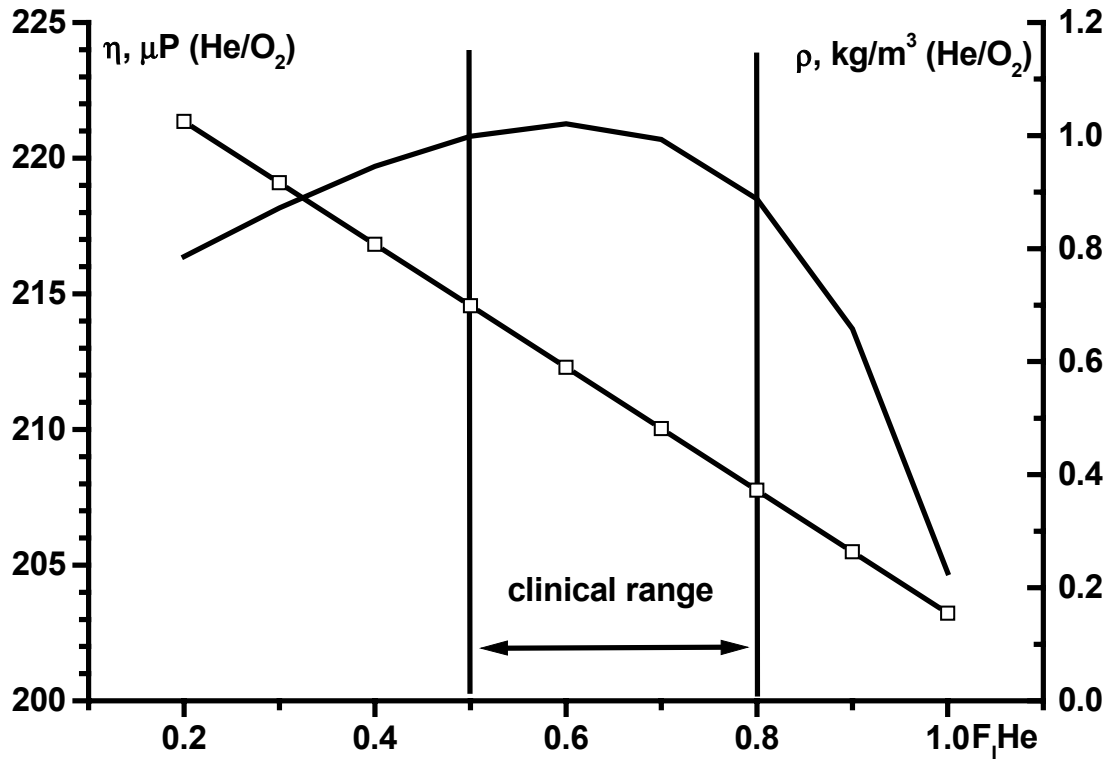


Figure 42. Relationship between viscosity (η , left y axis) of He/O₂-mixtures and F_{IHe} and relationship between density (ρ , right y axis) and F_{IHe} . The figure is based on Prestele (151). He/O₂ demonstrates increased viscosity in clinical range, this implies increased pressure drop at low flow levels.

Calibration of volume voltage signal from Datex-Ohmeda side stream spirometry when using low-density gas mixtures in relation to *measured volume* was performed under two conditions: controlled (VCV, PCV) and spontaneous breathing (SB). In controlled ventilation, *measured volume* was obtained from Biotek Ventilator Tester and in the case of spontaneous breathing, subjects were placed in a body plethysmograph. Three mixtures were used in VCV/PCV and two in SB.

Results of calibration of side stream spirometry (Paper III)

The relationship between voltage signal and BVT volume was perfectly linear for each density and ventilatory mode:

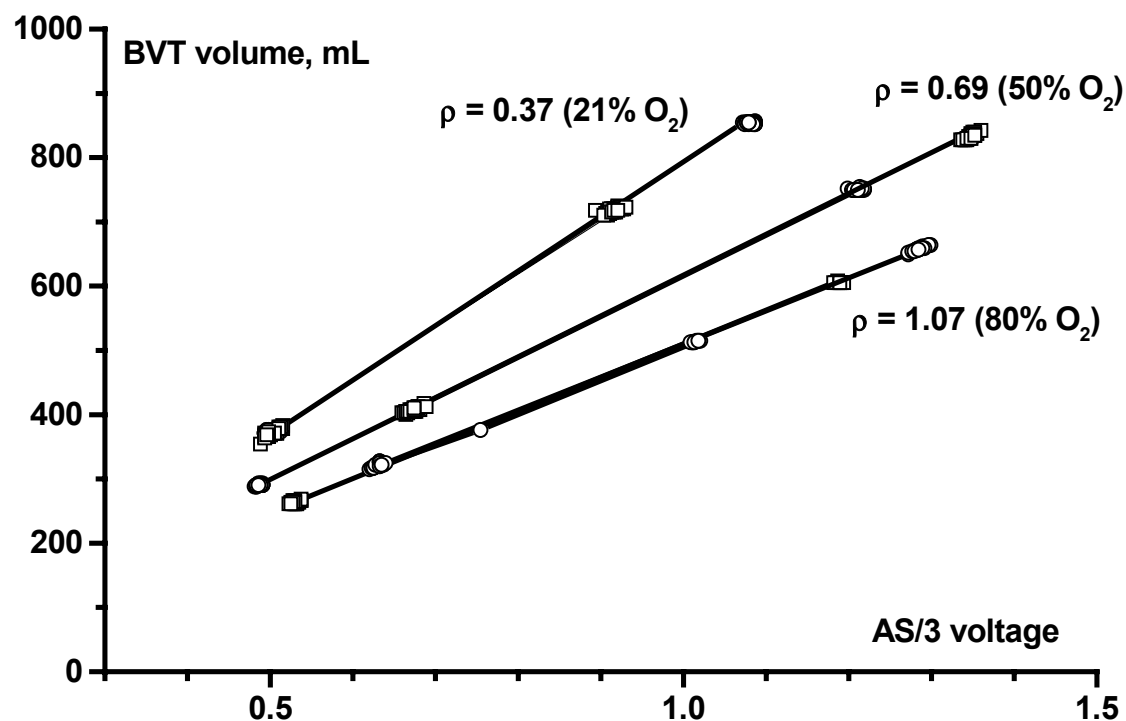


Figure 43. Calibration of D-lite in vitro. Measured BVT volume as function of Datex-Ohmeda AS/3 analogue volume signal and three mixtures of He/O₂. Open circles: PCV, open squares: VCV. Densities (ρ) and corresponding F_IO₂ are indicated in figure.

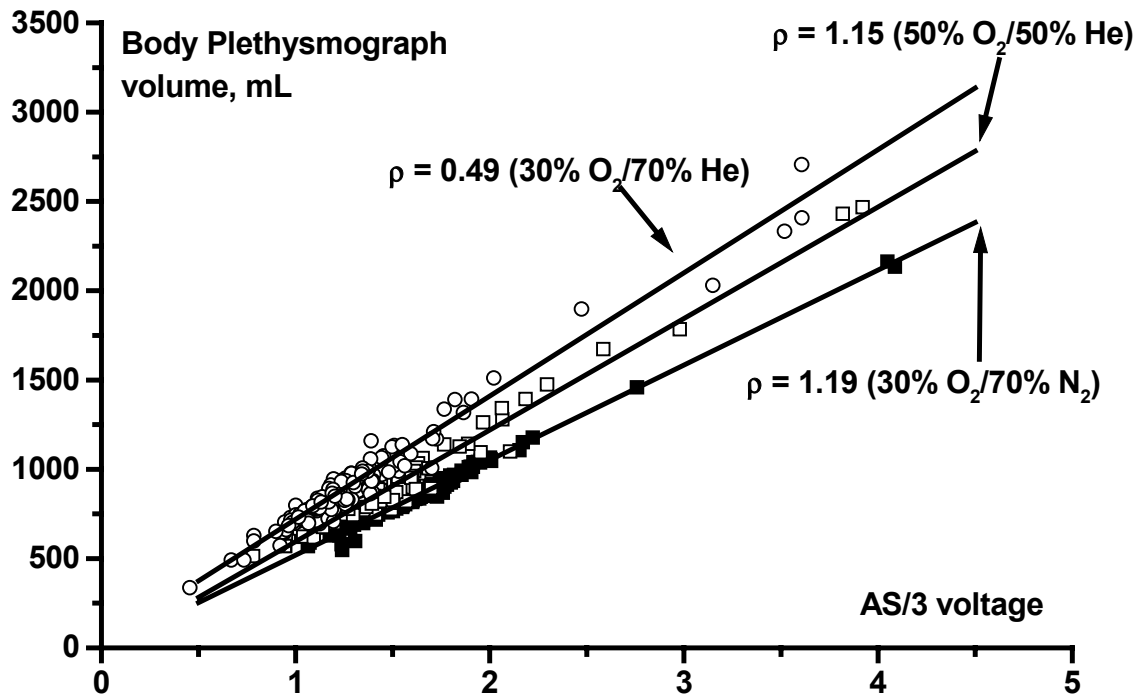


Figure 44. Calibration of D-lite in vivo. Measured body plethysmographic volume as function of Datex-Ohmeda AS/3 analogue signal and three mixtures of He/O₂ and N₂/O₂. Full lines: trends. Densities and corresponding F₁O₂/F₁He are indicated in figure.

As explained in the APPENDIX, p. 127, a corrected AS/3 voltage signal was calculated. This was entered into a multiple linear regression analysis according to a general expression:

$$\text{BVT/BP ("true volume")} = \text{corrected AS/3 voltage} \times k_1 + \rho \times k_2 + k_3 .$$

In the case of N₂/O₂, the density dependent constant was omitted as the software of the AS/3 monitor incorporates a correction for this:

$$\text{BVT/BP ("true volume")} = \text{AS/3 voltage} \times k_1 + k_2 .$$

Calculated constants and statistical measures are shown in Table 5.

Gas mixture and ventilatory mode		k ₁	k ₂	k ₃	R ²	SD %dev	CM
He/O ₂	VCV, PCV	481	67.5	-73.5	99.8	2.3	0.20
	SB	466	65	-39	96.9	5.6	0.68
N ₂ /O ₂	VCV, PCV	517	-18		98.4	2.7	0.35
	SB	532	-11		98.7	3.4	0.61

Table 5. Regression coefficients for ventilatory modes and gas mixtures. Confidence of the mean is calculated according to $\bar{x} \pm 1.96SD/\sqrt{n}$ at 95% confidence level.

The regression equation functioned satisfactorily as demonstrated in these Bland and Altman plots:

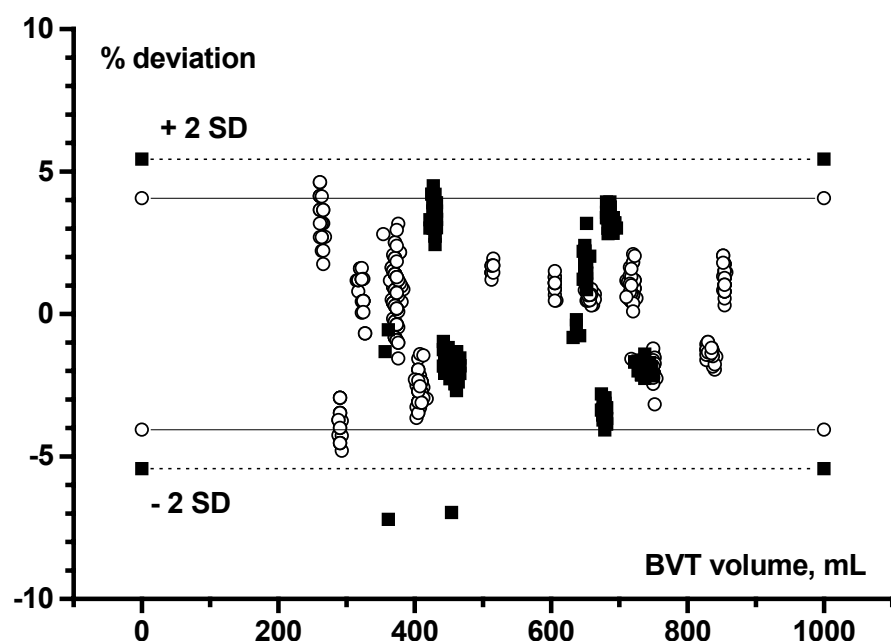


Figure 45. Bland and Altman plot of results of regression equation for CV. Agreement between calculated and BVT volume as percentage deviation of estimated tidal volume PC/VC He/O₂ (density corrected) and N₂/O₂ vs BVT volume. Black squares: N₂/O₂, dashed line: $\pm 2SD$. Open circles: He/O₂, full line: $\pm 2SD$.

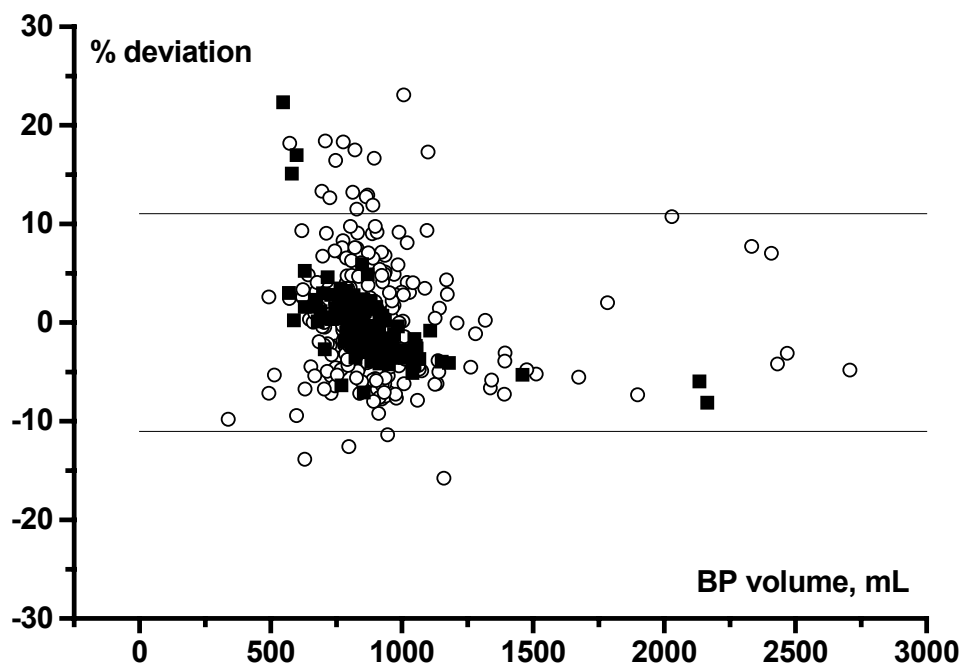


Figure 46. Bland and Altman plot of results of regression equation for SB. Agreement between calculated and BP volume as percentage deviation of AS/3 volume during spontaneous respiration. He/O₂ (open symbols) and N₂/O₂ (filled symbols) vs Body Plethysmographic volume. $\pm 2SD$ -lines for the complete measurement.

SAMPLING, PROCESSING, AND CALCULATIONS (Papers I-V)

Tracheal airway pressure (Papers I, II) was measured through an end-hole of a low compliant air-filled pressure line introduced through the ETT, its end positioned two cm distal to the tip of the tube. The pressure line was connected to a standard pressure transducer for intravascular measurements (pvh medizintechnik, GmbH, Kirchseeon, Germany). For effect on ETT resistance, see (100), and for validation of tracheal pressure measurements, see (102). In paediatric settings (Papers IV, V), a fibre-optic pressure transducer was used.

Oesophageal pressure was measured with a double lumen SalemTM stomach tube no. 16, length 120 cm (Argyle, Sherwood Medical Ltd., Belgium), ID 3 and 0.75 mm (Papers I, II) or conventional single-lumen stomach tube, paediatric size (Papers IV, V).

The tube was passed through the nose into the stomach; the narrow lumen was filled with saline and connected to a standard pressure transducer. The larger lumen was also filled with saline whereupon the proximal end was occluded. The tube was withdrawn slowly into the oesophagus until the pressure curves showed maximal respiratory-related pressure fluctuations and minimal artefacts from heart oscillations.

Correct positioning was verified by the rib cage compression occlusion test (97).

In the most recent version of the DSA, pressures are sampled at frequencies up to 3 kHz from a separate bridge amplifier.

Flow and volume were measured at the Y-piece with a D-lite Side Stream Spirometer connected to an AS/3 multi-module monitor (Datex-Ohmeda Ltd, Helsinki, Finland) (Papers I-III).

In Papers IV and V volume was calculated as time-integrated flow from Servo 300/900C analogue output, no compensation was included in TestPoint programmes for compressible volumes.

Inspiratory and expiratory vectors of flow and volume were identified manually off-line in Papers I and II (first version of DSA); in the second version, these vectors were delineated on-line based on an on-off inspiratory-expiratory analogue signal from the Servo ventilator.

Ventilators: Servo 900C (Papers I-V) and 300 (Papers IV, V) ventilator (Siemens Elema Ltd., Solna, Sweden) connected to a standard adult and paediatric breathing circuit.

Gas mixtures. N₂/O₂ were mixed in standard anaesthetic flow meters by enriching air with oxygen from wall outlet. He/O₂ were mixed from pressurised tank of helium 6.0 (AGA-Linde Gas, Lidingö, Sweden) and oxygen from wall outlet. Gas mixtures were connected to the low-pressure gas inlet of the ventilator (Paper III).

Data: were sampled with a frequency of 20 or 25 Hz from the AS/3 analogue output via an A/D converter (DI220, Keithley, Metrabyte, USA) (Papers I-III) or Data Translation, DT 9804 (Marlboro, MA, USA), (Papers IV, V) and analysed in TestPoint™ applications (CEC, Burlington, Billerica, Massachusetts, USA). These applications

were programmed by the author and Jan Wiklund and comprised the sampling, scaling, and saving of data to a database. Data were retrieved for analysis according to the DSA. In the model experiments, this analysis included a statistical part including regression and correlation, RMS, and Bland and Altman analysis with bias and precision. In clinical and model experiments, the analysis included the calculation of volume dependent compliance. The technical evaluation of the fibre-optic probe necessitated TestPoint applications handling response time, constant and dynamic flow dependent resistance as well as comparisons with mathematical models of calculation of flow resistance.

DISCUSSION

The **contributions** of the present work are:

- the establishing of tracheal pressure measurement in adults and children;
- the incorporation of tracheal pressure measurement in the DSA;
- the validation of the DSA for calculating the alveolar P/V curve as well as the alveolar P/t curve in adult and paediatric lung models. The calculation is performed continuously without calling for special manoeuvres or changing of ventilator settings. The feasibility of the algorithm was investigated clinically in adults and children.
- the establishing of a calibration algorithm for He/O₂ in combination with a Pitot type spirometer. The calibration worked very well in controlled ventilation modes and spontaneous breathing, and may easily be integrated in the DSA for future trials of possible clinical benefit of heliox in ARDS/ALI.

The introduction and application of the DSA naturally provokes a number a questions, which I intend to **discuss** under the following headings:

- Is the DSA related to a lung model?
- Can you really equate R_I with R_E ?
- What are the advantages of *tracheal pressure* measurement?
- Clinical impressions; and
- Low-density gas mixtures in severe lung disease.

Is the DSA related to a lung model?

The dynostatic algorithm rests on a long tradition of investigations into lung mechanics dating back to 1915. As detailed above, at least two approaches may be discerned: the interventional, and the computational, detailing the complex relationship between volume and pressure, and flow and pressure. The DSA belongs to the computational

group. Originally, the DSA was conceived as a method of *computing* alveolar pressure. The method of calculation may be apprehended by reference to a linear, one-compartment version of the equation of motion⁷. Instead of threading the usual way through multiple linear regression with a number of constants to account for linear as well as nonlinear phenomena, the DSA defines the relationship between pressure and flow at an arbitrary number of volume levels, making the assumption that inspiratory and expiratory resistances are equal – or almost equal. Understanding the DSA as a reflection of the one-compartment linear version is certainly without sophistication, but - for a start - it is completely transparent, easily implemented, simple, and modest in its description of physiological parameters (compliance and resistance). The choice of model and method of calculation becomes a trade-off between transparency (how do elements in the model/equation identify biological phenomena?), simplicity (Occam's razor⁸), implementation (incorporation in monitoring equipment), descriptive purpose (what do we wish to calculate and trend: tissue elastance/resistance, chest wall, and the clinical usefulness, &c.?).

The linear, one-compartment model cannot incorporate nonlinear phenomena, such as the curvilinear static P/V curve, nor frequency-dependent phenomena, such as viscoelasticity, nor the separate characteristics of lung and chest wall. As described in the historical parts, the assumption of linear relationships between pressure/flow and pressure/volume is “bending nature against her will”. Optimally, but unrealistically, one would like to include the Jaeger and Matthys formulation of the inspiratory pres-

⁷ The equation has its origin in Newton's third law (Axiomata sive leges motus, Philosophiae naturalis principia mathematica, 1687): *“To every action there is always opposed an equal reaction; or the mutual actions of two bodies upon each other are always equal, and directed to contrary parts.”*

⁸ Occam's razor is a principle attributed to the 14th century logician and Franciscan friar William of Occam. The principle states that ‘pluralitas non est ponenda sine necessitate’ (entities should not be multiplied unnecessarily).

sure/flow relationship, and the Hardin (78) or the Lambert (107) expiratory pressure/flow relationship instead of the term $(R \times \dot{V})$. In recognition of the nonlinear P/V relationship, one may wish to implement an exponential or polynomial expression as described by Venegas (202). Other attempts to include nonlinear phenomena are expressed in equations containing nonlinear components relating to elastance and/or resistance. In order to fathom the frequency dependent and multicompartment aspects of lung mechanics, one must look to the models of Otis, Bates, Bijaoui, Lutchen, or Suki.

A consequence of the assumption of equal resistances at isovolume levels somewhat modifies the *linear* aspect of the model/equation: it is important to realise that the algorithm only assumes *a* linear relationship, $P_1 = k_{F1} \times \dot{V}_1$, between pressure and flow at *each* isovolume level as well as pressure and volume $P_1 = k_{V1} \times V_1$. At neighbouring isovolume levels the relationship is still linear, $P_2 = k_{F2} \times \dot{V}_2$ and $P_2 = k_{V2} \times V_2$, but not necessarily identical to the former. The assumption implies that nothing is said about the relationship between neither compliance and tidal volume or flow, nor resistance and tidal volume or flow. Compliance as a function of volume, $C_1 = f(V_1)$, and resistance as a function of flow, $R_1 = f(\dot{V}_1)$, may turn out to be a sigmoidal or an nth order polynomial.

This makes it possible for the relations C/V and R/ \dot{V} to be nonlinear.

Inertance is not included in the DSA. This implies that the isovolume-specific values of C and R will have to “swallow” inertance at start inspiration and start expiration. Inertance is hardly of importance in adult ventilation, but in the paediatric setting with high respiratory frequency, small tube diameters and, as a corollary, fast acceleration of air during initial parts of inspiration and expiration, it may play a role and has been added in the description of endotracheal tube resistance (76).

The temporal expansion of the alveolar P/V curve is performed on a template of volume and time. The V/t-vectors work as a look-up table connecting the volume of the

P/V curve with a specific time, which is then plotted vs the pressure in the P/V curve in a P/t plot. Volume is constant during end-inspiratory pause in VCV, and consequently the alveolar pressure is constant, too. A rapid drop followed by a slowly decaying pressure is seen in the *tracheal pressure* during end-inspiratory pause, and one may expect this to be reflected in the alveolar pressure. The fact that this is not so in the DSA, may be seen as a drawback or it may raise the question whether this consequence of the viscoelastic properties, &c. is actually transmitted to the alveolar level? Other approaches to respiratory mechanics *do* demonstrate exponential decay during end-inspiratory pause in calculated alveolar pressure, but the same question may be raised: is it an artifact of the method or is it a real event?

The fact that the dynostatic algorithm is based on directly measured, narrow, tracheal P/V-loops is the main explanation for its tolerance against different inspiratory/expiratory resistance ratios. The total difference between inspiratory and expiratory pressures at isovolume levels is usually within 8 cm H₂O (Figure 47) and the alveolar pressure cannot be outside these limits. Therefore, even if the resistance difference between inspiration and expiration is doubled, the dynostatic pressure curve will be minimally displaced and the endpoints (to which the alveolar P/V curve is extrapolated) will remain the same whatever the resistance ratio.

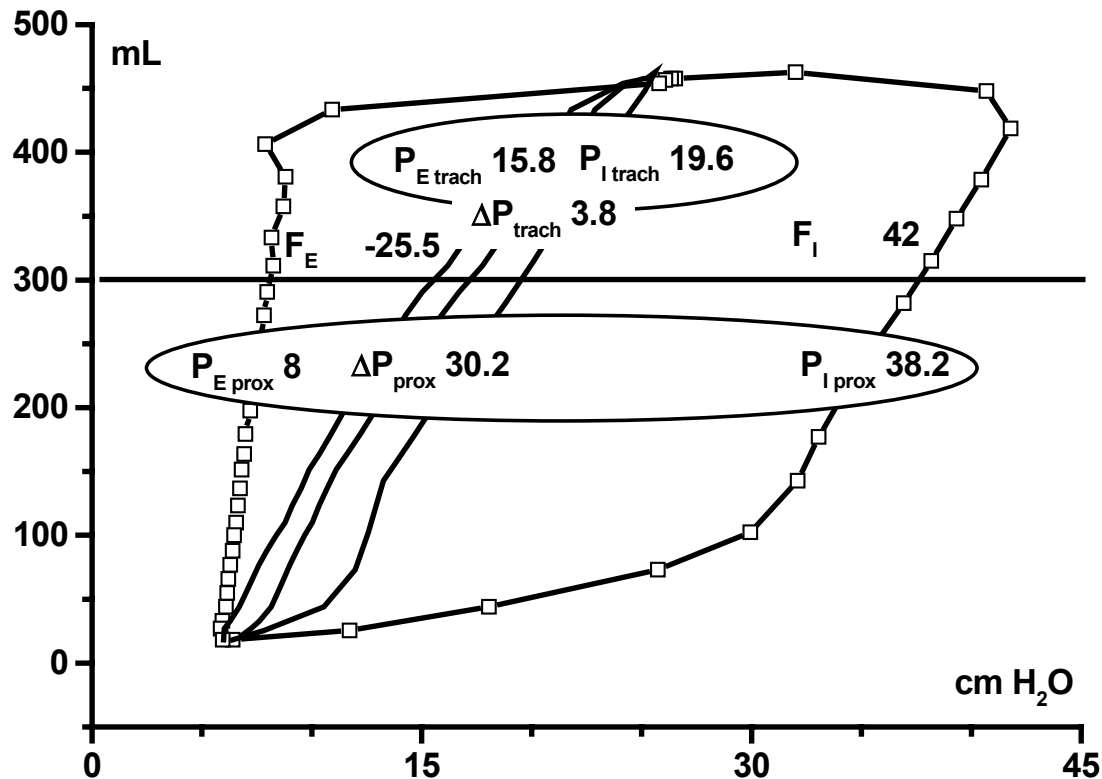


Figure 47. Robustness of dynostatic algorithm. A proximal (squares) and a tracheal P/V loop (full line). At the isovolume level of 300 mL, the pressure difference in proximal pressure is 30.2 cm H₂O, whereas the difference between inspiratory and expiratory tracheal pressure is only 3.8 cm H₂O. The algorithm is very robust even if the inspiratory and expiratory resistances are not on a par; in the above example, P_{dyn} at 300 mL is 17.3 cm H₂O. If expiratory resistance were doubled, P_{dyn} will increase by 0.6 cm H₂O to 17.9 cm H₂O. This difference is without clinical importance.

Can you really equate R_I with R_E ?

The DSA contains the assumption of equal - or almost equal - inspiratory and expiratory resistances at identical volumes during tidal breathing. Based on available evidence, this assumption does not seem farfetched. The position is somewhat modified as it is recognised that equality of resistances cannot exist at the beginning and end of inspiration/expiration. Therefore, an extrapolation algorithm is implemented based on

the central part of the alveolar P/V curve. The assumption of equal resistances releases the DSA from the vice-like grip of the MLR method. As explained above, the equation may cover the whole respiratory cycle, producing single values of compliance and resistance. Alternatively, it may be formulated to cover the inspiratory and expiratory limbs separately, thus producing a set of inspiratory compliance and resistance values and a set of expiratory compliance and resistance values (140, 197). Theoretically, the inspiratory and expiratory limb may even be subdivided into smaller parts, each of which may be subjected to MLR; the analysed part may even “slide” through the vectors. In my experience, this procedure does not give reasonable results as the variation of the constants C and R within the smaller vectors grow inversely with the size of the subvectors. It is an inherent feature of the MLR that it works better with values at “extremes” (182), which is why it cannot be applied to smaller sections of inspiratory or expiratory vectors. The signal-to-noise ratio becomes critically low. In order to handle the nonlinearities of resistance, additional constants have been applied in the equation of motion, increasing the congruence between measured and calculated values of pressure, but simultaneously clouding the relationship to the physiological modelling.

The “ $R_I=R_E$ ” axiom is not unique in the description of lung mechanics; the Nikischin modification (139) of the Mead and Whittenberger method (123), and the SLICE method (73, 127, 129) made the same assumption without specific motivation (personal communication, Mols). The assumption does not appear unfounded if looking at values reported for inspiratory and expiratory resistances, cf. Figure 24 and Table 1, though the methods of calculation are aimed at *overall* resistance values, rather than volume dependent resistances. It is noteworthy - with the same reservation - that the ratio $R_I:R_E$ in the Pesenti study of ARDS patients (147) was 1:1.4 at ZEEP, 1:1.5 at 5 cm H₂O, 1:1.6 at 10 cm H₂O and 1:2 at 15 cm H₂O PEEP. The corresponding ratios in COPD patients are 1:1.9, 1:1.4, 1:1.3, and 1:1.3. These ratios are well within the limits of the optimal “working range” of the DSA.

The 1:1 ratio is known to fail in cases with expiratory flow restriction (EFL). This is observed in COPD patients and in patients with ARDS (105, 198) in special circumstances, i.e. spontaneous ventilation, negative expiratory pressure, NEP, or zero end-expiratory pressures, ZEEP. The observation of EFL during controlled ventilation should make the physician act to eliminate it by changing I:E ratio, PEEP level, or tube size. EFL during spontaneous ventilation, NEP, and ZEEP is outside the scope of the DSA. A similar situation occurs in inspiratory flow limitation due to extrathoracic or upper airway obstruction and laryngomalacia. The question of the DSA in combination with COPD (including hyperreactivity) is more delicate: at the present stage of development, the DSA is not recommended in patients marked by obstructive lung disease.

Neither the interventional nor the computational approaches offer a gold standard for measuring airway resistance *at any point* during the respiratory cycle. Whatever method is used, it is important to realise the domain of the calculation: total respiratory system, lung and chest wall, lung and lung tissue, lung AND the assumptions: constant compliance, equal inspiratory and expiratory compliance (this is also the position of the DSA due to the “no hysteresis”-assumption), equal inspiratory and expiratory resistance during inspiratory and expiratory limb, in slices, in an arbitrary number of volume levels...&c.

What are the advantages of *tracheal pressure* measurement?

The resistance of the tube presents the largest single contribution to total airway impedance, and algorithms have been proposed in order to subtract the viscous pressure loss from proximal pressure to obtain tracheal pressure. First, several investigators have demonstrated the curvilinear pressure/flow relationship in *clean* endotracheal tubes of paediatric as well as adult dimensions during *constant* unidirectional flow (34, 71, 76, 196). This has led to second order polynomial expressions a.m. Rohrer (who formulated these for highly branching systems of tubes....) with constants spe-

cific for each diameter, length and flow direction. In paediatric tubes a constant for inertial forces has been included, and more complicated schemes have been proposed taking density, viscosity, and tube curvature into consideration (89). The prerogatives *clean tube* and *unidirectional flow* are obtainable only in the laboratory. In the clinical setting, ventilatory flows are oscillatory and tubes are seldom clean. A computer algorithm for the estimation of tube vs lung obstruction has been proposed, but necessitates calibration of tube obstruction vs changes in the pattern of time constants which the algorithm refers to (74). Furthermore, the bench test represents only one configuration of the transition from connector to tube and tube to trachea; these regions are recognised as containing flow profiles of contraction and expansion giving rise to highly unpredictable pressures (112, 178, 205, 213).

We have suggested a solution to these problems by using a catheter inserted into the ETT lumen and advanced to the region of the tip of the tube. The technical background of tracheal pressure measurement in adult-sized ETT was thoroughly described by Karason (102), cf. discussion (111). In conclusion, he demonstrated that an end-hole catheter, 2.0x0.9 mm, placed in a region from two cm above to two cm below the distal opening of the tube, reliably transmitted pressure variations with acceptable time constant. Objections concerning the possible differences between *static* pressure measurement during inspiration vs total (*dynamic+static*) pressure measurement during expiration turned out to be unimportant in this setting as the contribution of dynamic pressure ($=1/2 \times \rho \times \bar{V}^2$) is minimal owing to the low density of air (= 1.1 g/L). The drawback of the method is the encroachment on luminal area and emergence of intrinsic PEEP due to expiratory flow restriction in the tube. This can be minimised by choosing smaller dimensions of catheter, thus a polyethylene catheter OD 1.57 x ID 1.1, has a smaller influence on resistance and still shows a time constant of less than four milliseconds.

In paediatric tubes, it becomes unfeasible to use polyethylene catheters owing to small dimensions. In addition, time constants are incompatible with paediatric monitoring – the smaller the catheter, the longer the time constant, the greater the phase lag between

signal (tracheal pressure) and response (measured pressure). Algorithms for calculating tracheal pressure in paediatric tubes have been suggested (76, 89), and the same objections may be raised: these algorithms cannot possibly account for the influence of secretions, kinking, change of curvature, &c. which will invariably occur in the clinic, if not in the laboratory. A strong warning regarding varying tube resistance has been issued (178).

We have suggested a solution in the form of a fibre-optical pressure transducer, which is inserted into the lumen of the paediatric tube. We have shown that it is a reliable, fast responding pressure transducer for use in paediatric respiratory monitoring (Papers IV and V). The clinical implementation in terms of long-term use has yet to be investigated.

The DSA was developed and tested using conventional monitoring equipment, in our department Datex-Ohmeda monitoring equipment and Siemens ventilators, emphasizing the direct link between development and implementation of algorithms without recourse to advanced laboratory equipment. Today, we have replaced the pressure module of the Datex-Ohmeda AS/3 with a small bridge pressure amplifier in combination with a Servo ventilator 300 or 900, an A/D converter and a personal computer. The advantages are obvious. The equipment is ubiquitous and can be put up next to the patient whenever need arises for dynostatic respiratory monitoring. Software has been developed in continuing correspondence with manufacturers of monitoring equipment and clinicians in a constant exchange of ideas; the step from development to clinical implementation should not be insurmountable.

Clinical impressions

So far (August 2002) the DSA has been used clinically and experimentally in paediatric and adult patients (Papers I, II, IV, and V), in a preliminary heliox trial (unpublished observations), and in an animal endotoxin model of ARDS (98).

The Dynostatic Algorithm is – to my knowledge – **the first method for on-line, continuous calculation and display of tracheal and alveolar pressure**. The tracheal pressure is easily accomplished in monitoring of ventilator treatment of adult patients; the measuring catheter is introduced into the tube via a connector and delivers continuous registration of tracheal pressure independent of tube size and secretions. In cases of expiratory flow restriction due to bronchoconstriction, inverse I:E ratio or small tube size in combination with large tidal volumes, the tracheal pressure may deviate considerably from the conventional proximal pressure due to build-up of intrinsic PEEP, which will go completely undetected in the proximal pressure curve unless the clinician initiates end-inspiratory pauses. A mathematical method (LSF) has been proposed to estimate intrinsic PEEP (54), but this method still has to rely on the tube being clean and unobstructed, otherwise too large a portion of total pressure will be apportioned to the flow-resistive pressure component.

In ventilatory modes without end-inspiratory pause, proximal pressure differs from tracheal pressure due to tube resistance, and the more so the smaller the tube and shorter the I:E ratio. This is demonstrated only if a pressure line is inserted into the tube. Calculation of tracheal pressure from proximal pressure, flow and tube size is unreliable in the presence of secretions, but may possibly be remedied by mathematical methods analysing the time constant of expiration. The calculation, however, must repeatedly be verified by a pressure line inserted into the tube – which was our starting point.

A lower inflection point was not observed in the alveolar P/V curve during clinical monitoring, but could be produced by ventilator disconnection leading to reestablishment of atelectasis and re-expansion during inflation. Even though the external PEEP in some patients may not have been optimal (in the sense that it was higher than a hypothetical lower inflation point), lung collapse may have been avoided by short inter-breath period. More often, the alveolar P/V curve presented a decreasing compliance during inspiration. It was not evident *which* point should be designated upper inflection point, although definitions have been proposed, cf. (137); rather one would prefer

to designate it *upper inflection zone*, *UIZ*. In cases with decreasing compliance during inspiration, the conventional compliance happened to lie *outside* the tracheal P/V loop, which of course is not possible and points to the inability of semistatic or static compliance to capture the volume-dependent compliance.

In proximal pressure tracings, the difference between PCV and VCV is marked by step increase to constant pressure *vs* linear increase in pressure. In adult respiratory care, it is a time-honoured technique to change ventilation from VCV to PCV when oxygenation falters or insufflation pressure becomes “troublesome” (*proximal* insufflation pressures, N.B.). The effect may be explained by the phenomenon of ‘volume persistence’: the inspiratory volume is displaced to the alveoli faster in PCV compared with VCV, leaving more time for gas exchange, mean alveolar pressure is higher and incidence of PEEP_I likewise. In *paediatric* monitoring, the alveolar pressure *vs* time demonstrated an attenuation of the difference between PCV and VCV with the logical impact on the difference in volume displacement. This may be reflected in the discussion concerning choice of ventilatory mode in infants, cf. Sinha (175), who investigated VCV *vs* PCV in preterm infants and found that the group on VCV met “success criteria” faster: lower arterial-alveolar O₂-difference, shorter time on ventilator, and lower mean airway pressure compared to the group on PCV. The VCV-group of infants had a significantly lower incidence of intraventricular haemorrhages and abnormal periventricular echodensities on ultrasound. Bandy (9), tested VCV as a “rescue modality” in six babies and concluded that “preliminary analysis of pulmonary function during volume-controlled ventilation suggests differences in the patterns of delivery of tidal volume and minute ventilation, which are more consistent. This may improve stabilization of lung volume and decrease ventilation-perfusion mismatch”.

Low-density gas mixtures in severe lung disease

In the studies concerning protective lung ventilation, cf. Table 3, significance between groups was obtained with large differences in V_T and/or pressure. These differences are possible only in the experimental situation. Bedside, the clinician would (proba-

bly) not half the ventilation of the patient in one sweep; instead minor changes would be initiated and the clinical course followed by blood gases, CT, pulmonary X-ray, &c. The challenge in the clinical situation thus becomes one of diminishing the noxious stimuli by small steps without a guaranteed return in terms of lowered morbidity and mortality. The noxious stimuli to the lung are expressed in terms like volu-, baro-, atelec- or biotrauma. The question of which being primary culprit and which accomplice – volume, pressure, ventilator mode, focal (lung) or global disease – is still unanswered. Therefore, efforts must be directed towards reducing volume as well as pressure, searching the least deleterious ventilator mode (by adjusting the settings to the respiratory mechanics) and defining adjuvant treatment. The use of low-density gas mixtures *may* represent an option for lowering pressure and/or volume in selected cases. The primary mechanical feature of ARDS and ALI is a diminished compliance due to tissue oedema, inactivation of surfactant, and destruction of tensile elements. Less interest has been invested in the question of resistance changes in these disease states, though it may be expected that resistance will change, too, owing to exudation and transudation, secretion, increased bronchial reactivity, and cellular debris. Next, generation level of increased resistance in the bronchial tree must be established in order to ascertain type of flow (laminar/transitional/turbulent). As detailed above, laminar pressure/flow relation is “regulated” by the equation of Poiseuille, in which viscosity is determinant, whereas turbulent pressure/flow is determined by density. Thus, only pressure/flow in generations with turbulent flow due to diminished diameter and increased resistance, will benefit from a change to a low-density gas-mixture – if the density change is large enough to induce changes in pressure/flow. This can be estimated in the Jaeger and Matthys or Papamoschou models, see pp. 24ff. Spirometry with forced expiratory manoeuvres in a cooperative patient is necessary in order to diagnose “small airways disease” (lowered MMF) and/or EFL. This is hardly feasible in the ICU patient; other surrogate measures must be found (e.g. passive exhalation time constants) or the patient may be treated *ex juvantibus*.

The calibration of the Pitot type venturimeter is *instrumental* to a clinical evaluation of heliox. The construction of the D-lite provokes turbulent flow across a constriction with a short distance to normalize the flow profile. The sensors of the Datex-Ohmeda AS/3 measure O_2 , CO_2 , N_2O , and Anaesthetic Agent, and the software calculates density on the assumption that the balance is N_2 . Datex-Ohmeda AS/3 uses a paramagnetic principle which is undisturbed by the presence of helium (this is in contrast to the measurement of CO_2 based on extinction of infrared wavelength).

The present evaluation deviates from these presuppositions: using He/ O_2 -mixtures lowers resistance in the D-lite, converting a turbulent flow into a laminar. Under measuring conditions using “normal” gases, the software implements tabulated flow values when pressure difference is low and flow is expectedly laminar. Naturally, this algorithm is involved also when using low-density gas mixtures, and the more so as a greater proportion of flow states are laminar. This may explain the success of adding density to the linear estimate. This, however, was without effect when tried on data from spontaneous breathing, but it may be assumed that quiet breathing largely generates small pressure differences and laminar flow states, and the effect of adding density independently may be obscured by these circumstances. Spontaneous breathing entails much greater biological variation per se compared with controlled ventilation. Analysis proceeded from minimum and maximum values of the *inspiratory* limb, assuming a density correction based on exchanging He for N_2 . In the lung model, composition of inspiratory and expiratory gas is unchanged, but - theoretically - in vivo the use of inspiratory values (based on a two-gas mixture) introduces an error when these values are used for calculation of expiratory volumes, as the AS/3 corrects density including F_{ECO_2} . The error, though, is infinitesimal. Since the publication of our calibration study, Tassaux (193) has published an investigation of seven ventilators, calibrating them for use with heliox. He showed that the Servo 300 from Siemens performed equally well with air and heliox, and in fact was in no need of calibration.

CONCLUSIONS AND PERSPECTIVES.

The DSA is based on flow signal, flow integrated to volume, and tracheal pressure measured by polyethylene catheter in adult respiratory care or fibre-optic pressure transducer in paediatric respiratory care.

- Long-term measurement of tracheal pressure is feasible in the monitoring of respiratory mechanics in adults.
- Tracheal pressure measurement in paediatric patients is obtained by fibre-optic pressure transducer.
- The use of tracheal pressure measurement in adults and children obviates the need of calculating the pressure reduction of the tube and presents the true tracheal pressure, tracheal peak inspiratory pressure, and emergence of intrinsic PEEP. These features are not demonstrated in proximal pressure measurement.
- The DSA has been validated in adult and paediatric lung models including respiratory variables like I:E, PEEP, V_T , R_I : R_E , pause, viscoelasticity, linear and nonlinear pressure/flow, and pressure/volume relationships. There is a high degree of agreement between measured and calculated values of alveolar pressure in all models in terms of P/V loops and P/t curves. Calculation and display of alveolar P/V curve and alveolar pressure vs time are continuous and independent of ventilatory mode and special manoeuvres.
- The continuous display of the alveolar P/V curve reveals tendencies to overdistension, which does not appear in the conventional two-point compliance value calculated from values of volume and pressure at zero flow before inspiration and expiration after end-inspiratory pause.
- The calibration of spirometric volume signal in He/O₂-mixtures resulted in good agreement between measured and calculated volume. The calibration algorithm may be included in the DSA for investigational or clinical purposes.

ACKNOWLEDGEMENTS

The one aim of this thesis, which has not been declared so far, is the mere pleasure of the *exercitium mentale*. Numerous people have contributed to making this exercise an enjoyable one in terms of convening medical, technical, and mathematical dexterity and exploring - to me - unknown areas in the field of biotechnology in its broadest sense.

Professor **Ola Stenqvist** has been – and continues to be - a ceaseless source of ideas; I am most grateful for being enrolled in his combination of straightforwardness, openness, and insistence on making simple things simple and complex things possible. It has been a great experience to participate in this fruitful synergy of inventiveness, simplicity, endurance, and serendipity. Associate Professor **Stefan Lundin** has contributed with an eminent sense of coherence amidst confusing details, whether in laboratory work or in preparing manuscripts and presentations. His use of Occam’s razor is most admirable. My closest co-author, **Sigurbergur Kárasen**, MD; Ph.D. with great persistence has wrung the utmost out of experimental set-ups and clinical applications during the testing of the dynostatic algorithm. His systematic approach to respiratory mechanics, as expressed in his dissertation, has been a great inspiration and incitement in this continuation of work on respiratory mechanics in general and the dynostatic algorithm in particular. His personal calm and good humour have been a large part of the pleasant atmosphere of the project, and I greatly deplore his return to Iceland, despite the fact that Icelandic health care must profit tremendously from it. **Jan Wiklund** at the Department of Biomedical Engineering has been a safe haven when technical problems needed a solution, when programming did not work as expected or mathematical derivations were in need of confirmation. I am most grateful for his availability and interest in discussing these matters in intelligible “engineer talk”.

During the later part of the project, I made closer acquaintance with Associate Professor **Krister Nilsson** and **Angela Hanson**, MD at the Department of Paediatric Anaesthesia and Intensive Care, the Queen Silvia Children's Hospital. They have helped me include paediatric respiratory monitoring in a wider perspective. Krister, furthermore, has supplied the paediatric articles with an eminent stylistic sense in combination with a meticulous scrutiny of the "signifié", and Angela has showed me how to handle paediatric patients as well as their parents. In unproportionate return, I have shown her a few shortcuts when handling a personal computer.

Numerous, if not innumerable, people have contributed to the work through correspondence, discussion, and explanations. I wish to thank them all, pro- as well as antagonists.

Göran Hedenstierna, Professor of Clinical Physiology at the University of Uppsala; **Josef Brunner**, MD at Hamilton Medical AG, Rhaeuzens, Switzerland; and **René Coffeng**, Head Engineer, Datex-Ohmeda, Helsinki, Finland

- not to mention **Ola**, **Stefan**, **Krister**, **Jan**, and **Sigge**- have provided me with invaluable comments and feedback on preliminary versions of this manuscript for which I am most grateful. Their suggestions have certainly clarified my position.

Elisabeth Mourier Havrehed, state-authorized translator, has made every effort to correct my English and Greek usage. Whatever errors remain is my responsibility.

AGA-Linde, Datex-Ohmeda, Samba Sensors, Gothenburg Medical Society, and the Faculty of Health and Caring Sciences, Gothenburg University have generously provided financial support for the completion of the thesis.

It does *not* go without saying that my wife, **Kirsten**, has been a never-yielding companion throughout the project. She has brought to life and blooming our children, Anna and Niels, at the same time pursuing her own interests in anaesthesia and observing my mechanical breathing exercises with sound judgement and some astonish-

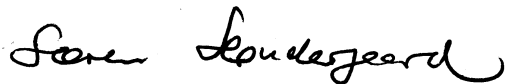
ment. She has provided the stage for this whole play. She is the answer to the saying
“Cherchez la femme” – here she is!

Without the constant wealth of ideas and suggestions from my colleagues, this thesis
would have been completed many years ago, and without my wife’s insistent interest
in the progress of the project, this thesis would never have reached completion.

I am most grateful for the patience of all parties involved and dedicate this work to
“my still patient family”:

Kirsten, Anna, Niels, Stine, and Marie.

Möln dal, October 1st, 2002

A handwritten signature in black ink, reading "Søren Lundegeard". The script is cursive and fluid, with the first name "Søren" and last name "Lundegeard" clearly distinguishable.

APPENDIX

Jaeger and Matthys

$$(xxx) \quad C_d = \frac{\dot{V}}{A} \sqrt{\frac{\rho}{2 \Delta P}}$$

Calculation of discharge coefficient.

$$(xxxii) \quad C_d = \frac{A_1 - A_2}{1 + (Re/Re_{\text{central}})^p}$$

Logistic fitting equation for curvilinear relation between C_d and Re . Constants:

A_1 0.25, A_2 0.89, p 1.4, and Re_{central} 549.0

$$(xxxiii) \quad \Delta P = \frac{1}{C_d^2} \times \frac{1}{A^2} \times \frac{\rho \times \dot{V}^2}{2}$$

Reorganising the equation of discharge coefficient for calculation of pressure drop.

Papamoschou

$$(xxxiiii) \quad \dot{V} = \pi \times \sqrt{\frac{1}{8} \frac{\Delta P}{L_{\text{eff}}} \frac{D_{\text{eff}}^5}{\rho f}},$$

Derivation of relation between flow, pressure, effective length and diameter according to Papamoschou. The friction factor, f , being dependent on the value of Reynolds' number.

Bates

$$(xxxv) \quad \Delta R = R_2 / (1 + \omega^2 \times \tau_2^2),$$

relating the resistance contribution from tissue to the time constant of the viscoelastic element and frequency.

$$(xxxvi) \quad \Delta E = \omega^2 \times \tau_2^2 E_2 / (1 + \omega^2 \times \tau_2^2),$$

relating the elastance contribution from tissue to the time constant of the viscoelastic element and frequency.

Otis

$$(xxxvii) \quad R_e = \frac{\omega^2 T_1 T_2 (T_2 C_1 + T_1 C_2) + (T_1 C_1 + T_2 C_2)}{\omega^2 (T_2 C_1 + T_1 C_2) + (C_1 + C_2)^2}$$

Calculation of *effective* resistance, R_e

$$(xxxviii) \quad C_e = \frac{\omega^2 (T_2 C_1 + T_1 C_2)^2 + (C_1 + C_2)^2}{\omega^2 (T_1^2 C_2 + T_2^2 C_2)^2 + (C_1 + C_2)^2}$$

Calculation of *effective* compliance, C_e

$$(xxxix) \quad \omega = 2\pi f$$

$$(xl) \quad T_1 = R_1 C_1$$

$$(xl) \quad T_2 = R_2 C_2$$

With equal time constants of lung compartments C_e and R_e become independent of frequency:

$$(xli) \quad C_e = C_1 + C_2$$

$$(xlii) \quad R_e = \frac{R_1 \times R_2}{R_1 + R_2}$$

Bijaoui

$$(xlili) \quad E_L \times P(t) + R_L \times \dot{P}(t) = \\ E_L \times E_{st,L} \times V(t) + [R_L \times (E_L \times E_{st,L}) + E_L \times R_{aw}] \times \dot{V}(t) \\ + R_L \times R_{aw} \times \ddot{V}(t) + R_L \times \ddot{R}_{aw} \times \dot{V}(t)$$

Bates-Bijaoui equation including a recursive multiple linear regression algorithm and frequently dependent elements.

$$(xliv) \quad \int_{\text{cycle}} P_{\text{res}} \times d\dot{V} = 0,$$

where $P_{\text{res}} = P_{\text{tot}} - E \times V - k = R \times \dot{V}$

This leads to

$$(xlv) \quad \int_{\text{cycle}} P \times d\dot{V} - \int_{\text{cycle}} K \times d\dot{V} - E \int_{\text{cycle}} V \times d\dot{V} = 0; \text{ and}$$

$$(xlvi) \quad E = \frac{\int_{\text{cycle}} P \times d\dot{V} - \int_{\text{cycle}} K \times d\dot{V}}{\int_{\text{cycle}} V \times d\dot{V}}$$

Calculation of “robust” elastance value.

Derivation of volume correction

The aerodynamic principle of the D-lite is based on the Bernoulli principle, stating that total pressure equals the sum of *potential*, *kinetic*, and *gravitational* energy:

$$(xlvii) \quad P_{\text{total}} = P_{\text{pot}} + P_{\text{kin}} + P_{\text{grav}};$$

the gravitational element ($\rho g z$) in this context is negligible. The sum of potential and kinetic energy is termed stagnation pressure.

$$(xlviii) \quad P_{\text{stagn}} = P_{\text{pot}} + 1/2 \times \rho \times \bar{V}^2$$

From this, linear velocity is isolated:

$$(xlix) \quad \bar{V} = \sqrt{2(P_{\text{stagn}} - P_{\text{pot}})/\rho}.$$

Multiplied by the cross-sectional area of conducting tube, volume flow is calculated, and integrated over time, volume is obtained. The software handling the signals from the D-lite contains an algorithm calculating density of mixture based on identification of gases. Oxygen is detected as well as carbon dioxide, nitrous oxide, and halogenated anaesthetics. The balance - as presumed by the software - is made up of nitrogen.

When using the D-lite with other gas mixtures the algorithm requires modification.

The AS/3-D-lite reports linear velocity or flow based on **presumed** density (ρ_p):
 $\bar{V}_p \propto \sqrt{(\Delta P/\rho_p)}$. To calculate the compensation between \bar{V}_p and $\bar{V}_a \propto \sqrt{(\Delta P/\rho_a)}$,
 linear velocity based on **actual** density ρ_a , the relation \bar{V}_a/\bar{V}_p is transformed to

$$\bar{V}_a = \sqrt{(\rho_p/\rho_a)} \times \bar{V}_p.$$

$V_{AS/3}$ Datex AS/3 flow signal

$V'_{AS/3}$ corrected Datex AS/3 flow signal in helium oxygen mixtures

$k_{1,2,3}$ constants

ΔP pressure difference

$\rho_{presumed}$ density of gas mixture of N_2 and O_2 as assumed by AS/3

ρ_{actual} density of gas mixture of He and O_2

ρ_{He} 0.1571 kg/m^3 , 1 ATA, 37°C

ρ_{N_2} 1.101 kg/m^3 , 1 ATA, 37°C

ρ_{O_2} 1.258 kg/m^3 , 1 ATA, 37°C

F_{O_2} fraction of oxygen

$$(I) V_{AS/3} = k \times \sqrt{\frac{\Delta p}{\rho_{presumed}}} \Rightarrow \Delta p = (V_{AS/3})^2 \times \rho_{presumed} \times \frac{1}{k^2}$$

(NB: mistyped in article)

$$(II) V'_{AS/3} = k \sqrt{\frac{\Delta p}{\rho_{actual}}}$$

Inserting ΔP

$$(III) V'_{AS/3} = k \sqrt{\frac{(V_{AS/3})^2 \rho_{presumed}}{k^2 \rho_{actual}}} = V_{AS/3} \sqrt{\frac{\rho_{presumed}}{\rho_{actual}}}$$

$$(III) \rho_{presumed} = F_{O_2} \rho_{O_2} + (1 - F_{O_2}) \rho_{N_2} = F_{O_2} (\rho_{O_2} - \rho_{N_2}) + \rho_{N_2}$$

$$(IV) \rho_{actual} = F_{O_2} \rho_{O_2} + (1 - F_{O_2}) \rho_{He} = F_{O_2} (\rho_{O_2} - \rho_{He}) + \rho_{He}$$

Thus

$$(IV) V'_{AS/3} = V_{AS/3} \sqrt{\frac{F_{O_2} (\rho_{O_2} - \rho_{N_2}) + \rho_{N_2}}{F_{O_2} (\rho_{O_2} - \rho_{He}) + \rho_{He}}}$$

ERRATA

1. In Paper IV, section Statistics and Calculations, Constant flow, p. 341: *t*-test was *not* performed.

2. In Paper IV, section Discussion, p.343, right column, first line: read: “6 and 64% of pressure drop. Guttman *et al.* (2) presented...etc.”

3. Paper IV, Figure 6. Lines of $\pm 2SD$ have been misplaced. Correct position is with line of bias as mid.

REFERENCES

1. Amato MB, Barbas CS, Medeiros DM, Magaldi RB, Schettino GP, Lorenzi-Filho G, Kairalla RA, Deheinzelin D, Munoz C, Oliveira R, Takagaki TY, Carvalho CR. Effect of a protective-ventilation strategy on mortality in the acute respiratory distress syndrome. *N Engl J Med* 1998; 338(6): 347-54.
2. Amato MB, Barbas CS, Medeiros DM, Schettino GdP, Lorenzi Filho G, Kairalla RA, Deheinzelin D, Moraes C, Fernandes EdO, Takagaki TY, et al. Beneficial effects of the "open lung approach" with low distending pressures in acute respiratory distress syndrome. A prospective randomized study on mechanical ventilation. *Am J Respir Crit Care Med* 1995; 152(6 Pt 1): 1835-46.
3. Anthony CM. Mechanical Modelling of Soft Tissue. A Literary Review. 2002
4. ARDSNet. Ventilation with lower tidal volumes as compared with traditional tidal volumes for acute lung injury and the acute respiratory distress syndrome. The Acute Respiratory Distress Syndrome Network. *N Engl J Med* 2000; 342(18): 1301-8.
5. Ashbaugh DG, Bigelow DB, Petty TL, Levine BE. Acute respiratory distress in adults. *Lancet* 1967; 2(7511): 319-23.
6. Bachofen H, Hildebrandt J. Area analysis of pressure-volume hysteresis in mammalian lungs. *J Appl Physiol* 1971; 30(4): 493-7.
7. Bachofen H, Hildebrandt J, Bachofen M. Pressure-volume curves of air- and liquid-filled excised lungs-surface tension in situ. *J Appl Physiol* 1970; 29(4): 422-31.
8. Ball J, Rhodes A, Grounds R. The Role of Helium in the Treatment of Acute Respiratory Failure. In: Vincent J-L, editor. *Yearbook of Intensive Care and Emergency Medicine*, pp 446-461. Berlin: Springer; 2001.
9. Bandy KP, Nicks JJ, Donn SM. Volume-controlled ventilation for severe neonatal respiratory failure. *Neonatal Intensive Care* 1992; 5(3): 70-3.
10. Barach A. Rare gases not essential to life. *Science* 1934; 80(2086): 593-94.
11. Barach A. Use of Helium as a New Therapeutic Gas. *Proc Soc Biol & Med* 1934; 32: 462-464.
12. Barach A. The Use of Helium as a New Therapeutic Gas. *Anaesth Analg* 1935; 14(5): 210-15.
13. Barach A. The Therapeutic Use of Helium. *JAMA* 1936; 107: 1273-80.
14. Barach A. Now Helium saves lives. *Sci Am* 1939; 160: 153.
15. Barach A, Martin J, Eckman M. Positive pressure respiration and its application to the treatment of acute pulmonary oedema. *Ann Int Med* 1938; 12(1): 754-95.
16. Barach A, Segal M. Helium-oxygen therapy in bronchial asthma. In: Weiss EB SM, editor. *Bronchial asthma. Mechanisms and therapeutics*, pp 983-89. Boston: Little, Brown & Co.; 1976.
17. Barach A, Swenson P. Effect of breathing gases under positive pressure on lumens of small and medium-sized bronchi. *Arch Intern Med* 1949; 63: 946-48.

18. Barach AL. Use of Helium in the Treatment of Asthma and Obstructive Lesions in the Larynx and Trachea. *Ann Int Med* 1935; 9(Dec): 739-65.
19. Barach AL. The Effects of Inhalation of Helium Mixed Oxygen on the Mechanics of Respiration. *J Clin Invest* 1936; 15: 47-61.
20. Barnas GM, Campbell DN, Mackenzie CF, Mendham JE, Fahy BG, Runcie CJ, Mendham GE. Lung, chest wall, and total respiratory system resistances and elastances in the normal range of breathing. *Am Rev Respir Dis* 1992; 145(1): 110-3.
21. Barnas GM, Mills PJ, Mackenzie CF, Ashby M, Sexton WL, Imle PC, Wilson PD. Dependencies of respiratory system resistance and elastance on amplitude and frequency in the normal range of breathing. *Am Rev Respir Dis* 1991; 143(2): 240-4.
22. Bassingthwaite JB, Liebovitch LS, West BJ. *Fractal physiology*. New York: Oxford University Press, 1994.
23. Bates J, Milic-Emili J. The Flow Interruption Technique for Measuring Respiratory Resistance. *J of Critical Care* 1991; 6(4): 227-38.
24. Bates JH, Ludwig MS, Sly PD, Brown K, Martin JG, Fredberg JJ. Interrupter resistance elucidated by alveolar pressure measurement in open-chest normal dogs. *J Appl Physiol* 1988; 65(1): 408-14.
25. Baydur A, Behrakis PK, Zin WA, Jaeger M, Milic-Emili J. A simple method for assessing the validity of the esophageal balloon technique. *Am Rev Respir Dis* 1982; 126(5): 788-91.
26. Bergman NA, Waltemath CL. A comparison of some methods for measuring total respiratory resistance. *J Appl Physiol* 1974; 36(1): 131-4.
27. Bersten AD, Doyle IR, Davidson KG, Barr HA, Nicholas TE, Kermeen F. Surfactant composition reflects lung overinflation and arterial oxygenation in patients with acute lung injury. *Eur Respir J* 1998; 12(2): 301-8.
28. Bersten AD, Edibam C, Hunt T, Moran J. Incidence and mortality of acute lung injury and the acute respiratory distress syndrome in three Australian States. *Am J Respir Crit Care Med* 2002; 165(4): 443-8.
29. Bertschmann W, Guttmann J, Zeravik J. Atemzugweise Bestimmung von Compliance und Resistance am Beatmeter. *Intensivmedizin und Notfallmedizin* 1990; 27: 42-47.
30. Beydon L, Svantesson C, Brauer K, Lemaire F, Jonson B. Respiratory mechanics in patients ventilated for critical lung disease. *Eur Respir J* 1996; 9(2): 262-73.
31. Bijaoui E, Tuck SA, Remmers JE, Bates JH. Estimating respiratory mechanics in the presence of flow limitation. *J Appl Physiol* 1999; 86(1): 418-26.
32. Bone RC. Toward a theory regarding the pathogenesis of the systemic inflammatory response syndrome: what we do and do not know about cytokine regulation. *Crit Care Med* 1996; 24(1): 163-72.
33. Briscoe W, Dubois A. The relationship between airway resistance, airway conductance and lung volume in subjects of different age and body size. *J Clin Invest* 1958; 37: 1279-1285.

34. Brochard L. Respiratory pressure-volume curves. In: Tobin M, editor. Principles and practice of intensive care monitoring, pp 597-616. New York: McGraw Hill; 1998.
35. Brochard L, Lemaire F. Tidal volume, positive end-expiratory pressure, and mortality in acute respiratory distress syndrome [editorial; comment]. *critical care medicine* 1999; 27(8): 1661-3.
36. Brochard L, Roudot-Thoraval F, Roupie E, Delclaux C, Chastre J, Fernandez-Mondejar E, Clementi E, Mancebo J, Factor P, Matamis D, Ranieri M, Blanch L, Rodi G, Mentec H, Dreyfuss D, Ferrer M, Brun-Buisson C, Tobin M, Lemaire F. Tidal volume reduction for prevention of ventilator-induced lung injury in acute respiratory distress syndrome. The Multicenter Trial Group on Tidal Volume reduction in ARDS. *Am J Respir Crit Care Med* 1998; 158(6): 1831-8.
37. Brower RG, Shanholtz CB, Fessler HE, Shade DM, White P, Jr., Wiener CM, Teeter JG, Dodd-o JM, Almog Y, Piantadosi S. Prospective, randomized, controlled clinical trial comparing traditional versus reduced tidal volume ventilation in acute respiratory distress syndrome patients. *Crit Care Med* 1999; 27(8): 1492-8.
38. Brunner JX, Laubscher TP, Banner MJ, Iotti G, Braschi A. Simple method to measure total expiratory time constant based on the passive expiratory flow-volume curve. *Crit Care Med* 1995; 23(6): 1117-22.
39. Carney DE, Bredenberg CE, Schiller HJ, Picone AL, McCann UG, Gatto LA, Bailey G, Fillinger M, Nieman GF. The mechanism of lung volume change during mechanical ventilation. *Am J Respir Crit Care Med* 1999; 160(5 Pt 1): 1697-702.
40. Chang HK. Flow Dynamics in the Respiratory Tract. In: Chang HK, editor. *Respiratory Physiology. An analytical approach*, pp 57-138. New York: Marcel Dekker, Inc.; 1989.
41. Chatburn RL, Primiano FPJ. Mathematical models of respiratory mechanics. In: Chatburn RL, editor. *Fundamentals of respiratory care research*, pp 59-100: Appleton & Lange; 1988.
42. Chelucci GL, Brunet F, Dall'Ava-Santucci J, Dhainaut JF, Paccaly D, Armaganidis A, Milic-Emili J, Lockhart A. A single-compartment model cannot describe passive expiration in intubated, paralysed humans. *Eur Respir J* 1991; 4(4): 458-64.
43. Chelucci GL, Dall' Ava-Santucci J, Dhainaut JF, Chelucci A, Allegra A, Paccaly D, Brunet F, Milic-Emili J, Lockhart A. Modelling of passive expiration in patients with adult respiratory distress syndrome. *Eur Respir J* 1993; 6(6): 785-90.
44. Collins JM, Shapiro AH, Kimmel E, Kamm RD. The steady expiratory pressure-flow relation in a model pulmonary bifurcation. *J Biomech Eng* 1993; 115(3): 299-305.
45. Dall'ava-Santucci J, Armaganidis A, Brunet F, Dhainaut JF, Nouria S, Morisseau D, Lockhart A. Mechanical effects of PEEP in patients with adult respiratory distress syndrome. *J Appl Physiol* 1990; 68(3): 843-8.
46. D'Angelo E. Static and dynamic behaviour of the respiratory system. In: Milic-Emili J, editor. *Applied physiology in respiratory mechanics*, pp 39-49. Milano: Springer Verlag; 1998.

47. D'Angelo E, Calderini E, Torri G, Robatto FM, Bono D, Milic-Emili J. Respiratory mechanics in anesthetized paralyzed humans: effects of flow, volume, and time. *J Appl Physiol* 1989; 67(6): 2556-64.
48. D'Angelo E, Prandi E, Tavola M, Calderini E, Milic-Emili J. Chest wall interrupter resistance in anesthetized paralyzed humans. *J Appl Physiol* 1994; 77(2): 883-7.
49. Davidson KG, Bersten AD, Barr HA, Dowling KD, Nicholas TE, Doyle IR. Endotoxin induces respiratory failure and increases surfactant turnover and respiration independent of alveolocapillary injury in rats. *Am J Respir Crit Care Med* 2002; 165(11): 1516-25.
50. Davis GM, Lands LC. Measurement of infant pulmonary mechanics: comparative analysis of techniques. *Pediatr Pulmonol* 1997; 23(2): 105-13.
51. De Blasi RA, Conti G, Antonelli M, Bufi M, Gasparetto A. A fibre optics system for the evaluation of airway pressure in mechanically ventilated patients. *Intensive Care Med* 1992; 18(7): 405-9.
52. Donaldson GC. The chaotic behaviour of resting human respiration. *Respir Physiol* 1992; 88(3): 313-21.
53. Drazen JM, Loring SH, Ingram RH, Jr. Distribution of pulmonary resistance: effects of gas density, viscosity, and flow rate. *J Appl Physiol* 1976; 41(3): 388-95.
54. Eberhard L, Guttman J, Wolff G, Bertschmann W, Minzer A, Kohl HJ, Zeravik J, Adolph M, Eckart J. Intrinsic PEEP monitored in the ventilated ARDS patient with a mathematical method. *J Appl Physiol* 1992; 73(2): 479-85.
55. Eissa NT, Ranieri VM, Corbeil C, Chasse M, Robatto FM, Braidy J, Milic-Emili J. Analysis of behavior of the respiratory system in ARDS patients: effects of flow, volume, and time. *J Appl Physiol* 1991; 70(6): 2719-29.
56. Falke KJ, Pontoppidan H, Kumar A, Leith DE, Geffin B, Laver MB. Ventilation with end-expiratory pressure in acute lung disease. *J Clin Invest* 1972; 51(9): 2315-23.
57. Fenn W. Mechanics of respiration. *Am J Med* 1951; 10: 77-91.
58. Fernandez R, Blanch L, Artigas A. Inflation static pressure-volume curves of the total respiratory system determined without any instrumentation other than the mechanical ventilator. *Intensive Care Med* 1993; 19(1): 33-8.
59. Fredberg JJ, Keefe DH, Glass GM, Castile RG, Frantz ID, 3rd. Alveolar pressure nonhomogeneity during small-amplitude high-frequency oscillation. *J Appl Physiol* 1984; 57(3): 788-800.
60. Fredberg JJ, Stamenovic D. On the imperfect elasticity of lung tissue. *J Appl Physiol* 1989; 67(6): 2408-19.
61. Gattinoni L, Mascheroni D, Basilico E, Foti G, Pesenti A, Avalli L. Volume/pressure curve of total respiratory system in paralysed patients: artefacts and correction factors. *Intensive Care Med* 1987; 13(1): 19-25.
62. Gattinoni L, Pesenti A, Caspani ML, Pelizzola A, Mascheroni D, Marcolin R, Iapichino G, Langer M, Agostoni A, Kolobow T, et al. The role of total static lung

- compliance in the management of severe ARDS unresponsive to conventional treatment. *Intensive Care Med* 1984; 10(3): 121-6.
63. Gattinoni L, Pesenti A, Mascheroni D, Marcolin R, Fumagalli R, Rossi F, Iapichino G, Romagnoli G, Uziel L, Agostoni A, et al. Low-frequency positive-pressure ventilation with extracorporeal CO₂ removal in severe acute respiratory failure. *JAMA* 1986; 256(7): 881-6.
 64. Glenn RW. Spatial correlation of regional pulmonary perfusion. *J Appl Physiol* 1992; 72(6): 2378-86.
 65. Glenn RW, Bernard S, Brinkley M. Validation of fluorescent-labeled microspheres for measurement of regional organ perfusion. *J Appl Physiol* 1993; 74(5): 2585-97.
 66. Glenn RW, Robertson HT. A computer simulation of pulmonary perfusion in three dimensions. *J Appl Physiol* 1995; 79(1): 357-69.
 67. Gottfried SB, Higgs BD, Rossi A, Carli F, Mingeot PM, Calverly PM, Zocchi L, Milic-Emili J. Interrupter technique for measurement of respiratory mechanics in anesthetized humans. *J Appl Physiol* 1985; 59(2): 647-52.
 68. Gottfried SB, Rossi A, Calverly PM, Zocchi L, Milic-Emili J. Interrupter technique for measurement of respiratory mechanics in anesthetized cats. *J Appl Physiol* 1984; 56(3): 681-90.
 69. Gottfried SB, Rossi A, Higgs BD, Calverly PM, Zocchi L, Bozic C, Milic-Emili J. Noninvasive determination of respiratory system mechanics during mechanical ventilation for acute respiratory failure. *Am Rev Respir Dis* 1985; 131(3): 414-20.
 70. Green MD, Ho G, Polu H, Ma Z, Agarwal M, Hu P, Barnas GM. Automated system for detailed measurement of respiratory mechanics. *J Clin Monit* 1996; 12(1): 61-7.
 71. Guttman J, Eberhard L, Fabry B, Bertschmann W, Wolff G. Continuous calculation of intratracheal pressure in tracheally intubated patients. *Anesthesiology* 1993; 79(3): 503-13.
 72. Guttman J, Eberhard L, Fabry B, Bertschmann W, Zeravik J, Adolph M, Eckart J, Wolff G. Time constant/volume relationship of passive expiration in mechanically ventilated ARDS patients. *Eur Respir J* 1995; 8(1): 114-20.
 73. Guttman J, Eberhard L, Fabry B, Zappe D, Bernhard H, Lichtwarck-Aschoff M, Adolph M, Wolff G. Determination of volume-dependent respiratory system mechanics in mechanically ventilated patients using the new SLICE method. *Technology and Health Care* 1994; 2: 175-191.
 74. Guttman J, Eberhard L, Haberthur C, Mols G, Kessler V, Lichtwarck-Aschoff M, Geiger K. Detection of endotracheal tube obstruction by analysis of the expiratory flow signal. *Intensive Care Med* 1998; 24(11): 1163-72.
 75. Guttman J, Eberhard L, Wolff G, Bertschmann W, Zeravik J, Adolph M. Maneuver-free determination of compliance and resistance in ventilated ARDS patients. *Chest* 1992; 102(4): 1235-42.

76. Guttman J, Kessler V, Mols G, Hentschel R, Haberthur C, Geiger K. Continuous calculation of intratracheal pressure in the presence of pediatric endotracheal tubes. *Crit Care Med* 2000; 28(4): 1018-26.
77. Hansen JJ, Jepsen SB, Lund J. [Symptomatic helium treatment of upper and lower airway obstruction]. *Ugeskr Laeger* 2000; 162(49): 6669-72.
78. Hardin J, Yu J. The pressure/flow relationship in bronchial airways on expiration. In: Schneck D, editor. *Biofluid Mechanics*, pp 39-55. New York: Plenum Press; 1980.
79. Hess D, Tabor T. Comparison of six methods to calculate airway resistance during mechanical ventilation in adults. *J Clin Monit* 1993; 9(4): 275-82.
80. Hickling KG. The pressure-volume curve is greatly modified by recruitment. A mathematical model of ARDS lungs. *Am J Respir Crit Care Med* 1998; 158(1): 194-202.
81. Hickling KG, Henderson SJ, Jackson R. Low mortality associated with low volume pressure limited ventilation with permissive hypercapnia in severe adult respiratory distress syndrome. *Intensive Care Med* 1990; 16(6): 372-7.
82. Hildebrandt J. Dynamic properties of air-filled excised cat lung determined by liquid plethysmograph. *J Appl Physiol* 1969; 27(2): 246-50.
83. Horsfield K. Diameters, generations, and orders of branches in the bronchial tree. *J Appl Physiol* 1990; 68(2): 457-61.
84. Horsfield K, Cumming G. Morphology of the bronchial tree in man. *J Appl Physiol* 1968; 24(3): 373-83.
85. Horsfield K, Kemp W, Phillips S. An asymmetrical model of the airways of the dog lung. *J Appl Physiol* 1982; 52(1): 21-6.
86. Iotti GA, Braschi A, Brunner JX, Smits T, Olivei M, Palo A, Veronesi R. Respiratory mechanics by least squares fitting in mechanically ventilated patients: applications during paralysis and during pressure support ventilation. *Intensive Care Med* 1995; 21(5): 406-13.
87. Jaeger M, Matthys H. The pressure flow characteristics of the human airways. In: Bouhuys A, editor. *Airway Dynamics. Physiology and Pharmacology*, pp 21-32. Springfield: Ch. C. Thomas Publ.; 1970.
88. Jaeger MJ, Matthys H. The pattern of flow in the upper human airways. *Respir Physiol* 1968; 6(1): 113-27.
89. Jarreau PH, Louis B, Dassieu G, Desfrere L, Blanchard PW, Moriette G, Isabey D, Harf A. Estimation of inspiratory pressure drop in neonatal and pediatric endotracheal tubes. *J Appl Physiol* 1999; 87(1): 36-46.
90. Johns DP, Pretto JJ, Streton JA. Measurement of gas viscosity with a Fleisch pneumotachograph. *J Appl Physiol* 1982; 53(1): 290-3.
91. Jonson B, Beydon L, Brauer K, Mansson C, Valind S, Grytzell H. Mechanics of respiratory system in healthy anesthetized humans with emphasis on viscoelastic properties. *J Appl Physiol* 1993; 75(1): 132-40.
92. Jonson B, Richard JC, Straus C, Mancebo J, Lemaire F, Brochard L. Pressure-volume curves and compliance in acute lung injury: evidence of recruitment above the lower inflection point. *Am J Respir Crit Care Med* 1999; 159(4 Pt 1): 1172-8.

93. Jonson B, Svantesson C. Elastic pressure-volume curves: what information do they convey? *Thorax* 1999; 54(1): 82-7.
94. Kano S, Lanteri CJ, Duncan AW, Sly PD. Influence of nonlinearities on estimates of respiratory mechanics using multilinear regression analysis. *J Appl Physiol* 1994; 77(3): 1185-97.
95. Karason S. Spirodynamics : new methods for continuous monitoring of respiratory mechanics in ventilator-treated patients: Göteborg; 2000.
96. Karason S, Antonsen K, Aneman A. Ventilator treatment in the Nordic countries. A multicenter survey. *Acta Anaesthesiol Scand* 2002; 46(9): 1053-1061.
97. Karason S, Karlsen KL, Lundin S, Stenqvist O. A simplified method for separate measurements of lung and chest wall mechanics in ventilator-treated patients. *Acta Anaesthesiol Scand* 1999; 43(3): 308-15.
98. Karason S, Sondergaard S, Aneman A, Lundin S, Stenqvist O. Respiratory mechanics during endotoxin infusion measured with the spiodynamic method. *Intensive Care Med* 2001.; 27(suppl 2): S452.
99. Karason S, Sondergaard S, Lundin S, Stenqvist O. Continuous on-line measurements of respiratory system, lung and chest wall mechanics during mechanic ventilation. *Intensive Care Med* 2001; 27(8): 1328-39.
100. Karason S, Sondergaard S, Lundin S, Wiklund J, Stenqvist O. Evaluation of pressure/volume loops based on intratracheal pressure measurements during dynamic conditions. *Acta Anaesthesiol Scand* 2000; 44(5): 571-7.
101. Karason S, Sondergaard S, Lundin S, Wiklund J, Stenqvist O. A new method for non-invasive, manoeuvre-free determination of "static" pressure-volume curves during dynamic/therapeutic mechanical ventilation. *Acta Anaesthesiol Scand* 2000; 44(5): 578-85.
102. Karason S, Sondergaard S, Lundin S, Wiklund J, Stenqvist O. Direct tracheal airway pressure measurements, essential for accurate and safe monitoring of tracheal pressures. A laboratory study. *Acta Anaesthesiol Scand* 2001; 45(2): 173-9.
103. Kessler V, Guttman J, Newth CJ. Dynamic respiratory system mechanics in infants during pressure and volume controlled ventilation. *Eur Respir J* 2001; 17(1): 115-21.
104. Koska J, Kelley E, Banner MJ, Blanch P. Evaluation of a fiberoptic system for airway pressure monitoring. *J Clin Monit* 1994; 10(4): 247-50.
105. Koutsoukou A, Armaganidis A, Stavrakaki-Kallergi C, Vassilakopoulos T, Lymberis A, Roussos C, Milic-Emili J. Expiratory flow limitation and intrinsic positive end-expiratory pressure at zero positive end-expiratory pressure in patients with adult respiratory distress syndrome. *Am J Respir Crit Care Med* 2000; 161(5): 1590-6.
106. Lachmann B. Open up the lung and keep the lung open. *Intensive Care Med* 1992; 18(6): 319-21.
107. Lambert RK, Wilson TA, Hyatt RE, Rodarte JR. A computational model for expiratory flow. *J Appl Physiol* 1982; 52(1): 44-56.
108. Lauzon AM, Bates JH. Estimation of time-varying respiratory mechanical parameters by recursive least squares. *J Appl Physiol* 1991; 71(3): 1159-65.

109. Lemaire F, Harf A, Simonneau G, Matamis D, Rivara D, Atlan G. Gas exchange, static pressure-volume curve and positive-pressure ventilation at the end of expiration. Study of 16 cases of acute respiratory insufficiency in adults. *Ann Anesthesiol Fr* 1981; 22(5): 435-41.
110. Levy P, Similowski T, Corbeil C, Albala M, Pariente R, Milic-Emili J, B. J. A method for studying the static volume-pressure curves of the respiratory system during mechanical ventilation. *J Crit Care* 1989; 4: 83-89.
111. Lichtwarck-Aschoff M, Guttman J. Letter: Direct tracheal airway pressure measurements. *Acta Anaesth Scand* 2001; 45: 1046-50.
112. Loring SH, Elliott EA, Drazen JM. Kinetic energy loss and convective acceleration in respiratory resistance measurements. *Lung* 1979; 156(1): 33-42.
113. Lu Q, Vieira SR, Richecoeur J, Puybasset L, Kalfon P, Coriat P, Rouby JJ. A simple automated method for measuring pressure-volume curves during mechanical ventilation. *Am J Respir Crit Care Med* 1999; 159(1): 275-82.
114. Luhr O, Karlsson M, Thorsteinsson A, Rylander C, Frostell C. The impact of respiratory variables on mortality in non-ARDS and ARDS patients requiring mechanical ventilation. *Intensive Care Med* 2000; 26: 508-517.
115. Luhr OR, Antonsen K, Karlsson M, Aardal S, Thorsteinsson A, Frostell CG, Bonde J. Incidence and mortality after acute respiratory failure and acute respiratory distress syndrome in Sweden, Denmark, and Iceland. The ARF Study Group. *Am J Respir Crit Care Med* 1999; 159(6): 1849-61.
116. Lutchen KR, Greenstein JL, Suki B. How inhomogeneities and airway walls affect frequency dependence and separation of airway and tissue properties. *J Appl Physiol* 1996; 80(5): 1696-707.
117. Lutchen KR, Hantos Z, Petak F, Adamicz A, Suki B. Airway inhomogeneities contribute to apparent lung tissue mechanics during constriction. *J Appl Physiol* 1996; 80(5): 1841-9.
118. Lutchen KR, Suki B, Zhang Q, Petak F, Daroczy B, Hantos Z. Airway and tissue mechanics during physiological breathing and bronchoconstriction in dogs. *J Appl Physiol* 1994; 77(1): 373-85.
119. Mandelbrot BB. The fractal geometry of nature. Rev. edn. San Francisco: Freeman, 1982.
120. Mankikian B, Lemaire F, Benito S, Brun-Buisson C, Harf A, Maillot JP, Becker J. A new device for measurement of pulmonary pressure-volume curves in patients on mechanical ventilation. *Crit Care Med* 1983; 11(11): 897-901.
121. Martynowicz M, Hubmayr R. Mechanics of regional lung expansion in acute respiratory distress syndrome. In: Vincent J, editor. 1999 Yearbook of intensive care and emergency medicine, pp 252-268. Berlin: Springer Verlag; 1999.
122. Matamis D, Lemaire F, Harf A, Brun-Buisson C, Ansquer JC, Atlan G. Total respiratory pressure-volume curves in the adult respiratory distress syndrome. *Chest* 1984; 86(1): 58-66.
123. Mead I, Whittenberger L. Physical properties of human lung measured during spontaneous respiration. *J Appl Physiol* 1953; 5: 779-796.

124. Mergoni M, Volpi A, Rossi A. Inflection point and alveolar recruitment in ARDS. In: Vincent J, editor. 1997 Yearbook of intensive and critical care medicine, pp 556-567. Berlin: Springer Verlag; 1997.
125. Merilainen P, Hanninen H, Tuomaala L. A novel sensor for routine continuous spirometry of intubated patients. *J Clin Monit* 1993; 9(5): 374-80.
126. Milic-Emili J, D'Angelo E. Mechanical implications of viscoelasticity. In: Milic-Emili J, Lucangelo U, Pesenti A, Zin W, editors. *Basics of Respiratory Mechanics and Artificial Ventilation*, pp 109-18. Berlin: Springer; 1999.
127. Mols G, Brandes I, Kessler V, Lichtwarck-Aschoff M, Loop T, Geiger K, Guttman J. Volume-dependent compliance in ARDS: proposal of a new diagnostic concept. *Intensive Care Med* 1999; 25(10): 1084-91.
128. Mols G, Hermle G, Schubert J, Miekisch W, Benzing A, Lichtwarck-Aschoff M, Geiger K, Walmrath D, Guttman J. Volume-dependent compliance and ventilation-perfusion mismatch in surfactant-depleted isolated rabbit lungs. *Crit Care Med* 2001; 29(1): 144-51.
129. Mols G, Kessler V, Benzing A, Lichtwarck-Aschoff M, Geiger K, Guttman J. Is pulmonary resistance constant, within the range of tidal volume ventilation, in patients with ARDS? *Br J Anaesth* 2001; 86(2): 176-82.
130. Mount L. The ventilation flow-resistance and compliance of rat lungs. *J Physiol* 1955; 127: 157-67.
131. Muramatsu K, Yukitake K. A new method to analyze lung compliance when pressure-volume relationship is nonlinear. *Am. J. Respir. Crit. Care Med.* 1999; 159(6): 2028-.
132. Murray JF, Matthay MA, Luce JM, Flick MR. An expanded definition of the adult respiratory distress syndrome. *Am Rev Respir Dis* 1988; 138(3): 720-3.
133. Musch G, Sparacino M, Pesenti A. Monitoring respiratory mechanics during controlled mechanical ventilation. In: Milic-Emili J, editor. *Applied physiology in respiratory mechanics*, pp 152-166. Milano: Springer-Verlag; 1998.
134. Navalesi P, Hernandez P, Laporta D, Landry JS, Maltais F, Navajas D, Gottfried SB. Influence of site of tracheal pressure measurement on in situ estimation of endotracheal tube resistance. *J Appl Physiol* 1994; 77(6): 2899-906.
135. Neergaard Kv, Wirz K. Die Messung der Strömungswiderstände in dem Atemwegen des Menschen, insbesondere bei Asthma und Emphysem. *Z. Klin. Med.* 1927; 105: 51-82.
136. Nelson TR, West BJ, Goldberger AL. The fractal lung: universal and species-related scaling patterns. *Experientia* 1990; 46(3): 251-4.
137. Neve V, de la Roque ED, Leclerc F, Leteurtre S, Dorkenoo A, Sadik A, Cremer R, Logier R. Ventilator-induced overdistension in children: dynamic versus low-flow inflation volume-pressure curves. *Am J Respir Crit Care Med* 2000; 162(1): 139-47.
138. Newman H. A simple method of measuring the compliance and the nonelastic resistance of the chest during anaesthesia. *Br J Anaesth* 1959; 31: 282-89.

139. Nikischin W, Gerhardt T, Everett R, Bancalari E. A new method to analyze lung compliance when pressure-volume relationship is nonlinear. *Am J Respir Crit Care Med* 1998; 158(4): 1052-60.
140. Officer TM, Pellegrino R, Brusasco V, Rodarte JR. Measurement of pulmonary resistance and dynamic compliance with airway obstruction. *J Appl Physiol* 1998; 85(5): 1982-8.
141. Otis A, McKerrow C, Bartlett R, Mead J, McIlroy M, Selverstone N, Radford EJ. Mechanical factors in distribution of pulmonary ventilation . *J Appl Physiol* 1956; 8: 427-43.
142. Papamoschou D. Theoretical validation of the respiratory benefits of helium-oxygen mixtures. *Respir Physiol* 1995; 99(1): 183-90.
143. Pedley JP, Kamm RD. Dynamics of Gas Flow and Pressure-Flow Relationships. In: Crystal RG, West JB, editors. *The Lung: Scientific Foundations*, pp 995-1010. New York: Raven Press; 1991.
144. Pedley TJ, Schroter RC, Sudlow MF. Energy losses and pressure drop in models of human airways. *Respir Physiol* 1970; 9(3): 371-86.
145. Pedley TJ, Schroter RC, Sudlow MF. The prediction of pressure drop and variation of resistance within the human bronchial airways. *Respir Physiol* 1970; 9(3): 387-405.
146. Pedley TJ, Schroter RC, Sudlow MF. Gas flow and mixing in the airways. In: West JB, editor. *Bioengineering Aspects of the Lung*, pp 163-265. New York: Marcel Dekker; 1977.
147. Pesenti A, Pelosi P. Respiratory Resistance in Mechanically Ventilated Patients: The Effects of PEEP. In: Vincent J-L, editor. *Yearbook of Intensive Care and Emergency Medicine*, pp 325-330. Berlin: Springer-Verlag; 1992.
148. Peslin R, da Silva JF, Chabot F, Duvivier C. Respiratory mechanics studied by multiple linear regression in unsedated ventilated patients. *Eur Respir J* 1992; 5(7): 871-8.
149. Pohlandt F, Saule H, Schroder H, Leonhardt A, Hornchen H, Wolff C, Bernsau U, Oppermann HC, Obladen M, Feilen KD. Decreased incidence of extra-alveolar air leakage or death prior to air leakage in high versus low rate positive pressure ventilation: results of a randomised seven-centre trial in preterm infants. *Eur J Pediatr* 1992; 151(12): 904-9.
150. Porszasz J, Barstow TJ, Wasserman K. Evaluation of a symmetrically disposed Pitot tube flowmeter for measuring gas flow during exercise. *J Appl Physiol* 1994; 77(6): 2659-65.
151. Prestele K, Franetzki M, Meerlender G. Viskositäts- und Dichteschwankungen von natürlichen Atemgasen und von Helium-Sauerstoff-Stickstoff-Gemischen in Abhängigkeit von Temperatur und Gaszusammensetzung. *Respiration* 1976; 33(2): 150-62.
152. Prezant DJ, Aldrich TK, Karpel JP, Park SS. Inspiratory flow dynamics during mechanical ventilation in patients with respiratory failure. *Am Rev Respir Dis* 1990; 142(6 Pt 1): 1284-7.

153. Putensen C, Baum M, Koller W, Putz G. The PEEP wave: an automated technic for bedside determination of the volume/pressure ratio in the lungs of ventilated patients. *Anaesthesist* 1989; 38(4): 214-9.
154. Raabe O, Yeh H, Schum G. Tracheobronchial Geometry: Human, Dog, Rat, Hamster. Albuquerque, NM: Lovelace Foundation, 1976.
155. Rahn H, Otis A, Chadwick L, Fenn W. The pressure-volume diagram of the thorax and lung. *Am J Physiol* 1946; 146: 1565-1570.
156. Ranieri VM, Giuliani R, Fiore T, Dambrosio M, Milic-Emili J. Volume-pressure curve of the respiratory system predicts effects of PEEP in ARDS: "occlusion" versus "constant flow" technique. *Am J Respir Crit Care Med* 1994; 149(1): 19-27.
157. Ranieri VM, Mascia L, Fiore T, Bruno F, Brienza A, Giuliani R. Cardiorespiratory effects of positive end-expiratory pressure during progressive tidal volume reduction (permissive hypercapnia) in patients with acute respiratory distress syndrome. *Anesthesiology* 1995; 83(4): 710-20.
158. Ranieri VM, Zhang H, Mascia L, Aubin M, Lin CY, Mullen JB, Grasso S, Binnie M, Volgyesi GA, Eng P, Slutsky AS. Pressure-time curve predicts minimally injurious ventilatory strategy in an isolated rat lung model. *Anesthesiology* 2000; 93(5): 1320-8.
159. Rodriguez L, Marquer B, Mardrus P, Molenat F, Le Grand JL, Reboul M, Garrigues B. A new simple method to perform pressure-volume curves obtained under quasi-static conditions during mechanical ventilation. *Intensive Care Med* 1999; 25(2): 173-9.
160. Rohrer F. Der Strömungswiderstand in den menschlichen Atemwegen unter der Einfluß unregelmässigen Verzweigung des Bronchialsystems auf den Atmungsverlauf in verschiedenen Lungenbezirken. *Pfluegers Arch Ges Physiol* 1915; 162: 225-59.
161. Rohrer F. Flow resistance in human air passages and the effect of irregular branching of the bronchial system on the respiratory process in various regions of the lungs. In: West JB, editor. *Translations in respiratory physiology*, pp 3-66. Stroudsburg; 1975.
162. Rohrer F, Nakasone K, Wirz K. Physiologie der Atembewegung. In: Bethe A, Embden B, Ellinger A, editors. *Handbuch der normalen und pathologischen Physiologie*, pp 70-127. Berlin: Springer; 1925.
163. Rossi A, Polese G. As simple as possible, but not simpler. *Intensive Care Med* 2000; 26(11): 1591-4.
164. Rossi A, Polese G, Milic-Emili J. Monitoring respiratory mechanics in ventilator-dependent patients. In: Tobin M, editor. *Principles and practice of intensive care monitoring*, pp 553-596. New York: McGraw-Hill; 1998.
165. Rousselot JM, Peslin R, Duvivier C. Evaluation of the multiple linear regression method to monitor respiratory mechanics in ventilated neonates and young children. *Pediatr Pulmonol* 1992; 13(3): 161-8.
166. Santos C, Slutsky AS. Advances in ARDS: How do they impact Bedside Management? In: Vincent J-L, editor. *Yearbook of Intensive Care and Emergency Medicine*, pp 320-36. Berlin: Springer; 2002.

167. Saxe JG, Galdone P. The blind men and the elephant. New York,: Whittlesey House, 1963.
168. Segal M. Inhalational therapy in the treatment of serious respiratory disease. *New Eng J Med* 1943; 229(6): 235-41.
169. Segal MS. Advances in inhalation therapy, with particular reference to cardio-respiratory disease. *New Eng J Med* 1944; 231(16): 553-556.
170. Segal MS. Inhalation therapy. *New Eng J Med* 1944; 230: 456-65, 485-93.
171. Servillo G, De Robertis E, Coppola M, Blasi F, Rossano F, Tufano R. Application of a computerised method to measure static pressure volume curve in acute respiratory distress syndrome. *Intensive Care Med* 2000; 26(1): 11-4.
172. Servillo G, De Robertis E, Maggiore S, Lemaire F, Brochard L, Tufano R. The upper inflection point of the pressure-volume curve. Influence of methodology and of different modes of ventilation. *Intensive Care Med* 2002; 28(7): 842-9.
173. Servillo G, Svantesson C, Beydon L, Roupie E, Brochard L, Lemaire F, Jonson B. Pressure-volume curves in acute respiratory failure: automated low flow inflation versus occlusion. *Am J Respir Crit Care Med* 1997; 155(5): 1629-36.
174. Similowski T, Levy P, Corbeil C, Albala M, Pariente R, Derenne JP, Bates JH, Jonson B, Milic-Emili J. Viscoelastic behavior of lung and chest wall in dogs determined by flow interruption. *J Appl Physiol* 1989; 67(6): 2219-29.
175. Sinha SK, Donn SM, Gavey J, McCarty M. Randomised trial of volume controlled versus time cycled, pressure limited ventilation in preterm infants with respiratory distress syndrome. *Arch Dis Child Fetal Neonatal Ed* 1997; 77(3): F202-5.
176. Slutsky AS. Mechanical ventilation. American College of Chest Physicians' Consensus Conference. *Chest* 1993; 104(6): 1833-59.
177. Slutsky AS, Berdine GG, Drazen JM. Steady flow in a model of human central airways. *J Appl Physiol* 1980; 49(3): 417-23.
178. Sly PD, Lanteri CJ, Nicolai T. Measurement of Respiratory Function in the Intensive Care Unit. In: Stocks J, Sly PD, Tepper RS, Morgan JW, editors. Infant respiratory function testing, pp 445-484. New York: Wiley-Liss; 1996.
179. Sondergaard S, Karason S, Hanson A, Nilsson K, Hojer S, Lundin S, Stenqvist O. Direct measurement of intratracheal pressure in pediatric respiratory monitoring. *Pediatr Res* 2002; 51(3): 339-45.
180. Sondergaard S, Karason S, Hanson A, Nilsson K, Wiklund J, Lundin S, Stenqvist O. The Dynostatic Algorithm accurately calculates alveolar pressure on-line during ventilator treatment in children. submitted 2002.
181. Sondergaard S, Karason S, Wiklund J, Lundin S, Stenqvist O. Alveolar pressure monitoring - an evaluation in a lung model and in patients with acute lung injury. submitted 2002.
182. Stegmaier PA, Zollinger A, Brunner JX, Pasch T. Assessment of pulmonary mechanics in mechanical ventilation: effects of imprecise breath detection, phase shift and noise. *J Clin Monit Comput* 1998; 14(2): 127-34.
183. Stewart TE, Meade MO, Cook DJ, Granton JT, Hodder RV, Lapinsky SE, Mazer CD, McLean RF, Rogovein TS, Schouten BD, Todd TR, Slutsky AS. Evaluation of a

ventilation strategy to prevent barotrauma in patients at high risk for acute respiratory distress syndrome. Pressure- and Volume-Limited Ventilation Strategy Group. *N Engl J Med* 1998; 338(6): 355-61.

184. Stick S. Measurements during tidal breathing. In: Stocks J, Sly PD, Tepper RS, Morgan JW, editors. *Infant respiratory function testing*, pp 117-138. New York: Wiley-Liss; 1996.

185. Suki B, Alencar AM, Tolnai J, Asztalos T, Petak F, Sujeer MK, Patel K, Patel J, Stanley HE, Hantos Z. Size distribution of recruited alveolar volumes in airway re-opening. *J Appl Physiol* 2000; 89(5): 2030-40.

186. Suki B, Barabasi AL, Hantos Z, Petak F, Stanley HE. Avalanches and power-law behaviour in lung inflation. *Nature* 1994; 368(6472): 615-8.

187. Suratt PM, Owens D. A pulse method of measuring respiratory system compliance in ventilated patients. *Chest* 1981; 80(1): 34-8.

188. Suter PM, Fairley B, Isenberg MD. Optimum end-expiratory airway pressure in patients with acute pulmonary failure. *N Engl J Med* 1975; 292(6): 284-9.

189. Suter PM, Fairley HB, Isenberg MD. Effect of tidal volume and positive end-expiratory pressure on compliance during mechanical ventilation. *Chest* 1978; 73(2): 158-62.

190. Svantesson C, Drefeldt B, Jonson B. The static pressure-volume relationship of the respiratory system determined with a computer-controlled ventilator. *Clin Physiol* 1997; 17: 419-430.

191. Svantesson C, Sigurdsson S, Larsson A, Jonson B. Effects of recruitment of collapsed lung units on the elastic pressure-volume relationship in anaesthetised healthy adults. *Acta Anaesthesiol Scand* 1998; 42(10): 1149-56.

192. Sydow M, Burchardi H, Zinserling J, Ische H, Crozier TA, Weyland W. Improved determination of static compliance by automated single volume steps in ventilated patients. *Intensive Care Med* 1991; 17(2): 108-14.

193. Tassaux D, Jolliet P, Thouret JM, Roeseler J, Dorne R, Chevrolet JC. Calibration of seven ICU ventilators for mechanical ventilation with helium-oxygen mixtures. *Am J Respir Crit Care Med* 1999; 160(1): 22-32.

194. The Acute Respiratory Distress Syndrome Network. Ventilation with lower tidal volumes as compared with traditional tidal volumes for acute lung injury and the acute respiratory distress syndrome. *N Engl J Med* 2000; 342(18): 1301-8.

195. Tibby SM, Cheema IU, Sekaran D, Hatherill M, Murdoch IA. Use of permissive hypercapnia in the ventilation of infants with respiratory syncytial virus infection. *Eur J Pediatr* 1999; 158(1): 42-5.

196. Tipping TR, Sykes MK. Tracheal tube resistance and airway and alveolar pressures during mechanical ventilation in the neonate. *Anaesthesia* 1991; 46(7): 565-9.

197. Uhl RR, Lewis FJ. Digital computer calculation of human pulmonary mechanics using a least squares fit technique. *Comput Biomed Res* 1974; 7(5): 489-95.

198. Valta P, Takala J, Eissa NT, Milic-Emili J. Does alveolar recruitment occur with positive end-expiratory pressure in adult respiratory distress syndrome patients? *J Crit Care* 1993; 8(1): 34-42.

199. Varene P, Jacquemin C. Airways resistance: a new method of computation. In: Bouyhuys A, editor. *Airway dynamics: Physiology and pharmacology*, pp 99-108. Springfield: Charles C Thomas; 1970.
200. Vassiliou MP, Petri L, Amygdalou A, Patrani M, Psarakis C, Nikolaki D, Georgiadis G, Behrakis PK. Linear and nonlinear analysis of pressure and flow during mechanical ventilation. *Intensive Care Med* 2000; 26(8): 1057-64.
201. Vassiliou MP, Saunier C, Duvivier C, Behrakis PK, Peslin R. Volume dependence of respiratory system resistance during artificial ventilation in rabbits. *Intensive Care Medicine* 2001; 27: 898-904.
202. Venegas JG, Harris RS, Simon BA. A comprehensive equation for the pulmonary pressure-volume curve. *J Appl Physiol* 1998; 84(1): 389-95.
203. Vieira SR, Puybasset L, Lu Q, Richecoeur J, Cluzel P, Coriat P, Rouby JJ. A scanographic assessment of pulmonary morphology in acute lung injury. Significance of the lower inflection point detected on the lung pressure-volume curve. *Am J Respir Crit Care Med* 1999; 159(5 Pt 1): 1612-23.
204. Wald A, Jason D, Murphy TW, Mazzia VD. A computers system for respiratory parameters. *Comput Biomed Res* 1969; 2(5): 411-29.
205. Warters RD, Allen SJ, Tonnesen AS. Intratracheal pressure monitoring during synchronized intermittent mandatory ventilation and pressure controlled-inverse ratio ventilation. *Crit Care Med* 1997; 25(2): 227-30.
206. Weibel E, editor. *Design of Biological Organisms and Fractal Geometry*. Basel: Birkhäuser Verlag; 1993.
207. Weibel E, Gomez D. Architecture of the human lung. *Science* 1962; 137: 577-85.
208. West BJ, Bhargava V, Goldberger AL. Beyond the principle of similitude: re-normalization in the bronchial tree. *J Appl Physiol* 1986; 60(3): 1089-97.
209. West JB, American Physiological Society (1887-). *Respiratory physiology : people and ideas*. New York: Published for the American Physiological Society by Oxford University Press, 1996.
210. Wilson TA. The Mechanics of Lung Parenchyma. In: Chang HK, Paiva M, editors. *Lung biology in health and disease*, pp 317-42. New York: Dekker; 1989.
211. Wolf AR, Volgyesi GA. A modified Pitot tube for the accurate measurement of tidal volume in children. *Anesthesiology* 1987; 67(5): 775-8.
212. Wood LD, Engel LA, Griffin P, Despas P, Macklem PT. Effect of gas physical properties and flow on lower pulmonary resistance. *J Appl Physiol* 1976; 41(2): 234-44.
213. Wright PE, Marini JJ, Bernard GR. In vitro versus in vivo comparison of endotracheal tube airflow resistance. *Am Rev Respir Dis* 1989; 140(1): 10-6.
214. Xiao Z. *Applications of artificial microcavities in wafer bonded silicon*. Gothenburg: Chalmers University of Technology; 1996.

ISBN 91-628-5385-6